# DESIGN, PRODUCTION AND TESTING OF A LABORATORY SCALE ORGANIC RANKINE CYCLE SYSTEM

by

Onur Kardaş

B.S., Mechanical Engineering, Dokuz Eylül University, 2013

Submitted to the Institute for Graduate Studies in
Science and Engineering in partial fulfillment of
the requirements for the degree of
Master of Science

Graduate Program in Mechanical Engineering

Boğaziçi University

2017

# ACKNOWLEDGEMENTS

I would like to thank the entire BURET team for their amazing collaboration. Together, we established this laboratory, and hopefully, greater research will be conducted in future time. My supervisor and co-supervisor, Dr. Günay Anlaş and Dr. Hasan Bedir, have been such great mentors and gave me encouragement and initiative to reach my stride.

I would like to give special thanks to Bora Işık for his great deal of attention, motivation, and knowledge. I could not have imagined building a better system without his engineering experience.

I gratefully acknowledge the funding from the Istanbul Development Agency (ISTKA). I would not have the practical experience I do now if it were not for them.

My sincere thanks also go to my labmates: Emre Sezerkan, Umut Soysal, Mehdi Nebati, Hamed Shafiei, and Alpay Asma for their support and for all the fun we have had.

Last but not the least, I would like to thank my family, my parents and my little sister, for their limitless support. You were always there for me and I really appreciate it. Finally, I want to thank my dear Melike for always standing by me and for making me a better person.

# ABSTRACT

## DESIGN, PRODUCTION AND TESTING OF A LABORATORY SCALE ORGANIC RANKINE CYCLE SYSTEM

This study presents the thermodynamic design, implementation and commissioning of a small scale organic Rankine cycle test rig. The objective was to design a flexible organic Rankine cycle test rig to study performance of different working fluids and cycle components. The test rig was instrumented with pressure, temperature and flowmeter sensors to collect data from cycle operation. These data was used to validate various thermodynamic models. During the design process; environmental, safety and physical characteristics of 13 different fluids were studied to obtain suitable working fluids. Four fluids namely R134a, R141b, R245ca and R245fa were taken into consideration for further detailed analyses. Maximum cycle efficiency and maximum net power output were considered as performance indicators. A recuperator was integrated into the system to investigate its effect on the cycle efficiency. From the thermodynamic analyses, R134a was adopted as the working fluid for the experimental setup. Detailed commissioning procedures were prepared and preliminary testing were conducted. Maximum net power output and maximum cycle efficiency were found to be 4.13 kW and 7.64%, respectively.

# ÖZET

## LABORATUVAR ÖLÇEKLİ ORGANİK RANKİNE ÇEVRİM SİSTEMİNİN TASARIMI, ÜRETİMİ VE TEST EDİLMESİ

Bu çalışma küçük ölçekli organik Rankine çevrim test düzeneğinin tasarımını, uygulamasını ve devreye alınmasını içermektedir. Buradaki amaç, değişik çevrim akışkanlarının ve ekipmanların performanslarını incelemeye olanak sağlayan esnek bir deney düzeneği oluşturmaktır. Bu çevrim düzeneği, operasyon sırasında veri toplamak amacıyla basınç, sıcaklık ve akış sensörleri ile beraber kurulmuştur. Bu veriler, değişik termodinamik modelleri doğrulamakta kullanılmıştır. Uygun çevrim akışkanlarını bulmak amacıyla 13 akışkan çevresel, fiziksel ve güvenlilik karakteristikleri göz önüne alınarak kıyaslanmıştır. Bu kriterleri sağlayan ve isimleri R134a, R141b, R245ca ve R245fa olmak üzere dört akışkan daha detaylı analiz için seçilmiştir. Maksimum çevrim verimi ve maksimum alınan güç performans göstergeleri olarak seçilmiştir. Çevrim verimine etkisi araştırılmak üzere bir adet ısı geri kazanıcı eşanjör sisteme dahil edilmiştir. Termodinamik analizlerin sonucunda, deney düzeneği için çevrim akışkanı olarak R134a seçilmiştir. Detaylı devreye alma prosedürleri hazırlanmış ve ön testler yapılmıştır. Maksimum alınan güç ve maksimum çevrim verimi sırasıyla 4.13 kW ve %7.64 bulunmuştur.

# TABLE OF CONTENTS

ACKNOWLEDGEMENTS . . . iii
ABSTRACT . . . iv
ÖZET . . . v
LIST OF FIGURES . . . ix
LIST OF TABLES . . . xv
LIST OF SYMBOLS . . . xvii
LIST OF ACRONYMS/ABBREVIATIONS . . . xviii
1. INTRODUCTION . . . 1
1.1. Organic Rankine Cycle . . . 4
1.2. Literature Review . . . 8
1.2.1. Geothermal applications . . . 9
1.2.2. Waste heat recovery applications . . . 10
1.2.3. Solar applications . . . 11
1.2.4. Biomass applications . . . 12
1.2.5. Other applications . . . 14
1.2.6. Expander applications . . . 15
2. THERMODYNAMIC ANALYSIS . . . 18
2.1. Investigation of Working Fluids . . . 20
2.2. Cycle Analyses . . . 24
2.2.1. The effect of expander pressure ratio . . . 25
2.2.2. The effect of expander inlet pressure . . . 27
2.2.3. The effect of superheating . . . 33
2.2.4. Selection of state points . . . 39
3. HEAT EXCHANGER DESIGN . . . 43
3.1. Heat Transfer Calculations . . . 44
3.2. Pressure Drop Calculations . . . 49
4. ORC Test Rig . . . 51
4.1. Main Equipment . . . 53
4.1.1. Scroll expander . . . 53

4.1.2. Feed pump . . . 54
4.1.3. Evaporator . . . 56
4.1.4. Condenser . . . 57
4.1.5. Recuperator . . . 60
4.1.6. Expander simulator . . . 62
4.2. Balance of Plant . . . 64
4.2.1. Heater . . . 64
4.2.2. Heat transfer oil pump . . . 65
4.2.3. Expansion Vessel . . . 66
4.2.4. Chiller . . . 67
4.2.5. Dynamometer . . . 68
4.2.6. Liquid collector . . . 69
4.2.7. Fluid recovery exchanger . . . 70
4.3. Sensors and Data Acquisition . . . 70
5. COMMISSIONING AND PRELIMINARY TESTING . . . 76
5.1. Procedures . . . 76
5.2. Cold Run of the System . . . 80
6. CONCLUSION . . . 84
REFERENCES . . . 86
APPENDIX A: SECTION DRAWING OF THE SCROLL EXPANDER . . . 94
APPENDIX B: SECTION DRAWING OF THE SIDE CHANNEL PUMP . . . 95
APPENDIX C: SECTION DRAWING OF THE INTERNAL GEAR PUMP . . . 96
APPENDIX D: SECTION DRAWING OF THE HEAT EXCHANGERS . . . 97
APPENDIX E: DATASHEET OF THE HEATER . . . 98
APPENDIX F: SECTION DRAWING OF THE BOILER VESSEL . . . 99
APPENDIX G: SECTION DRAWING OF THE LIQUID COLLECTOR . . . 101
APPENDIX H: SECTION DRAWING OF THE EXPANSION VESSEL . . . 102
APPENDIX I: SECTION DRAWING OF THE FLUID RECOVERY HEX . . . 103
APPENDIX J: EXPERIMENTAL PROCEDURE . . . 105
J.1. Checking of Safety Valve and Adjusting Pressure Reducing Valve . . . 106
J.2. Vacuuming . . . 106

J.3. Filling . . . . . 106
J.4. Putting Heater and Chiller into Operation . . . . . 107
J.5. Start-up, Testing and Shut-down Operations . . . . . 108
J.6. Actions to Be Taken . . . . . 118

# LIST OF FIGURES

Figure 1.1. Electricity generation by energy source in Turkey according to Republic of Turkey Ministry of Energy and Natural Resources . . . . 2

Figure 1.2. Schematic diagram of the simple ORC. . . . . 5

Figure 1.3. T-s diagram of R134a. . . . . 5

Figure 1.4. Schematic diagram of the recuperator integrated ORC. . . . . 7

Figure 2.1. Flow diagram of the proposed ORC. . . . . 18

Figure 2.2. T-s diagrams of each fluid types. . . . . 20

Figure 2.3. Specific net power output variation for different condensation temperatures depending on the pressure ratio of the expander. . . . . 26

Figure 2.4. Net power output variation depending on the expander inlet pressure. 27

Figure 2.5. T-s diagram for R134a with different pressure states. . . . . 28

Figure 2.6. Heat input rate variation depending on the expander inlet pressure. 29

Figure 2.7. Mass flow rate variation depending on the expander inlet pressure for simple ORC. . . . . 29

Figure 2.8. Mass flow rate variation depending on the expander inlet pressure for regenerative ORC. . . . . 30

Figure 2.9. Cycle efficiency variation depending on the expander inlet pressure for R245fa. . . . . 30

Figure 2.10. Cycle efficiency variation depending on the expander inlet pressure for R245ca. . . . . 31

Figure 2.11. Cycle efficiency variation depending on the expander inlet pressure for R141b. . . . . 31

Figure 2.12. Cycle efficiency variation depending on the expander inlet pressure for R134a. . . . . 32

Figure 2.13. Net power output variation depending on the degree of superheat. 33

Figure 2.14. T-s diagram of R245fa. . . . . 34

Figure 2.15. Heat input rate variation depending on the degree of superheat for simple ORC. . . . . 34

Figure 2.16. Mass flow rate variation depending on the degree of superheat for simple ORC. . . . . 35

Figure 2.17. Mass flow rate variation depending on the degree of superheat for regenerative ORC. . . . . 36

Figure 2.18. Cycle efficiency variation depending on the degree of superheat for R245fa. . . . . 36

Figure 2.19. Cycle efficiency variation depending on the degree of superheat for R245ca. . . . . 37

Figure 2.20. Cycle efficiency variation depending on the degree of superheat for R141b. . . . . 37

Figure 2.21. Cycle efficiency variation depending on the degree of superheat for R134a. . . . . 38

Figure 2.22. T-s diagram of R134a with two different pressure and two different temperature states. . . . . 39

Figure 3.1. Section drawing of a plate type heat exchanger . . . . . 48

Figure 4.1. P&ID of the ORC. . . . . 52

Figure 4.2. Installed scroll type expander on ORC test rig. . . . . 54

Figure 4.3. Installed side channel pump on ORC test rig. . . . . 55

Figure 4.4. T-Q curves of the evaporator. . . . . 56

Figure 4.5. Installed brazed type heat exchanger on ORC test rig. . . . . 58

Figure 4.6. T-Q curves of the condenser. . . . . 58

Figure 4.7. T-Q curves of the recuperator. . . . . 60

Figure 4.8. Installed throttle valve on ORC test rig. . . . . 62

Figure 4.9. T-Q curves of the pre-cooler. . . . . 64

Figure 4.10. Installed heater on ORC test rig. . . . . 65

Figure 4.11. Installed internal gear pump on ORC test rig. . . . . 66

Figure 4.12. Installed expansion vessel on ORC test rig. . . . . 67

Figure 4.13. Installed chiller on ORC test rig. . . . . 68

Figure 4.14. Installed dynamometer on ORC test rig. . . . . 69

Figure 4.15. Installed liquid collector on ORC test rig. . . . . 69

Figure 4.16. Installed fluid recovery exchanger on ORC test rig. . . . . 70

Figure 4.17. Installation specifications of electromagnetic flowmeter for pipe sections with elbows. . . . . 71

Figure 4.18. Installation specifications of vortex flowmeter for straight pipe sections. . . . . 71

Figure 4.19. Installation specifications of vortex flowmeter for pipe sections with elbows. . . . . 72

Figure 4.20. Installed transmitters and flowmeters. . . . . 73

Figure 4.21. Installed M-SENS module on ORC test rig. . . . . 74

Figure 4.22. 3D model of the proposed ORC. . . . . 75

Figure 4.23. Image of the proposed ORC. . . . . 75

Figure 5.1. Feed pump cold run testing. . . . . 82

Figure A.1. Section drawing of the scroll expander. . . . . 94

Figure B.1. Section drawing of the side channel pump. . . . . 95

Figure C.1. Section drawing of the internal gear pump. . . . . 96

Figure D.1. Section drawing of the heat exchangers. . . . . 97

Figure E.1. Datasheet of the heater. . . . . 98

Figure F.1. Section drawing of the boiler vessel. . . . . 99

Figure G.1. Section drawing of the liquid collector. . . . . 101

Figure H.1. Section drawing of the expansion vessel. . . . . 102

Figure I.1. Section drawing of the fluid recovery hex. . . . . 103

Figure J.1. Piping and instrumentation diagram of the proposed ORC with valve and sensor numbers. . . . . 105

Figure J.2. Start-up A operation conditions. . . . . 109

Figure J.3. Start-up B operation conditions. . . . . 110

Figure J.4. Start-up C operation conditions. . . . . 110

Figure J.5. Start-up D operation conditions. . . . . 111

Figure J.6. Start-up E operation conditions. . . . . 111

Figure J.7. Testing A operation conditions. . . . . 112

Figure J.8. Testing B operation conditions. . . . . 112

Figure J.9. Testing C operation conditions. . . . . 113

Figure J.10. Shut-down A operation conditions. . . . . 113

Figure J.11. Shut-down B operation conditions. . . . . 114

Figure J.12. Shut-down C operation conditions. . . . . 114

# LIST OF TABLES

Table 1.1. Experimental results of small-scale organic Rankine cycles from literature. . . . . 16

Table 2.1. Fluid comparison with respect to physical, safety, environmental and numerical data. . . . . 23

Table 2.2. Net power output and cycle efficiency variation with respect to different variables and constants. . . . . 24

Table 2.3. Saturation pressures of different fluids at 30 °C. . . . . 25

Table 2.4. Max. net power output and cycle efficiency conditions for simple ORC. . . . . 40

Table 2.5. Max. net power output and cycle efficiency conditions for regenerative ORC. . . . . 41

Table 2.6. Max. net power output and maximum cycle efficiency values for each working fluid. . . . . 42

Table 3.1. Heat transfer and pressure drop equation constants . . . . . 50

Table 4.1. Specifications of the scroll type expander. . . . . 54

Table 4.2. Specifications of the feed pump. . . . . 55

Table 4.3. Evaporator performance and geometry results. . . . . 57

Table 4.4. Condenser performance and geometry results. . . . . 59

Table 4.5. Recuperator performance and geometry results. . . . . 61

Table 4.6. Pre-cooler performance and geometry results. . . . . 63

Table 4.7. Specifications of the internal gear pump. . . . . 66

Table 4.8. Specifications of the chiller. . . . . 68

Table 4.9. Specifications of the sensors. . . . . 72

Table 4.10. Specifications of the data acquisition modules. . . . . 74

Table 5.1. Pre-commissioning procedure of the proposed ORC test rig. . . . . 77

Table 5.2. Commissioning procedure of the working fluid circuit. . . . . 78

Table 5.3. Commissioning procedure of the heating circuit. . . . . 79

Table 5.4. Commissioning procedure of the cooling circuit. . . . . 79

Table 5.5. Error analysis parameters. . . . . 80

Table 5.6. Cold run testing with 100% pump motor frequency. . . . . 82

Table 5.7. Cold run testing with 90% pump motor frequency. . . . . 82

Table J.1. Start-up, testing and shut-down conditions . . . . . 109

# LIST OF SYMBOLS

| | |
|---|---|
| a,b | PR parameters |
| b | Mean Channel Spacing, m |
| $b$ | (subscript) boiling point |
| $c$ | (subscript) condensation / critical point |
| $c_p$ | Specific Heat at Constant Pressure, kJ/(kg· K) |
| $e$ | (subscript) evaporation |
| $G_c$ | Mass Velocity Through a Channel, kg/(m$^2$· s) |
| h | Specific Enthalpy, kJ/(kg· K) |
| k | Thermal Conductivity, W/(m· K) |
| m | Intermediate Function in PR |
| p | Plate Pitch, m |
| $pc$ | (subscript) phase change |
| R | Fouling Factor, (m$^2$· K)/W |
| $rg$ | (subscript) regenerative cycle |
| $s$ | (subscript) isentropic / simple |
| U | Overall Heat Transfer Coefficient, W/(m· K) |
| $w$ | (subscript) wall |
| | |
| $\alpha$ | Heat Transfer Coefficient, W/(m· K) |
| $\beta$ | Chevron Angle, degree |
| $\eta$ | Efficiency |
| $\mu$ | Dynamic Viscosity, Pa· s |
| $\nu$ | Molar Volume, cm$^3$/mol |
| $\omega$ | Acentric Factor |
| $\phi$ | Surface Enlargement Factor |
| $\rho$ | Density, kg/m$^3$ |
| $\xi$ | Inverse of the Slope of the Saturation Vapor Curve |

# LIST OF ACRONYMS/ABBREVIATIONS

| | |
|---|---|
| 2D | Two Dimensional |
| 3D | Three Dimensional |
| BURET | Boğaziçi University Renewable Energy Technologies |
| CCHP | Combined Cooling Heating and Power |
| CHP | Combined Heating and Power |
| CW | Cooling Water |
| DAQ | Data Acquisition |
| EOS | Equation of State |
| GWP | Global Warming Potential |
| HEX | Heat Exchanger |
| HTO | Heat Transfer Oil |
| ODP | Ozone Depletion Potential |
| ORC | Organic Rankine Cycle |
| OTEC | Ocean Thermal Energy Conversion |
| P&ID | Piping and Instrumentation Diagram |
| PR | Peng-Robinson |
| RC | Rankine Cycle / Recuperator |
| RG | Regenerative |
| UCTEA | Union of Chambers of Turkish Engineers and Architects |
| WF | Working Fluid |
| WHR | Waste Heat Recovery |

# 1. INTRODUCTION

Global primary energy demand could increase by 50% by the middle of the century according to World Energy Council 2013 Survey [1]. This huge increase in energy demand comes mainly from the population increase and growing rate of usage of electricity which is directly proportional to advancing technology. Therefore, this increasing demand for energy pushes countries to take actions to maintain the welfare of its people.

Usage of fossil fuels like natural gas, coal, and oil correspond to approximately 70% of the total electricity production and they are widely used to meet a significant part of power demand by developing countries and/or governments that have big fossil reserves [2]. The usage of fossil fuels that keeps increasing progressively brings some drawbacks such as increasing carbon dioxide emission which leads to air pollution and global warming. Other than the disadvantages above, fossil fuels are not sustainable and their prices fluctuate substantially. In order to produce sustainable and emission-free energy, renewable energy sources would be the solution. However, fuel-switching does not happen in a snap. Renewable energy must be put into the consideration in the case of extinction of fossil fuels and devastation caused by global warming.

Renewable energy sources are basically biomass, solar, wind, waste heat and geothermal. Their total contribution to the Turkey's national power generation is only 6.3% but have risen exponentially for the past 10 years. Turkey's total power demand has been increasing rapidly and it reached 264 TWh in 2015. According to the Ministry of Energy and Natural Resources [3], electricity demand of Turkey is expected to reach at 416 TWh in 2023. Considering Turkey's fossil fuel potential, renewable energy sources are expected to increase their share on total power generation.

The pie chart showing total net electricity generated by each type of energy source in Turkey in 2015 is illustrated in Figure 1.1.

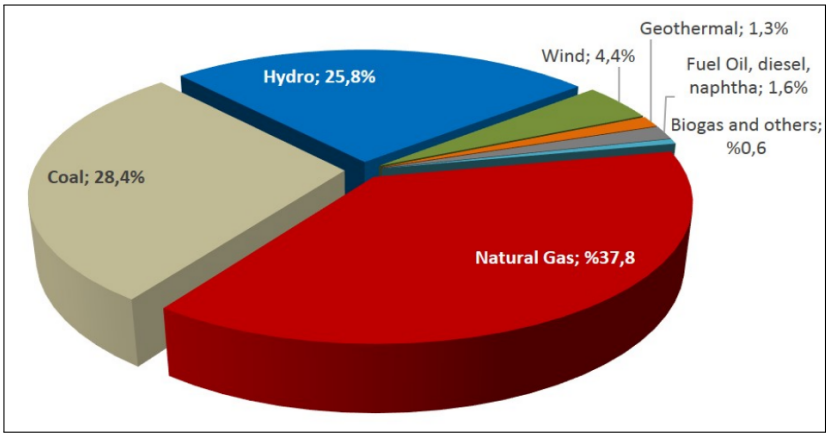


Figure 1.1. Electricity generation by energy source in Turkey according to Republic of Turkey Ministry of Energy and Natural Resources [3].

Solar, biomass and waste heat are considered as other renewable sources at the pie chart. Geothermal has a share of 1.3% while other renewables have only 0.6%.

Waste Heat Recovery (WHR) is mostly used in the industrial applications. The exhaust heat in the steel, cement, petroleum and glass industries are decently high and for that reason, there is a big interest in waste heat recovery systems [4]. Temperatures below 370 °C is not economically feasible and it usually becomes an exhaust. Since WHR leads to significant fuel savings, emissions are often reduced. Therefore, WHR enables not only electricity generation but also reduction of carbon dioxide emissions [5].

Solar ORCs are being established gradually in kW scale in rural areas to generate remote electricity and in MW scale in large areas of land to generate high voltage grid power. Concentrated solar power with parabolic troughs or solar towers are used for heating the heat transfer fluid. The most difficult problem of solar ORCs is the unsteady heat source since the heat input fluctuates during the day and dies out after the sunset. This means there is no constant electricity at daytime and no electricity at nighttime. However, people need constant and sustainable energy for improving their quality of life. That is why thermal storage is the most important consideration of a solar power generation system.

Biomass would be a promising choice to play a role in the replacement of fossil fuels and in the reduction of greenhouse gas emissions. Generally, ORC integrated biomass-fired power plants are located near to biomass production sites because of the huge available heat, such as furniture manufacturing industries, district heating systems, biomass drying plants and pellet producers [6, 7]. CHP (combined heat and power) power plants and CCHP (trigeneration or combined cooling, heat, and power) power plants are commercially used in biomass and waste heat applications in order to utilize available heat as much as possible.

ORC integrated systems are able to use with geothermal sources as well. Considering Turkey's geothermal potential, it would be a feasible solution for decreasing dependency on foreign energy sources. 227 geothermal fields have been discovered in Turkey since 1960. Geothermal heating applications have reached 2886 MWt and geothermal electricity production has reached 400 MWe by a total of 17 geothermal power plants [8].

These renewable sources such as solar, geothermal, waste heat and biomass, which have a temperature range of 60 and 200 °C, can be considered as low-grade heat sources [9]. Organic Rankine cycles allow utilization of heat for power generation from heat sources, having a temperature as low as 65 °C [10].

Organic Rankine cycle (ORC) represents a powerful solution for small to medium scale power generation applications with utilizing low-grade and renewable heat sources like biomass, waste heat, solar or geothermal. Furthermore, it is used to increase the plant efficiency in the industry and to desalinate of seawater. Detailed technical information about organic Rankine cycle is indicated in the next section.

## 1.1. Organic Rankine Cycle

The ORC process is same of the Rankine cycle (RC) process except the working fluid. Rankine cycle uses water and conventional steam in the integrated process while organic Rankine cycle uses organic fluids such as ammonia, carbon dioxide, fluorocarbons, and hydrocarbons. These working fluids have high molecular weight and relatively low boiling point than water make them advantageous in low-grade heat conversion.

The specific advantages of ORC technology are simplicity, robustness, availability of its components, long service life, fast start-up and stop procedures, low maintenance costs, and good partial load behavior. Furthermore, adopting a suitable dry organic fluid with lower boiling point allows low-grade heat conversion into power and ensures no erosion problem for the turbine blades because of the absence of liquid droplets [11, 12].

The usual lifetime of ORC systems is greater than twenty years [13]. Utilization of higher density fluids results in smaller plant size compared to the conventional Rankine cycle. Adopting dry working fluids leads to single vapor phase at the turbine outlet and eliminates the possible problem which is the possession of liquid droplets and reduces the capital and maintenance costs [14].

A simple ORC consists of a pump, expander, evaporator and condenser units. The process starts with the heat transfer fluid passing through the evaporator and changing the working fluids liquid phase into gaseous form. Pressurized and vaporized working fluid goes into the expander where it expands and loses its enthalpy. This enthalpy difference corresponds to the obtainable work per mass. Then, the working fluid leaves the expander and passes through the condenser where it cools down and change its gaseous phase into liquid. Finally, the liquid fluid flows into the inlet of the pump and forms a closed loop system. The schematic diagram of the simple organic Rankine cycle and temperature versus entropy (T-s) diagram of the cycle are shown in Figures 1.2 and 1.3.

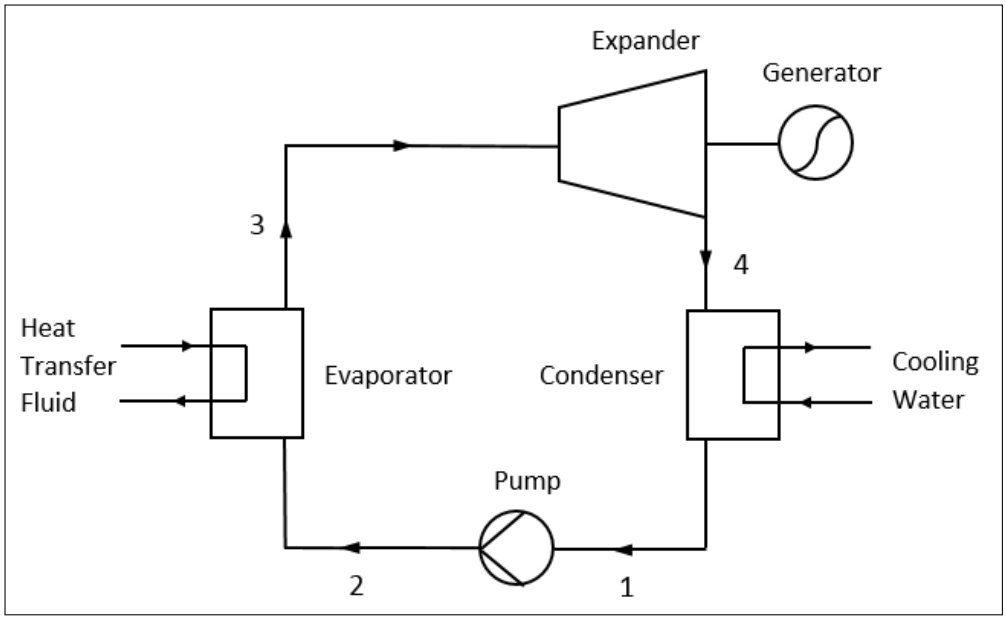


Figure 1.2. Schematic diagram of the simple ORC.

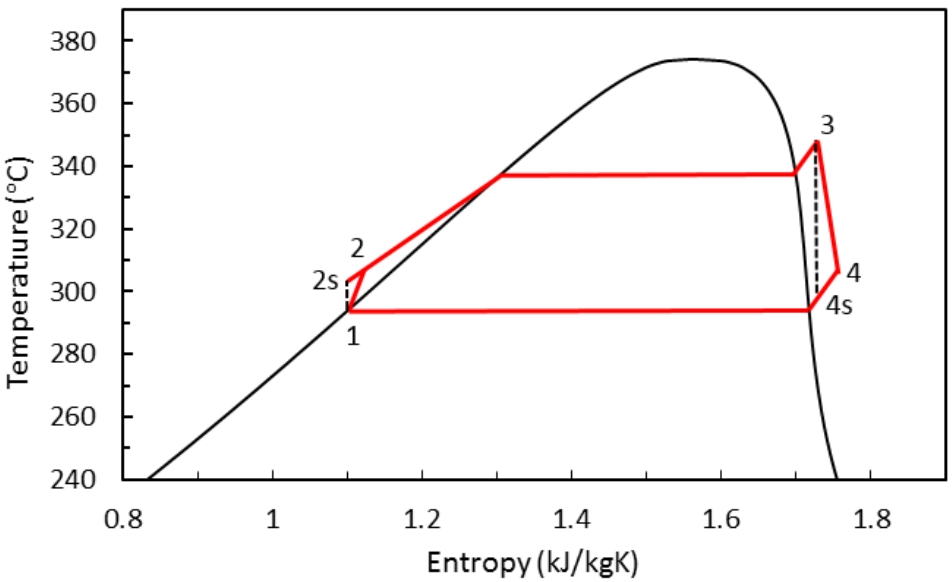


Figure 1.3. T-s diagram of R134a.

Processes of the simple cycle are indicated below:

*Process* 1 *to* 2: It can be considered as a non-isentropic compression process where the working fluid is compressed at the pump. The work rate done by the pump and pump isentropic efficiency are given as:

$$\dot{W}_p = \dot{m}(h_{2s} - h_1)/\eta_p \tag{1.1}$$

$$\eta_p = \frac{h_{2s} - h_1}{h_2 - h_1} \tag{1.2}$$

where $\dot{m}$ and $h$ are the mass flow rate and enthalpy of the working fluid and $\eta_p$ is the pump isentropic efficiency.

*Process* 2 *to* 3: It can be considered as an isobaric heat addition process where the evaporation occurs in the evaporator. The rate of heat addition via heat transfer fluid is:

$$\dot{Q}_{ev} = \dot{m}(h_3 - h_2) \tag{1.3}$$

*Process* 3 *to* 4: It can be considered as an adiabatic expansion process at the expander. The obtained power from the expander and expander isentropic efficiency are given as:

$$\dot{W}_{ex} = \dot{m}(h_3 - h_{4s})\eta_{ex} \tag{1.4}$$

$$\eta_{ex} = \frac{h_3 - h_4}{h_3 - h_{4s}} \tag{1.5}$$

where $\eta_{ex}$ is the expander isentropic efficiency.

*Process* 4 *to* 1: It can be considered as an isobaric heat rejection process where the condensation occurs at the condenser. The rate of heat rejection via cooling water is:

$$\dot{Q}_c = \dot{m}(h_4 - h_1) \tag{1.6}$$

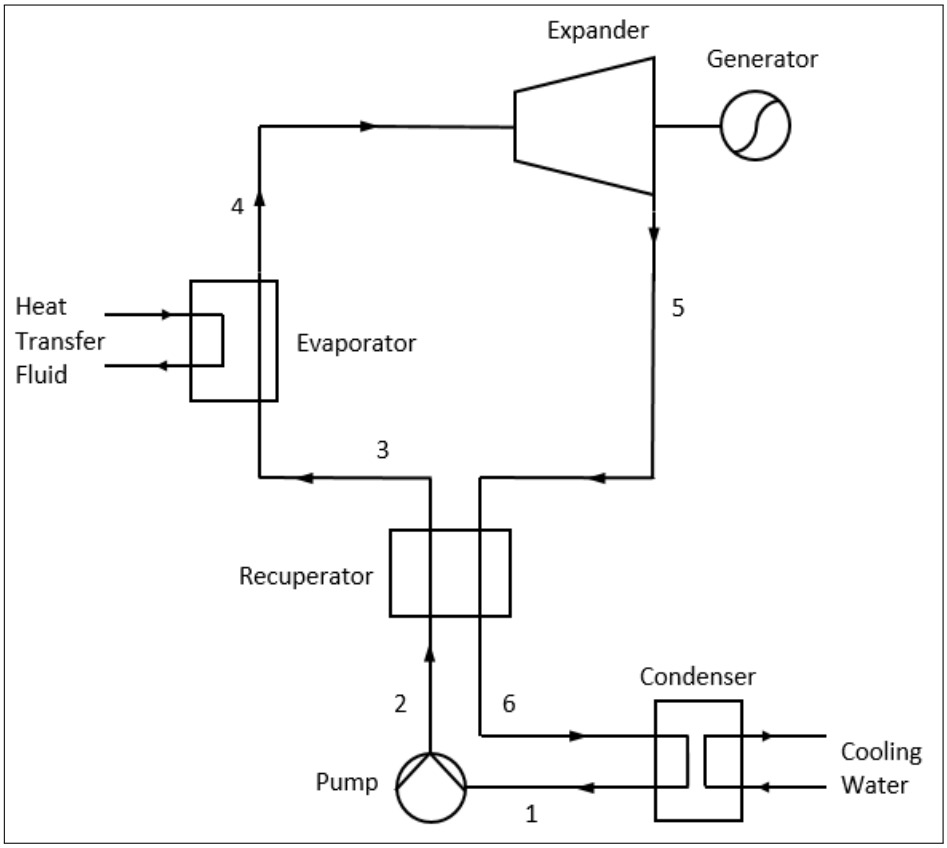


Figure 1.4. Schematic diagram of the recuperator integrated ORC.

Cycle thermal efficiency is defined as the ratio of the net power output to the rate of heat input and it is indicated in Equation 1.7.

$$\eta_{th} = \frac{\dot{W}_{ex} - \dot{W}_p}{\dot{Q}_{ev}} \tag{1.7}$$

Regenerative ORC can be used instead of basic ORC in order to increase cycle thermal efficiency. Here, expanded vapor at the expander outlet goes into an internal heat exchanger called recuperator where the vapor working fluid loses its enthalpy. At the same time, liquid working fluid at the pump outlet passes into recuperator to gain heat and reduce the evaporators duty. The schematic of the recuperator integrated organic Rankine cycle is shown in Figure 1.4.

## 1.2. Literature Review

Several authors tried various working fluids to obtain maximum cycle efficiency for their ORC system. R123, R134a, R245fa, R245ca, isobutane, isopentane, Solkatherm SES36 are only a couple of these fluids. G. Pei *et al.* [15] demonstrated a small scale ORC with adopting R123 while Farrokhi *et al.* [16] conducted an experimental study for residential buildings with adopting isopentane and S.H. Kang [17] is adopted R245fa as the working fluid. Experimental results showed that maximum cycle efficiency was found to be 6.8%, 1.66%, and 5.22%, respectively.

Cycle efficiency highly depends on the condenser exit temperature which is affected and limited by ambient temperature. When all other variables are constant, decreasing condenser exit temperature gives better cycle efficiency values. As a result, locations which have lower ambient temperature values are preferable for ORC installations [5, 18].

Yamamoto *et al.* [9] designed an ORC system with R123 and water as the working fluids. They used an electric heater to simulate the heat source during the experiments. Maximum net power and cycle efficiency are found to be 150 W and 1.25%. Moreover, they suggested that low latent heat and high density are preferable to increase mass flow rate and if such a fluid is to be used, the saturated vapor at the turbine inlet would give the best results.

However, H. Chen *et al.* [19] conducted a theoretical analysis and claimed that high latent heat and high density give better results because the area formed by the main points of the closed loop cycle would increase if the horizontal evaporation line in T-s diagram elongates. Since the area is proportional that of the obtainable work, larger power outputs can be obtained.

J.-C. Chang *et al.* [20] claimed that cycle and expander efficiency increase with increasing of superheating.

However, many researchers pointed out an opposite statement which is superheating has a deteriorating effect on cycle efficiency and the saturation point of the working fluid at the turbine inlet would give the best efficiency results [5, 19, 21–24].

A brief review of electricity generation techniques from low-temperature heat sources is presented by N. Galanis *et al.* [25]. They pointed out that net work does not depend on the effectiveness of the recuperator; however, it highly depends on the cycle efficiency which increases as the recuperator effectiveness improves. Also, maximum cycle efficiency and maximum power output do not correspond to the same pressure and temperature values at the turbine inlet.

### 1.2.1. Geothermal applications

Geothermal heat sources vary in temperature between 50 - 350 °C. The reservoir could be dry steam, steam and water mixture or only liquid water [26]. Generally, there are three types of geothermal water utilization processes namely dry steam systems, flash steam systems and binary cycles. Dry and flash steam systems use geothermal reservoir directly in the main cycle while in binary cycles, hot reservoir heats a secondary fluid which is vaporized and drives the turbine. The difference between dry and flash steam systems is that dry ones use steam directly in the main cycle; however, flash steam cycles use the effect of pressure relief to convert high-pressure hot water into steam. Cycle efficiencies are around 5-9% for low-temperature geothermal sources utilization and in case of medium temperatures, efficiencies are around 10-15% [26].

Meyer *et al.* [27] introduced a 1 kW ORC system which utilizes geothermal sources. HFC-M1, which is a mix of 50% R245fa and 50% R365mfc, was selected to be used as the working fluid mostly for its ease of availability in New Zeland. An automotive turbocharger as a radial turbine and a scroll expander will be used in the future experiments for the expansion device. Theoretical cycle efficiency is 5.7% with a pressure ratio of 3.5 and max. pressure of 13.8 bar.

M. Li *et al.* [28] constructed a low-temperature regenerative ORC test bed with a power output of 6 kW. Geothermal source temperature is fixed at 130 °C. A single stage axial flow turbine was used in this experiments and a regenerative cycle efficiency of 7.98% was found, which is higher than that of the simple cycle by 1.83%.

Nikolskiy *et al.* [29] presented a binary ORC power plant of 2.5 MWe power output was installed in Kamchatka, Russia. The heat source is waste geothermal brine with a temperature of 120 °C.

M. Astolfi *et al.* [24] modeled a geothermal ORC considering the heat source temperature varying from 120 to 180 °C. They defined two variables namely turbine inlet pressure and the difference between turbine inlet temperature and the inlet temperature of the geothermal brine for optimization. The results showed that organic fluids with critical temperatures slightly lower than the geothermal brine gave 6 % higher efficiency values than fluids with higher critical temperatures for supercritical cycles.

R.S. El-Emam and I. Dincer [30] analyzed a binary ORC considering geothermal water source and brine reinjection temperature difference was around 38 °C. For a 5 MWe power output, plant efficiency was found to be 16.37% when adopting isobutane as the working fluid.

### 1.2.2. Waste heat recovery applications

Waste Heat Recovery is one of the widely used heat sources in the literature of organic Rankine cycle applications. There is a big interest of waste heat recovery especially on the industrial side since exhaust heat in the cement, steel, petroleum and glass industries are very high.

N. Zhou *et al.* [31] constructed an experimental test bed and used an LPG (liquefied petroleum gas) stove to simulate industrial waste heat. Results showed that increasing evaporating pressure has a positive effect on both cycle efficiency and power output.

Maximum cycle efficiency and max. net power output are obtained 8.5% and 645 W, respectively.

Wei *et al.* [18] performed an analysis and optimization of an ORC system using R245fa as the working fluid for a waste heat recovery application. They reported that in order to keep system efficiency and net work at their peaks, the utilization of exhaust heat should be maximized and the degree of subcooling in the condenser should be in the range of 0.5-0.6 K. Y.

Dai *et al.* [22] performed a parametric optimization and comparative study with 10 different fluids for utilizing waste heat sources. They found that under their waste heat configurations, using a recuperator would not improve the cycle efficiency. Additionally, it is shown that there is an optimum operating pressure at the expander inlet where the net power output reaches its peak and then it reduces dramatically. Azeotropic mixtures are defined as the mixtures of liquids which boil at constant temperature and retain same composition in vapor as well as in liquid phase.

S. Quoilin *et al.* [12] investigated R245fa, R123, n-butane, n-pentane, R1234yf and Solkatherm SES36, which is an azeotropic mixture, working fluids with respect to economic optimization parameters for recovering waste heat. Results indicated that maximum work output does not correspond to that of minimum specific investment cost.

### 1.2.3. Solar applications

Concentrating Solar Power (CSP) technologies use mirrors to focus the energy of sunlight and convert it into heat. There are two types of CSP systems namely parabolic trough collector and solar tower. Parabolic trough systems use U-shaped reflectors to focus the energy towards the focal point where receiver tubes are positioned. Solar tower systems use a central receiver system, which allows for higher operating temperatures. Flat mirrors focus solar energy towards a solar tower. The focused energy is used to heat a transfer fluid likewise parabolic trough.

G. Cohen *et al.* [32] presented a parabolic trough solar ORC power plant in Arizona, USA. This 1 MWe solar ORC, for a solar field size of 10340 $m^2$, showed solar to electric efficiency of 7.5% with using n-pentane as the working fluid.

S. Quoilin *et al.* [33] conducted a performance analysis and design optimization for a low-cost solar ORC installed in Lesotho for rural power generation. Different working fluids such as R134a, R245fa, Solkatherm SES36, and n-pentane are studied and overall efficiencies are found in a range of 3.6 to 7.9%, respectively.

Tchanche *et al.* [34] examined twenty organic fluids with respect to first and second law efficiencies, mass and volume flow rates, pressure ratio of the turbine, ODP, GDP, flammability and toxicity for a low-temperature solar ORC. Second law efficiency, is also known as exergy efficiency, deals with the entropy which is used to define unavailable energy in a system. Their examination showed that R134a appeared to have the most favorable characteristics with a heat source temperature below 90 °C. Moreover, they suggested that ambient temperature and condenser temperature difference should be taken in the range of 5-15 °C.

Twomey *et al.* [35] carried out a dynamic performance analysis of a small-scale solar CHP with integrated an ORC system. A scroll expander is modeled and simulation results showed that the maximum cycle and expander efficiencies are 3.47% and 59%, respectively.

Saitoh *et al.* [36] constructed a solar ORC with a scroll expander and tested for cogeneration application. Maximum cycle, total cogeneration, and expander efficiencies are obtained 7%, 42%, and 63%, respectively.

### 1.2.4. Biomass applications

Biomass applications are generally used in CHP and CCHP power plants rather than only power generation systems. By this way, district heating is utilized with higher efficiencies.

If the net electrical power output of a CHP plant is less than 100 kW, it is considered as small scale; the power output is less than 15 kW than it is considered a micro scale CHP plant [37].

I. Obernberger *et al.* [13] introduced a decentralized biomass-fired CHP plant with an integrated ORC system located in Lienz, Austria. It had a nominal electricity capacity of 1 MWe and a nominal thermal capacity of 4.4 MWth with an electrical efficiency of 15% and total efficiency (heat and electricity) of 80%. Again, the same author presented 400 kWe biomass-fired power plant in Admont, Austria. At nominal load, net electric efficiency 17.7% was obtained with silicon oil used as the working fluid [38].

C. Perilhon *et al.* [39] compared two different capacities of biomass-fired CHP plants: a 2 MW and a 10MW. Former one had an integrated ORC which its electrical efficiency of 16.2% and cogeneration efficiency of 80% while latter had a steam cycle with an electrical efficiency of 19% and cogeneration efficiency of 51%.

Y. Huang *et al.* [40] conducted an economic analysis of trigeneration system integrated with an ORC and using biomass as the heat source. The waste heat from ORC used for space heating with supplying hot water and for cooling with driving an absorption chiller. Simulation results showed that 11.1% for maximum electrical efficiency, 85% for maximum cogeneration efficiency and 71.7% for maximum trigeneration efficiency.

Since the heat input is constant for any cases, cogeneration efficiency is higher than that of trigeneration efficiency due to higher losses in cooling process when comparing with heating process. In order to construct an economically feasible biomass ORC, more than 5 MWe power output is needed [41].

A. Algieri and P. Morrone [11] analyzed the energetic performance of a biomass-fired ORC in Italy with three working fluids namely toluene, decane, and cyclohexane with three operating conditions: saturated, superheated, and transcritical cycle.

For saturated cycle conditions, toluene gave the best cycle efficiency which was 14.6%; for superheated cycle conditions, the largest cycle efficiency 20% was found when cyclohexane was used; and for transcritical conditions are applied, maximum cycle efficiency 21.7% was found when decane was used as the working fluid.

### 1.2.5. Other applications

Another ORC integrated application is the reverse osmosis desalination. The access to water is a basic need and it can be a challenge especially in rural areas. This technology can be the most energy-efficient technology for seawater within the small to medium power output range [42].

D. Manolakos *et al.* [43] presented an experimental evaluation of a low-temperature ORC for reverse osmosis desalination system. They simulated solar collectors with an electric heater of 100 kW and considered a fix pressure difference of 13 bar through the expansion process. Obtained results with adopting R134a as the working fluid are: 2 kW maximum power output and 4% maximum overall system efficiency when using an expander which had an overall efficiency of 65%.

Tchanche *et al.* [44] presented a relatively new approach called OTEC (Ocean Thermal Energy Conversion). An OTEC system utilizes very low-grade energy and that leads a very lower efficiency output of about 3–5%. Therefore, instead of generating electricity, it could be used in other areas such as fresh water production, air conditioning and refrigeration, cold water agriculture, etc.

There are several worldwide ORC manufacturers namely ORMAT [45], which is the most representative one in U.S, Turboden [46] and Exergy [47] in Europe, especially active in biomass and geothermal heat sources utilization. However, plants generating lower power outputs are still at the prototype stage mainly due to the lack of suitable expander or turbine [41].

### 1.2.6. Expander applications

Expander is the most critical part of the ORC system. It directly affects the efficiency and net power output of the plant. Expanders can be categorized into two main groups that are turbo-machines (also called velocity type expanders) and positive displacement types. Former one consists of axial turbines and radial turbines while the latter consists of scroll expanders, screw expanders, rotary vane expanders and piston expanders [48]. Axial and radial turbines are usually used in the large capacity systems. Within the positive displacement types, screw and reciprocating piston expanders can also be adopted for relatively high power output, which generally denotes medium-sized systems. The power output of scroll and rotary vane expanders are relatively low; therefore, they are adopted for small or micro ORC systems [49].

Usually in small scale ORC applications, scroll expanders are preferred. Since the scroll compressor types had been used in air-conditioning and refrigeration industry, it could be considered as a proven technology. A scroll type expander is a good candidate for the ORC applications, because of its reliability and reduced number of moving parts. Scroll type expanders have higher pressure ratios, lower flow rates, lower rotational speeds and proportionally fewer windage losses than radial or axial turbines. These machines can tolerate two-phase conditions, which can be crucial because of the fact that the expander outlet may have liquid drops and can harm the machinery [50, 51]. Moreover, the usage of scroll expanders is very feasible for small scale ORCs since turbines with low power outputs have relatively higher gap losses. On the other hand, for larger scale applications, radial and axial turbines are preferable since the gap losses are reduced by using higher mass flow rates [52].

Internal leakages, mechanical losses, and the supply pressure drop are the main losses deteriorating the expanders performance [50]. Various actions could be taken to increase the expander efficiency such as improved lubrication and better sealing. Also, there exists a rotational speed that maximizes the expander effectiveness. When the rotational speed exceeds a specific point; friction losses, internal leakages, and the supply pressure drop effects are more dominant on expander efficiency [53].

J.-C. Chang *et al.* [20] investigated an experimental study with using hot water as a dummy waste heat source and adopting R245fa as the working fluid. The expander used in this research was modified from an oil-free scroll type air compressor with a volume ratio of 4.05. Obtained maximum power output, expander efficiency and cycle efficiency was found 2.3 kW, 73%, and 9.43%, respectively.

K. Rahbar *et al.* [14] presented a modeling and optimization of an ORC where dynamic efficiency approach was used for the radial inflow turbine instead of a constant turbine efficiency, which is used for a wide range of ORC models. Six organic fluids were compared and the results showed that maximum turbine efficiency was obtained for isobutane which was 76.36%, while maximum cycle efficiency was obtained for n-pentane which was 11.55%. Table 1.1 shows the experimental results of small-scale ORCs from literature.

Table 1.1. Experimental results of small-scale organic Rankine cycles from literature.

| Authors | Heat source | Working fluid | Expander type | Performance indicator | $\dot{W}_{\text{net}}$ | $\eta_{\text{cycle}}$ |
|---|---|---|---|---|---|---|
| Yamamoto *et al.* [9] | Electric heater | R123 | Radial turbine | Net power and cycle thermal efficiency | 150 W | 1.25% |
| Chang *et al.* [20] | Electric heater | R245fa | Scroll expander | Net power and cycle thermal efficiency | 2.3 kW | 9.43% |
| Peris *et al.* [4] | Ceramic furnace | R245fa | Volumetric expander | Net power and cycle thermal efficiency | 18.51 kW | 10.94% |
| Zhou *et al.* [31] | LPG stove | R123 | Scroll expander | Net power, cycle thermal efficiency, and exergetic efficiency | 645 W | 8.5% |
| Li *et al.* [28] | Electric heater | R123 | Axial turbine | Net power and cycle thermal efficiency | 6 kW | 7.98% |
| Manolakos *et al.* [43] | Electric heater | R134a | Scroll expander | Net power and cycle thermal efficiency | 2.05 kW | 4% |
| Lemort *et al.* [50] | Boiler | R123 | Scroll expander | Net power | 1.82 kW | No information |
| Quoilin *et al.* [53] | Boiler | R123 | Scroll expander | Cycle thermal efficiency | No information | 7.4% |
| Pei *et al.* [15] | No information | R123 | Radial turbine | Cycle thermal efficiency | 1 kW | 6.8% |
| S..H. Kang [17] | Gas-fired boiler | R245fa | Radial turbine | Net power and cycle thermal efficiency | 32.7 kW | 5.22% |
| Farrokki *et al.* [16] | Gas-fired boiler | Isopentane | Vane expander | Net power and cycle thermal efficiency | 77 W | 1.66% |
| Nguyen *et al.* [54] | Boiler | N-pentane | Radial turbine | Capital cost | 1.44 kW | 4.3% |
| Torique *et al.* [55] | Electric heater | R134a | Scroll expander | Net power, cycle thermal efficiency, and exergetic efficiency | 920 W | 8.5% |

Although small scale ORC systems have significant potential for power generation, desalination, cogeneration, and trigeneration applications; the utilization of renewable sources with integrated ORC units have not become widespread at the present time. However; uncertainty in the availability of fossil fuel reserves, government incentives for the utilization of renewable sources to create sustainable energy and more strict carbon dioxide emission regulations will make ORC systems more popular. Waste heat recovery systems will become more interesting especially in steel, cement, petroleum and glass industries where the exhaust temperatures are relatively high. Similarly, biomass-fired ORC systems will draw the attention of industries like furniture manufacturers, pellet producers, district heating suppliers, biomass drying plant owners. Solar ORCs, on the other hand, can be one of the most feasible implementations in rural areas to generate remote electricity in small to medium scale as well as generating high voltage grid power if enough large areas and solar collectors can be provided. Geothermal ORCs can be implemented if only geothermal sources exist as one can imagine and in this case, Turkey has a big potential to establish geothermal power generation systems. Finally, there are other applications such as water desalination and ocean thermal energy conversion systems which are still at the development stage.

The motivation of this study is to establish a fully-instrumented laboratory scale organic Rankine cycle system that enables to test various working fluids and to test different expanders with installed expander simulator unit. In order to achieve the aim, thermodynamic analysis is conducted, suitable equipment is selected or designed, a test rig is build, a complete data acquisition system is installed, and preliminary testing is conducted. The most suitable state points of the cycle are investigated as they were argued in the previous literature and results are discussed.

In Chapter 2, thermodynamic analysis is conducted. Optimum state points are identified in terms of simple and regenerative ORC. Theoretical cycle efficiency and net power output values are indicated. In Chapter 3, ORC test rig is presented. Technical data of selected and/or designed equipment is indicated. Piping and instrumentation diagram and 3D model of ORC test rig are created. Finally, in Chapter 4, commissioning procedures are prepared and preliminary testing is conducted.

# 2. THERMODYNAMIC ANALYSIS

Organic Rankine cycle in BURET (Boğaziçi University Renewable Energy Technologies Laboratory) differs from the simple cycle with two specific equipment. Former one is the recuperator which is surrounded with ball valves. The recuperator enables testing the cycle with both simple and regenerative conditions. Latter one is the expander simulator which consists of two throttle valves and an additional heat exchanger called pre-cooler. The expander simulator enables commissioning process without using the expander, hence protect the expander from potential damage due to liquid drops.

Thermodynamic analysis of the ORC was conducted by using Aspen Plus by AspenTech software to determine pressure and temperatures of each state, mass flow rate of the fluids, exchanger duties, net power output and cycle efficiency values. REFPROP from National Institute of Standards and Technology is used to determine fluids thermodynamic properties [56]. Pipe lengths and angles are given for each pipeline to check the pressure drops. Flow diagram of the proposed ORC is given in Figure 2.1. Red lines show heat transfer fluid circuit while blue and black lines indicate cooling water and working fluid circuit, respectively.

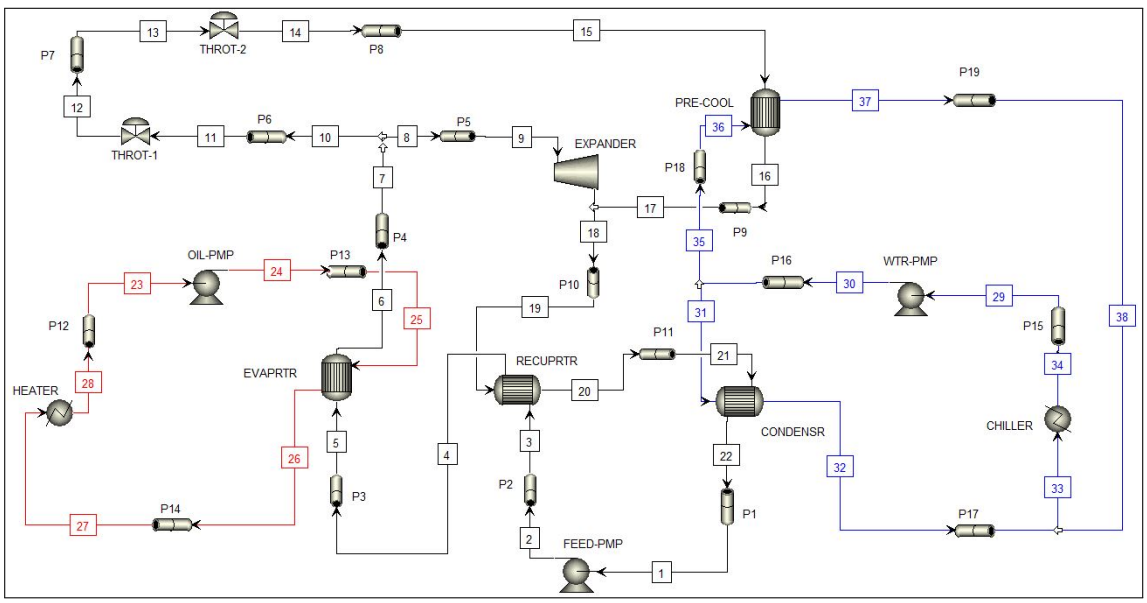


Figure 2.1. Flow diagram of the proposed ORC.

Peng-Robinson Equation of State (PR EOS) is chosen as property calculation method to specify each state of the closed loop cycle. The reason for that is PR approach gives better results near to the critical region for ideal gas [57]. The PR EOS [58] can be written as

$$P = \frac{RT}{\nu - b} - \frac{a(T)}{\nu(\nu + b) + b(\nu - b)} \tag{2.1}$$

where $P$ is pressure, $R$ is the universal gas constant, $T$ is temperature and $\nu$ is molar volume. The PR EOS parameters a and b can be expressed as

$$b = 0.07780\frac{RT_c}{P_c} \tag{2.2}$$

$$a(T) = a_c \left[1 + m\left(1 - \sqrt{\frac{T}{T_c}}\right)\right]^2 \tag{2.3}$$

where $T_c$ is critical temperature and $P_c$ is critical pressure. PR parameter at the critical temperature, $a_c$ and intermediate function in PR, $m$ which is defined by the acentric factor, $\omega$ are also indicated below.

$$a_c = 0.45724\frac{R^2T_c^2}{P_c} \tag{2.4}$$

$$m = 0.37464 + 1.54226\omega - 0.26992\omega^2 \tag{2.5}$$

Thus far the flow diagram is created and the EOS method is determined. The next step is to find the most suitable working fluid for the proposed ORC system. Various fluids are selected and analyzed with respect to numerous selection criteria which is explained in the following section.

## 2.1. Investigation of Working Fluids

Working fluids play a vital role in organic Rankine cycle applications. As it mentioned above, the only difference between conventional Rankine cycle and organic Rankine cycle is that ORC adopts organic fluids instead of water and steam which are used in the RC systems. There are three types of fluids with respect to the slope of the saturation vapor curve on the temperature-entropy diagram such as dry, wet and isentropic. The inverse of the slope of the saturation vapor curve is commonly used to express the fluid type and denoted by the symbol $\xi$.

$$\xi = \frac{ds}{dT} \tag{2.6}$$

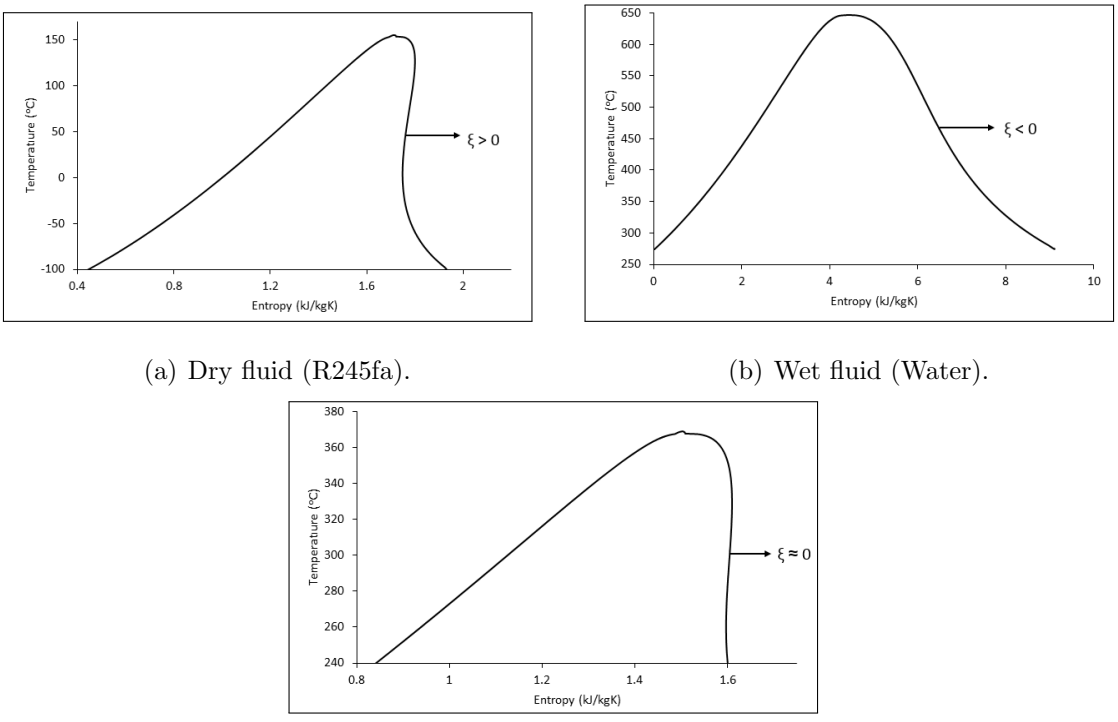


(a) Dry fluid (R245fa).

(b) Wet fluid (Water).

(c) Isentropic fluid (R1234yf).

Figure 2.2. T-s diagrams of each fluid types.

From the equation 2.6, if the value of $\xi > 0$, it is a dry fluid; if $\xi < 0$ : wet fluid and $\xi \approx 0$ : isentropic fluid. Figure 2.2 shows the T-s curves of each fluid types.

These three types of fluids have different characteristics which have a substantial effect on the working fluid selection. Dry and isentropic fluids are usually preferred over wet fluids in ORC setups. The reason for that is the expansion process ends in the vapor region, hence the superheating is not required for these types of fluids. However, wet fluids with a small need of superheat are also used in ORC applications. Required qualifications of a working fluid for an organic Rankine cycle are [44, 59–61]:

- High enthalpy drop during the expansion
- Easy to handle at ambient temperature
- Large heat conductivity
- Large vaporization latent heat
- High molecular weight
- Low viscosity
- Good chemical and thermal stability
- Low environmental impacts
- Good safety characteristics
- Good compatibility
- Good availability and low cost

Working fluids should have high enthalpy difference during the expansion process since higher enthalpy difference gives higher power outputs. They should be easy to handle at the ambient temperature because the condensing temperature is generally close to the ambient temperature. Large heat conductivity and large vaporization latent heat correspond smaller heat exchanger areas mainly at the evaporator and condenser. High molecular weight increases the mass flow rate for the same size of expander. It also reveals fewer expander losses, hence gives better expander efficiency values. Low viscosity corresponds to lower power consumption at the process pump. Good chemical and thermal stability prohibit these fluids suffering from chemical deterioration and decomposition at high temperatures. Low environmental impacts stand for low or zero global warming potential (GWP) and ozone depletion potential (ODP).

Kyoto protocol limits the usage of some fluids which have high GWP and Montreal Protocol limits the usage of some fluids which have high ODP values. Good safety characteristics correspond to low or non-toxicity and low or non-flammability. ASHRAE Standard 34 is used for the security classification of refrigerants [62]. Compatibility of the fluid with another mechanical equipment prevents corrosion, therefore it is vital for chemical systems. Finally, being available and cost effective are important parameters for a working fluid when looking from the financial aspect. 13 fluids are analyzed with respect to physical, safety, environmental and numerical data and indicated in Table 2.1.

Table 2.1 shows that maximum simple and maximum regenerative cycle efficiencies are achieved when isobutane is adopted as the working fluid. Detailed analysis is not conducted at this stage, only heat duties and power outputs are taken into consideration. Even though fluids that include benzene, butane and pentane give better efficiency values rather than refrigerants, they require strict safety supervision before the operation.

Environmental and safety characteristics are prioritized to determine the working fluid selection criteria; therefore, four fluids are taken into consideration for further detailed analyses namely R134a, R141b, R245ca and R245fa which are shown good environmental and safety characteristics.

In this proposed ORC system, R134a is selected as the working fluid because of its superior performance in small heat inputs, zero ODP value, low GWP value which is 1300 relative to $CO_2$, non-flammability and non-toxicity, high molecular weight, good chemical and thermal stability [63], broad availability, and cost-effectiveness. On the other hand, Renolin Therm 320 heat transfer oil is selected as the heat transfer oil because of its low viscosity, large heat conductivity, good availability and good compatibility.

Table 2.1. Fluid comparison with respect to physical, safety, environmental and numerical data.

| | | Physical data | | | | Safety data | Environmental data | | | Numerical data | | |
|---|---|---|---|---|---|---|---|---|---|---|---|---|
| Working fluid | Chemical formula | Molecular mass (kg/kmol) | $T_b$ (C) | $T_c$ (C) | $P_c$ (bar) | ASHRAE 34 safety group | ODP | GWP | Atmospheric life time (yr) | $W_{net}$ | $\eta_s$ | $\eta_{rg}$ |
| Benzene | $C_6H_6$ | 78.11 | 80.07 | 288.87 | 49.07 | n.a | n.a | n.a | n.a | 8.1 | 8.59 | 10.15 |
| Isobutane | $C_4H_{10}$ | 58.12 | -11.75 | 134.66 | 36.29 | A3 | 0 | 4±2 | 12±3 | 8.67 | 8.96 | 10.33 |
| Isopentane | $C_5H_{12}$ | 72.15 | 27.83 | 187.2 | 33.78 | A3 | 0 | 3 | 12±3 | 8.05 | 8.34 | 10.16 |
| N-butane | $C_4H_{10}$ | 58.12 | -0.49 | 151.98 | 37.96 | A3 | 0 | 4±2 | 12±3 | 9.06 | 8.84 | 10.18 |
| N-pentane | $C_5H_{12}$ | 72.15 | 36.06 | 196.55 | 33.7 | A3 | 0 | 4 | 12±3 | 8.25 | 8.21 | 9.97 |
| R113 | $C_2Cl_3F_3$ | 187.38 | 47.59 | 214.06 | 33.92 | A1 | 1 | 6130 | 85 | 7.45 | 8.23 | 9.91 |
| R123 | $C_2HCl_2F_3$ | 152.93 | 27.82 | 183.68 | 36.62 | B1 | 0.02 | 77 | 1.3 | 8.51 | 8.43 | 9.62 |
| R134a | $C_2H_2F_4$ | 102.03 | -26.07 | 101.06 | 40.59 | A1 | 0 | 1430 | 14 | 9.35 | 8.66 | 9.18 |
| R141b | $C_2H_3Cl_2F$ | 116.95 | 32.05 | 204.35 | 42.12 | n.a | 0.12 | 725 | 9.3 | 9.12 | 8.83 | 9.85 |
| R245ca | $C_3H_3F_5$ | 134.05 | 25.26 | 174.42 | 39.41 | A1 | 0 | 693 | 6.2 | 8.75 | 7.96 | 9.83 |
| R245fa | $C_3H_3F_5$ | 134.05 | 15.14 | 154.01 | 36.51 | A1 | 0 | 1030 | 7.6 | 8.37 | 7.97 | 9.13 |
| R365mfc | $C_4H_5F_5$ | 148.07 | 40.15 | 186.85 | 32.66 | n.a | 0 | 794 | 8.6 | 7.42 | 7.97 | 9.99 |
| Toluene | $C_7H_8$ | 92.14 | 110.6 | 318.6 | 41.26 | n.a | n.a | n.a | n.a | 7.42 | 7.99 | 9.89 |

*Pressure ratio of the expander is selected 4.

** Expander and pump isentropic efficiencies are assumed 0.7 and 0.75, respectively.

## 2.2. Cycle Analyses

In the beginning of the cycle analyses, capacity of the heat source needs to be determined. In this laboratory scale ORC test rig, a heater with 100 kW maximum capacity is taken into consideration. With regard to the cooling unit, likewise, maximum capacity of 100 kW chiller unit is selected. Isentropic efficiencies of the expander and pump are assumed as 0.7 and 0.75, respectively. A recuperator is integrated into the system to decrease the heat duty of the evaporator. Thermodynamic analyses are conducted to calculate net power output and cycle efficiency values. In the calculations, pressure ratio of the expander, expander inlet pressure and the degree of superheating at the evaporator are varied for both simple and regenerative ORC. Maximum cycle pressure is selected 30 bar as a laboratory safety precaution. Conducted analyses regarding the effect of pressure ratio, expander inlet pressure and degree of superheat at the evaporator on specific net power output and cycle efficiency are summarized in Table 2.2.

Table 2.2. Net power output and cycle efficiency variation with respect to different variables and constants.

| Sets of analysis | Constants | State points |
|---|---|---|
| Set 1. Specific net power output vs expander pressure ratio | $T_{cond}$ = 30 °C | Saturated liquid at pump inlet<br>Saturated vapor at expander inlet |
| Set 2. Net power output vs expander inlet pressure | $\dot{m}$ = 0.25 kg/s<br>PR = 3 | Saturated liquid at pump inlet<br>Saturated vapor at expander inlet |
| Set 3. Cycle efficiency vs expander inlet pressure | $\dot{Q}_{in}$ = 60 kW<br>PR = 3 | Saturated liquid at pump inlet<br>Saturated vapor at expander inlet |
| Set 4. Net power output vs degree of superheat at the evaporator | $\dot{m}$ = 0.25 kg/s<br>PR = 3<br>EIP = * | Saturated liquid at pump inlet |
| Set 5. Cycle efficiency vs degree of superheat at the evaporator | $\dot{Q}_{in}$ = 60 kW<br>PR = 3<br>EIP = ** | Saturated liquid at pump inlet |

$T_{cond}$ : Condenser temperature, PR : Pressure ratio,

EIP : Expander inlet pressure, DSE : Degree of superheat at the evaporator.

* : Pressure that gives best result in the net power output vs DSE analysis.

** : Pressure that gives best result in the cycle efficiency vs DSE analysis.

*** :$\eta_{ex}$ and $\eta_p$ are assumed as 0.7 and 0.75.

### 2.2.1. The effect of expander pressure ratio

As the starting point of the analyses, condenser temperature (minimum cycle temperature) is selected as 30 °C which is approximately 5 °C above the ambient temperature and minimum cycle pressure is determined from the corresponding saturation point of the working fluid. Minimum cycle temperature selection is made to avoid negative gage pressure at the condenser. Table 2.3 shows the saturation pressures for each working fluid when the minimum cycle temperature is 30 °C.

Table 2.3. Saturation pressures of different fluids at 30 °C.

| Working fluid | Saturation pressure (bar) |
|---|---|
| R134a | 7.70 |
| R141b | 0.94 |
| R245ca | 1.21 |
| R245fa | 1.78 |

$$PR = \frac{P_{ex,in}}{P_{ex,out}} \tag{2.7}$$

Pressure ratio of the expander is the expander inlet pressure divided by the outlet pressure as shown in Equation (2.7). Thermodynamic calculations show that specific net power output and cycle efficiency are affected strongly from the change in the pressure ratio.

Pressure ratio of the expander is varied in the range between 1.5 to 4.5 to obtain the effect of pressure ratio on the net power output hence the cycle efficiency since the heat input rate is constant. Lowest pressure ratio is chosen as 1.5 because obtainable work from expander is significantly low at lower values. On the other hand, highest pressure ratio is chosen as 4.5 since higher values are really hard to reach when single stage expansion machines are considered.

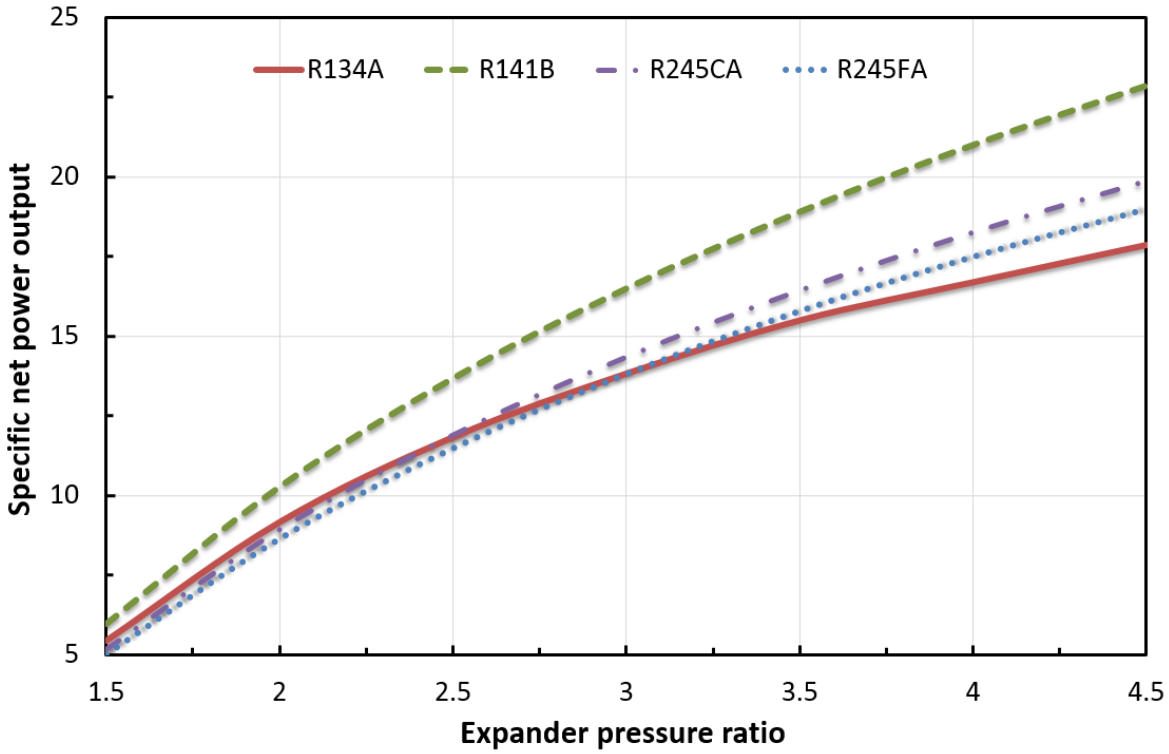


Figure 2.3. Specific net power output variation for different condensation temperatures depending on the pressure ratio of the expander.

Figure 2.3 shows the effect of the pressure ratio on the specific net power output for various working fluids namely R134a, R141b, R245ca and R245fa. It can be seen that increasing pressure ratio improves specific net power output of the cycle for all working fluids. The reason is the increment of the enthalpy difference between expander inlet and outlet.

In order to continue cycle analyses, pressure ratio of the expander needs to be decided. As mentioned before, to be able to obtain higher power outputs, higher pressure ratios are needed. However, higher pressure ratios than 4 are not feasible for single stage expanders.

The pressure ratio of the expander is selected as 3, which can be found suitable for a single stage expander unit for the future analyses.

### 2.2.2. The effect of expander inlet pressure

Expander inlet pressure is an essential parameter to determine the design points of the cycle. Expander inlet pressure is varied in the range between 3, which is minimum expander inlet pressure to avoid negative gage pressures at the condenser since the pressure ratio is selected as 3, to 30 bar, which is the maximum allowable pressure for the proposed ORC system. Net power output and cycle efficiency variation depending on the expander inlet pressure are analyzed. Saturated liquid at pump inlet and saturated vapor at expander inlet are considered for all working fluids. Figure 2.4 shows the expander inlet pressure effect on the net power output for each fluid. Heat input rate is varied to supply constant mass flow rate which is 0.25 kg/s. Regenerative ORC is not taken into consideration in the net power output analysis since it only affects the cycle efficiency.

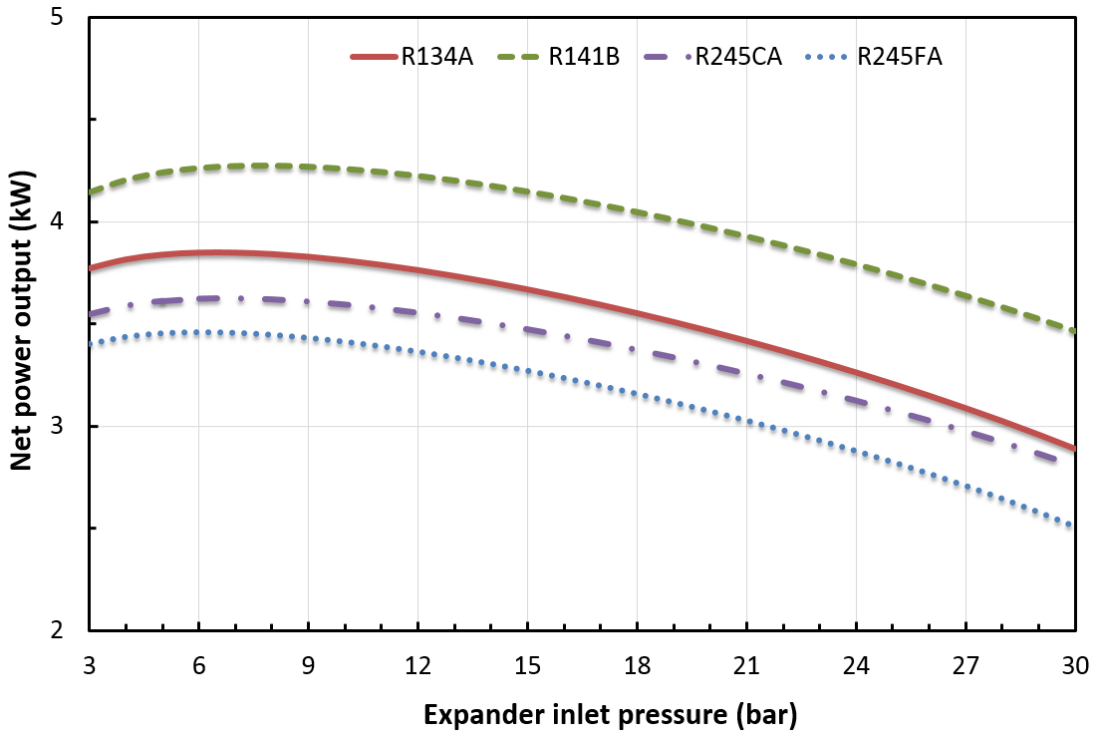


Figure 2.4. Net power output variation depending on the expander inlet pressure.

As shown in Figure 2.4, there is a single expander inlet pressure where the net power output is maximized. Net power output increases until this single point and then it starts to decrease. The enthalpy difference between the expander inlet and outlet is the reason for the change in net power output since mass flow rate is kept constant.

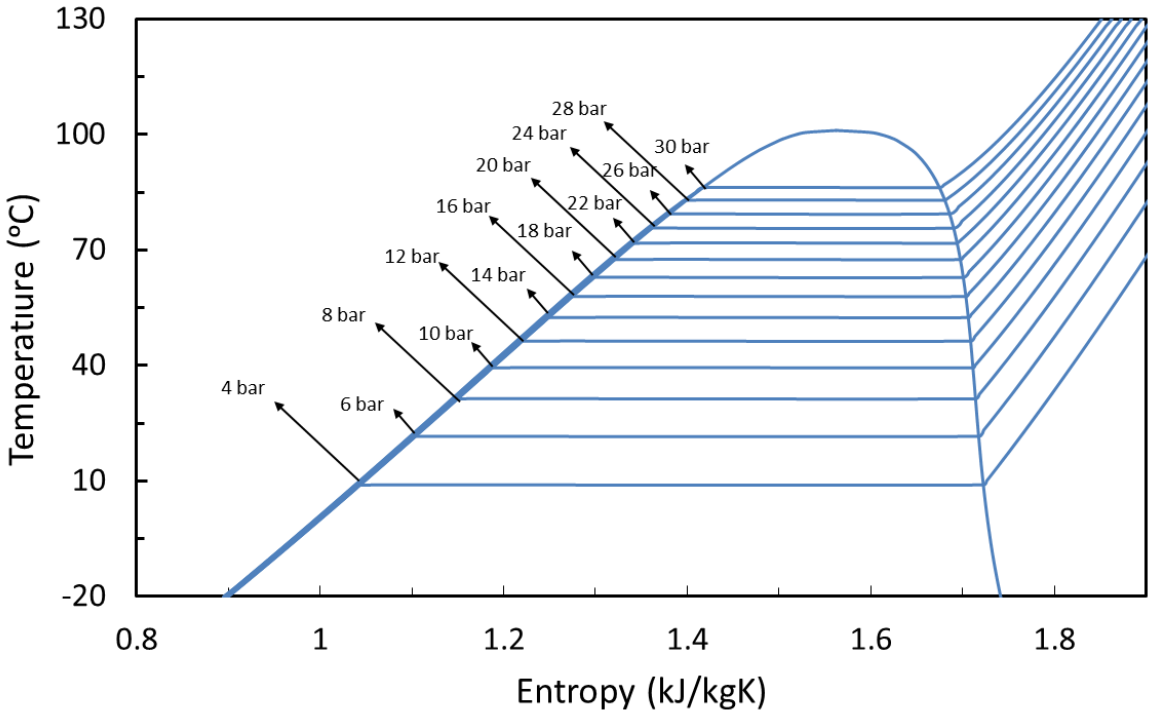


Figure 2.5. T-s diagram for R134a with different pressure states.

When the range is considered, lower expander inlet pressures with a constant pressure ratio give higher enthalpy differences and therefore, they give higher net power outputs.

As shown in Figure 2.5, when the pressure increases, the area enclosed with two different consecutive pressure states are becoming smaller. This means more enthalpy difference can be obtained when operating lower pressures with the same pressure ratio.

As indicated in Figure 2.6, if the expander inlet pressure increases, required heat input rate decreases almost linearly. This means the enthalpy difference between evaporator inlet and outlet is decreased since the mass flow rate is constant. As a result of this, as it is shown in Figures 2.7 and 2.8, when the heat input rate is fixed at a predetermined heat source capacity above the required heat input rate, mass flow rate is expected to increase since the enthalpy difference for the same conditions stays constant. Figures 2.9 to 2.12 show the expander inlet pressure effect on cycle efficiency for each fluid for simple and regenerative ORC.

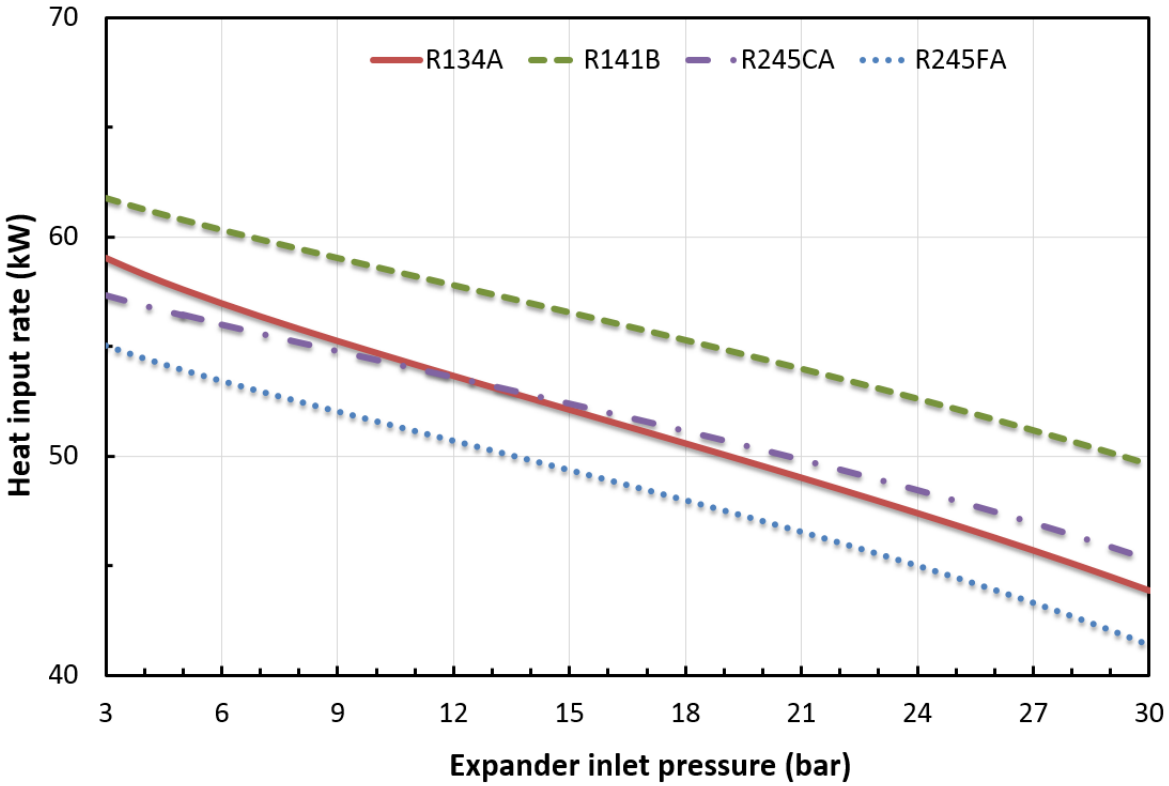


Figure 2.6. Heat input rate variation depending on the expander inlet pressure.

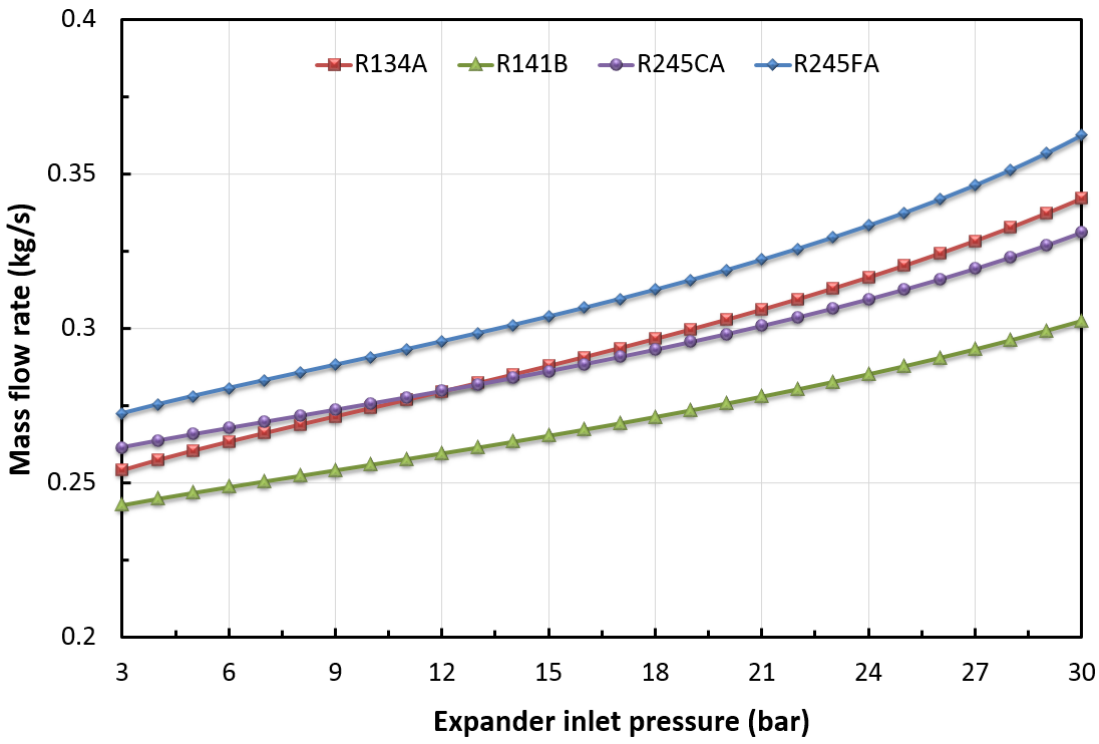


Figure 2.7. Mass flow rate variation depending on the expander inlet pressure for simple ORC.

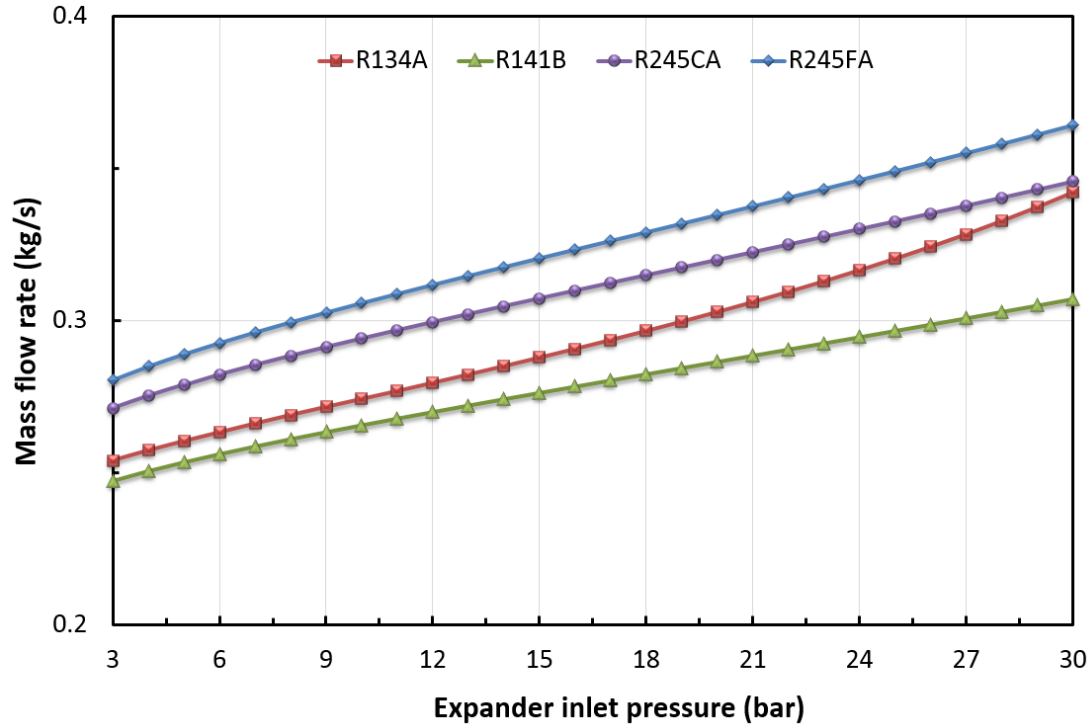


Figure 2.8. Mass flow rate variation depending on the expander inlet pressure for regenerative ORC.

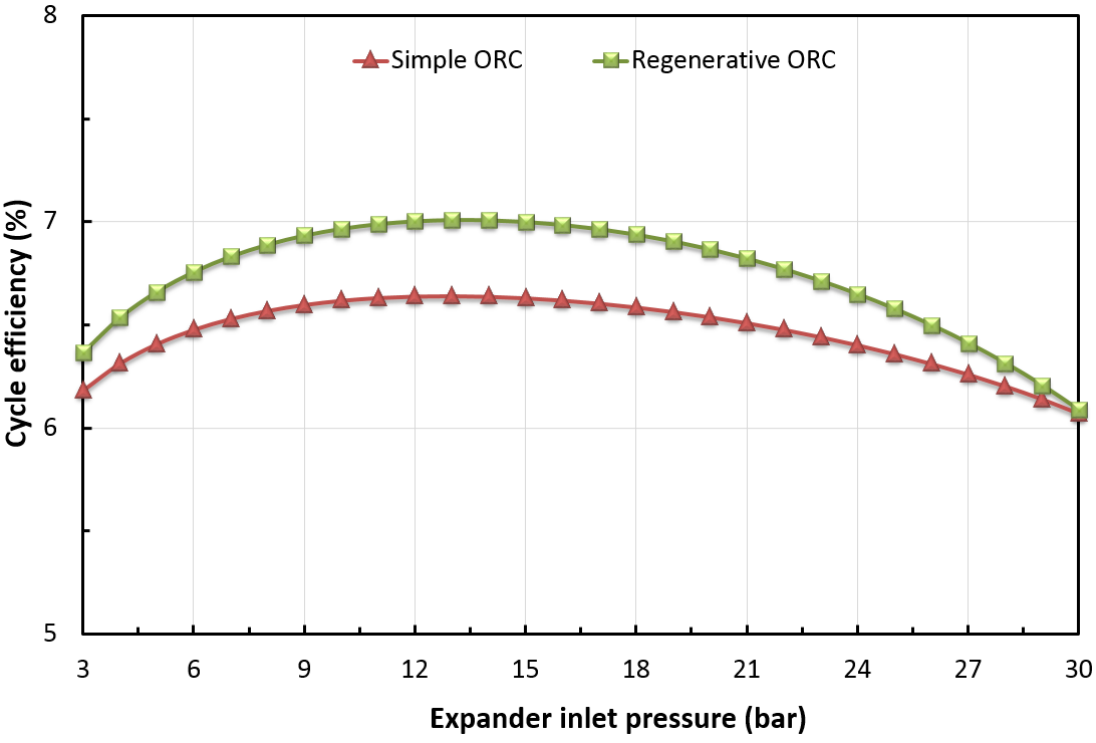


Figure 2.9. Cycle efficiency variation depending on the expander inlet pressure for R245fa.

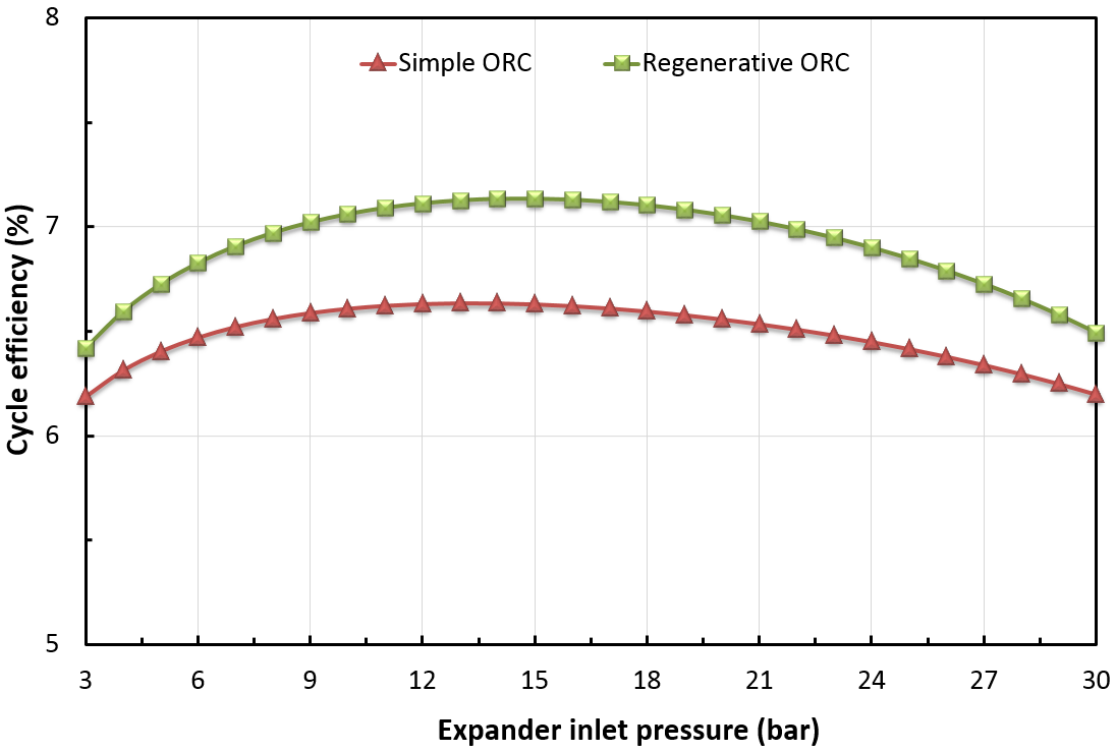


Figure 2.10. Cycle efficiency variation depending on the expander inlet pressure for R245ca.

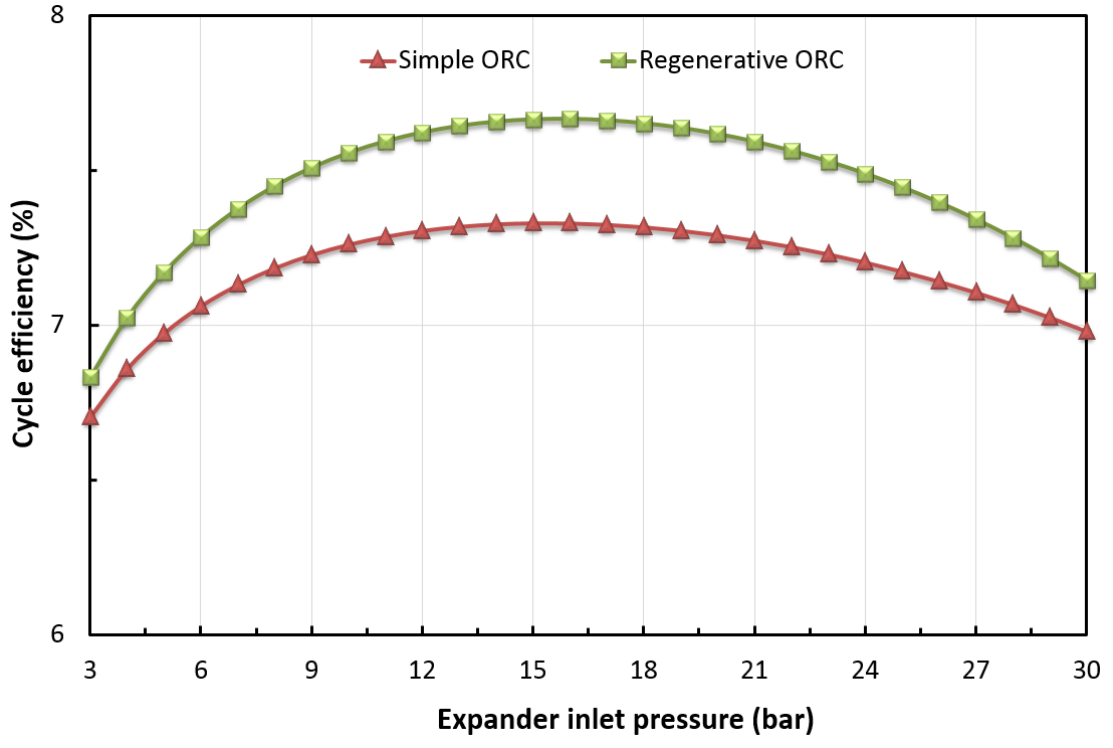


Figure 2.11. Cycle efficiency variation depending on the expander inlet pressure for R141b.

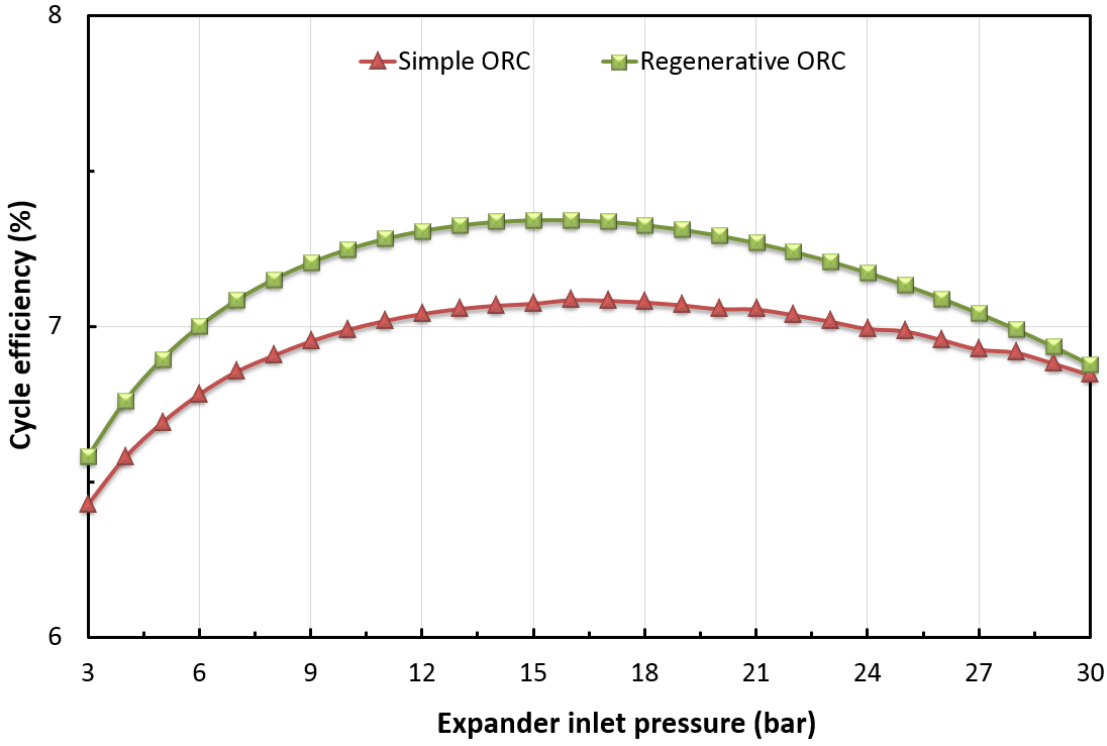


Figure 2.12. Cycle efficiency variation depending on the expander inlet pressure for R134a.

As it shown in Figures 2.9 to 2.12, regenerative ORC improves the cycle efficiency mostly at the mid-level expander inlet pressures when the minimum is 3 and the maximum is 30. At lower and higher expander inlet pressures, the temperature difference between cold fluid outlet and hot fluid inlet at the recuperator is relatively low. This leads to lower heat transfer rates at the recuperator; thus, regenerative effect would be negligible. However, at the middle expander inlet pressures, cold fluid outlet and hot fluid inlet temperature difference at the recuperator is relatively high. Higher temperature difference brings higher heat transfer rates at the recuperator, so regenerative effect would be remarkable.

As a summary, at low or high expander inlet pressures, the change is too small for any further consideration. It can be said that regenerative ORCs are not feasible for extremely low or extremely high pressure operations.

### 2.2.3. The effect of superheating

Degree of superheat at the evaporator is an important variable to determine the state points of the cycle. Superheating is varied in the range between 0 to 15 °C. Net power output and cycle efficiency variation depending on the degree of superheat at the evaporator are analyzed. Pressure ratio is selected 3 as pre-determined before. Saturation liquid at the pump inlet is considered for all working fluids.

As shown in Figure 2.13, superheating effect on the net power output for each fluid. Heat input rate is varied to supply constant mass flow rate which is 0.25 kg/s. Again, regenerative ORC is not taken into consideration in the net power output analysis since it only affects the cycle efficiency.

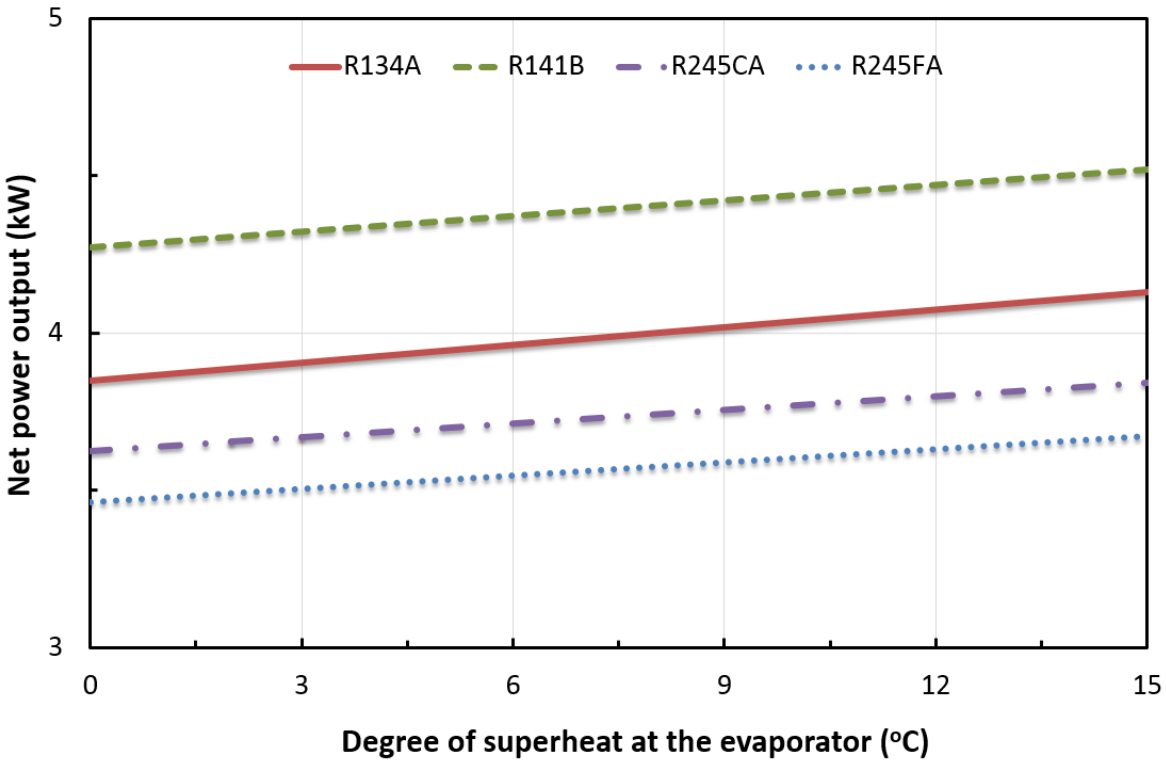


Figure 2.13. Net power output variation depending on the degree of superheat.

As indicated in Figure 2.13, superheating linearly increases the net power output. It is logical since the enthalpy of the working fluid is increasing with the increasing temperature at the evaporator.

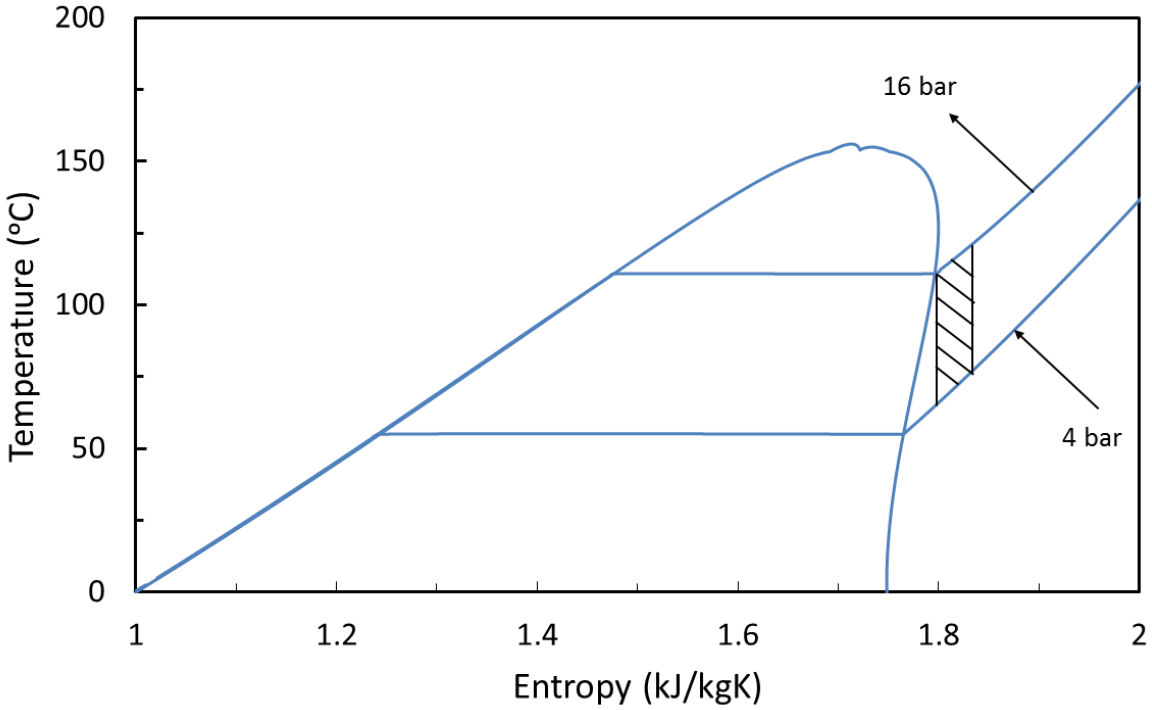


Figure 2.14. T-s diagram of R245fa.

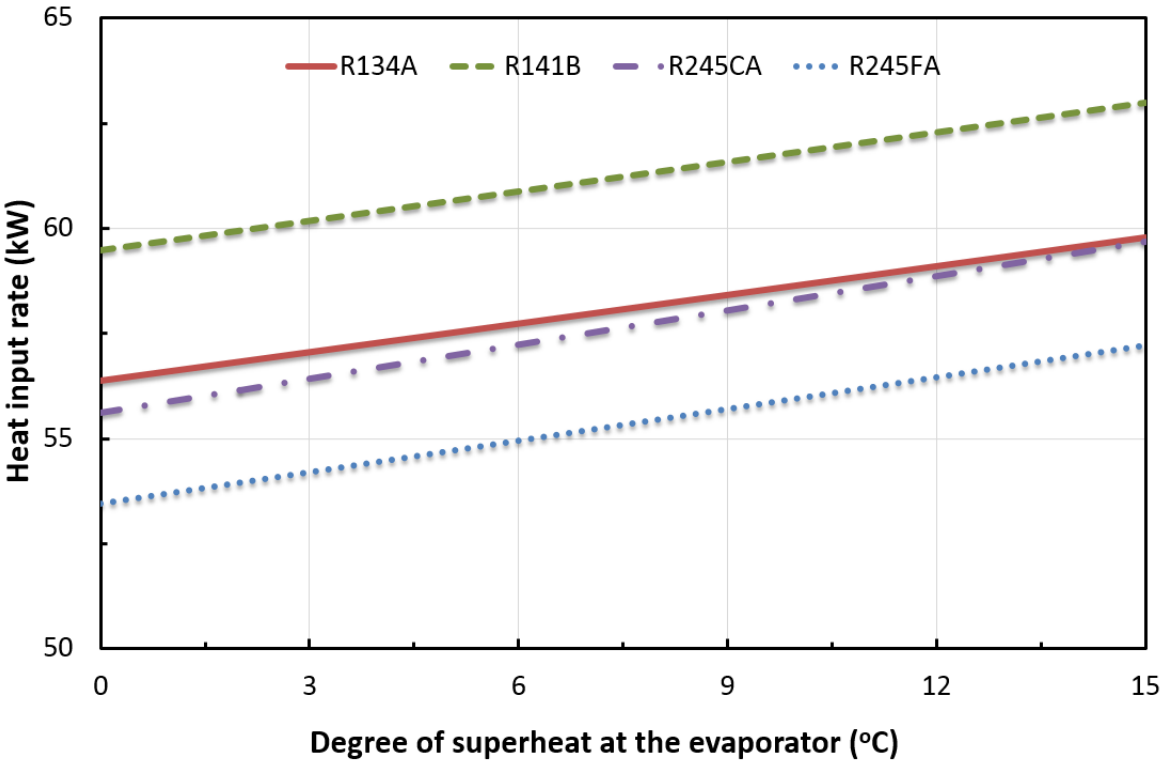


Figure 2.15. Heat input rate variation depending on the degree of superheat for simple ORC.

T-s diagram of R245fa is indicated in Figure 2.14. Since the net power output is the enclosed area of the two pressure curves in T-s diagram, superheating effect increases the obtainable power by the shaded area. The dashed area indicates the net power output increase when the degree of superheat is 10 °C. Required heat input rate with respect to degree of superheat at the evaporator is given in Figure 2.15.

As it shown in Figure 2.15, if the degree of superheat is increased, required heat input rate is increased linearly. As a result of this, when the heat input rate is fixed at a predetermined heat source capacity, mass flow rate is slightly decreased with the increasing of superheat. Figures 2.16 and 2.17 indicate the mass flow rate variation for both simple and regenerative ORC when the heat input rate is fixed at 60 kW. In contrast to simple ORC, mass flow rate stays nearly constant for regenerative ORC because the heat transfer in the recuperator has a detrimental effect on the heat input rate. Calculations up to 4 °C superheat is trivial for R134a since it is a wet fluid.

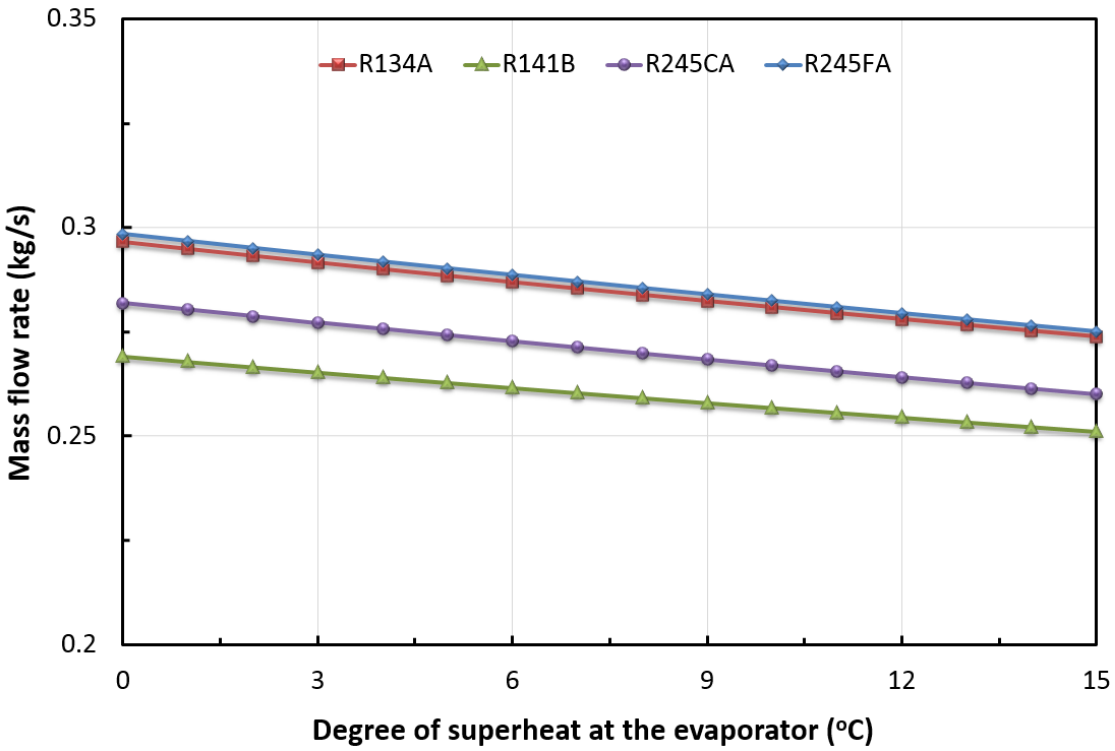


Figure 2.16. Mass flow rate variation depending on the degree of superheat for simple ORC.

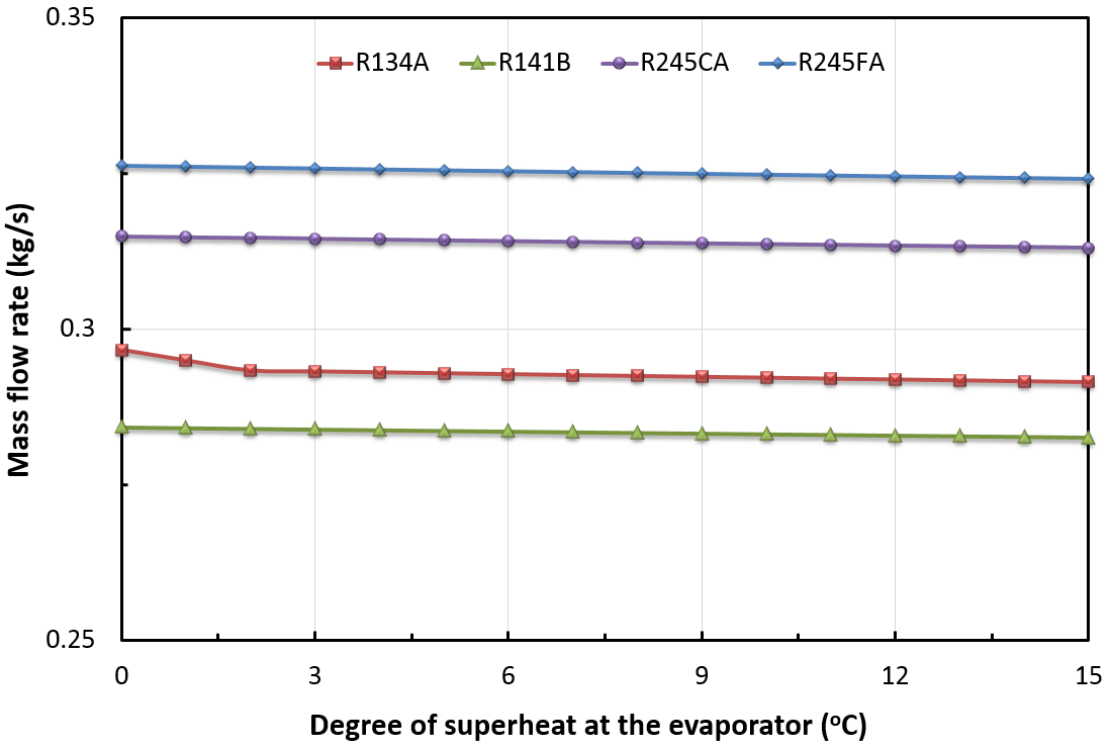


Figure 2.17. Mass flow rate variation depending on the degree of superheat for regenerative ORC.

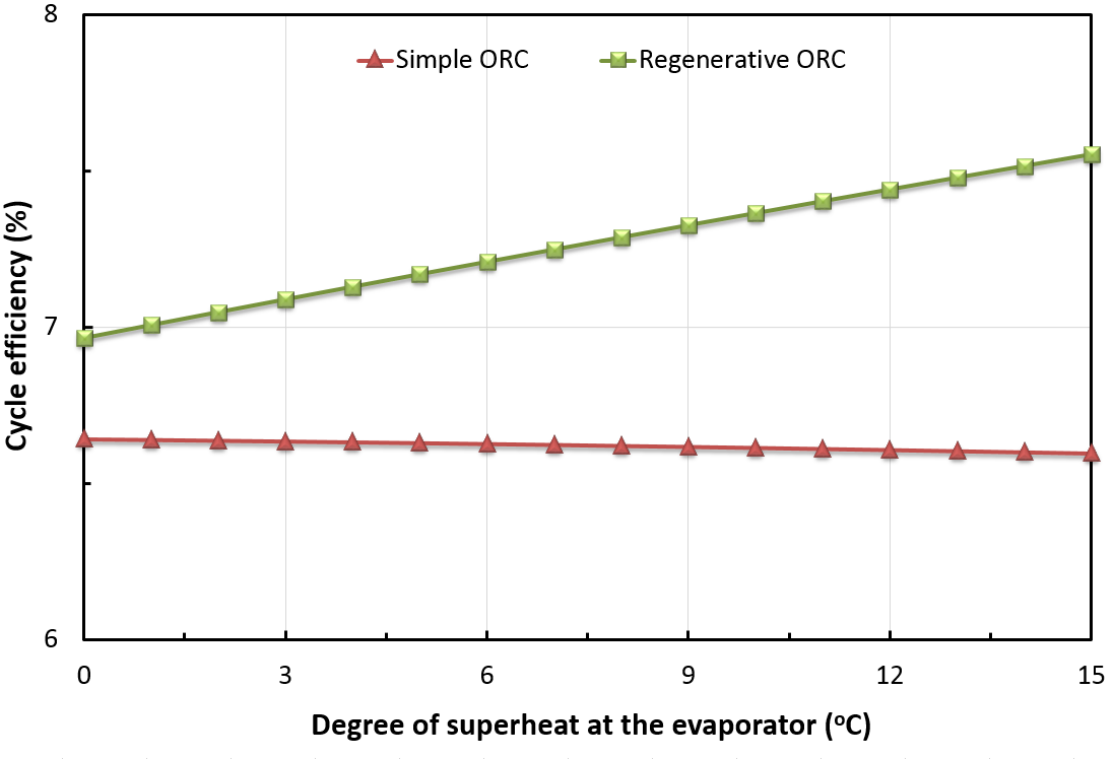


Figure 2.18. Cycle efficiency variation depending on the degree of superheat for R245fa.

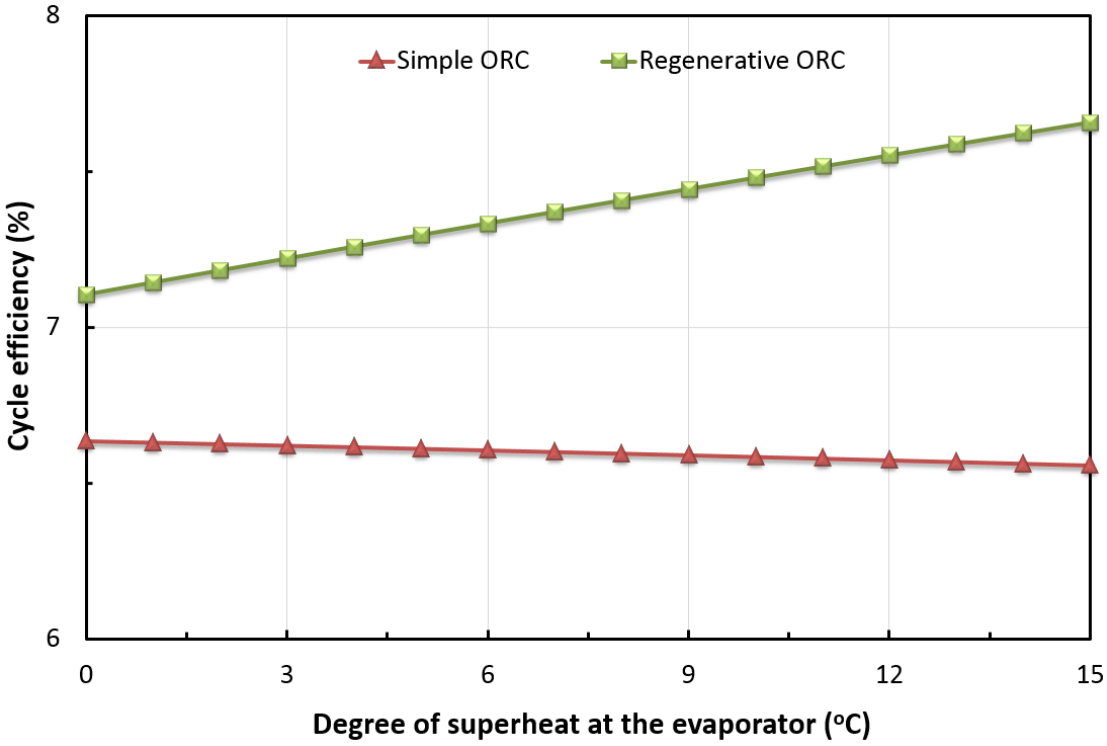


Figure 2.19. Cycle efficiency variation depending on the degree of superheat for R245ca.

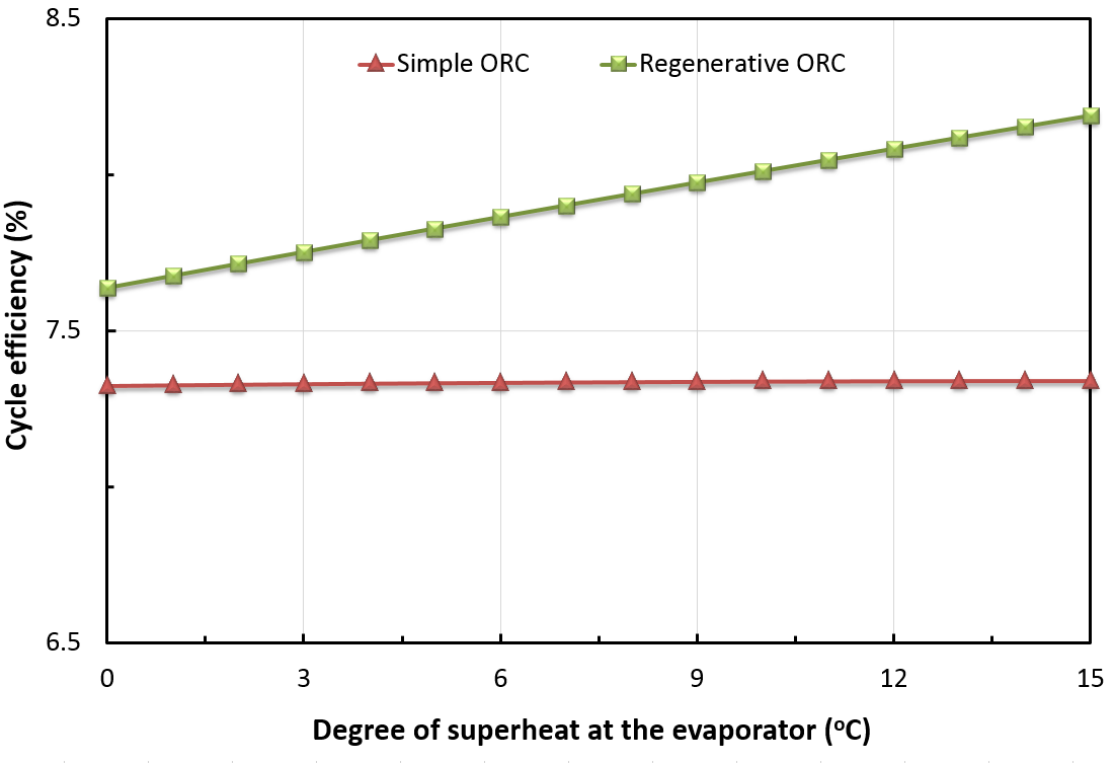


Figure 2.20. Cycle efficiency variation depending on the degree of superheat for R141b.

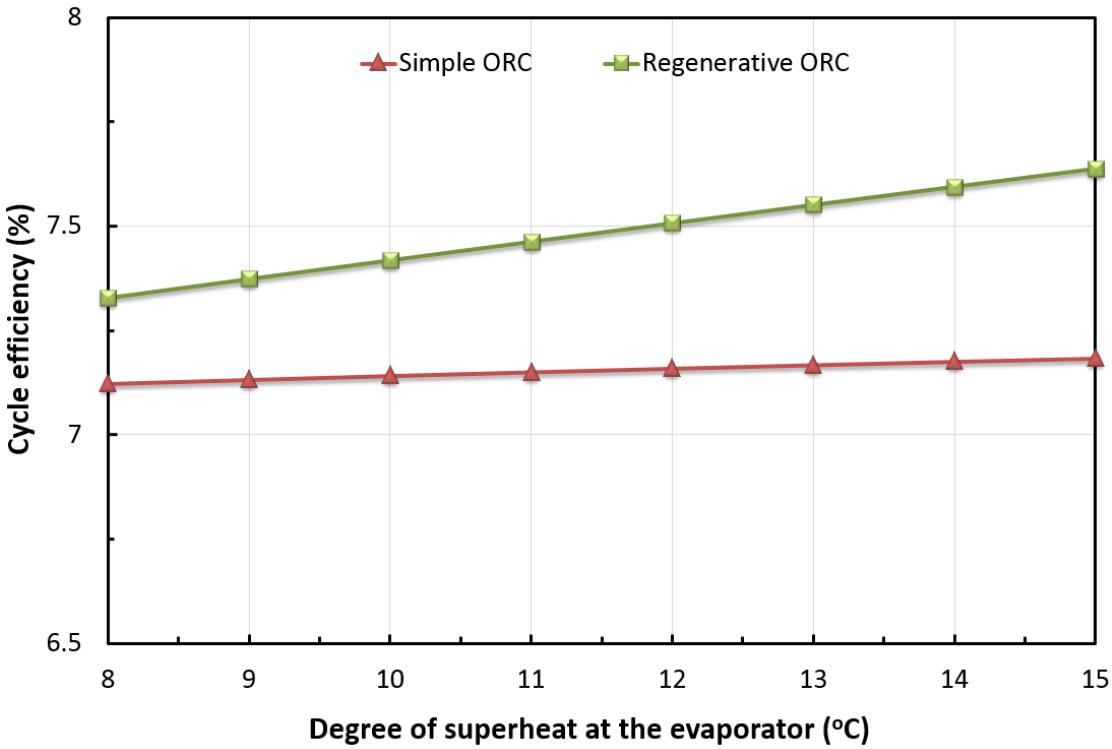


Figure 2.21. Cycle efficiency variation depending on the degree of superheat for R134a.

As it is shown in the Figures 2.18 to 2.21, regenerative ORC improves the net power output mostly when highest superheating is conducted. The reason is; recuperator into the system is designed to supply constant 5 °C temperature difference between cold fluid outlet and hot fluid inlet temperatures. When superheating increases, hot fluid inlet temperature increases, too. Thus, cold fluid outlet temperature increases and heat duty of the recuperator is improved.

Additionally, if R134a is adopted, the change of the cycle efficiency is too small for any further consideration up to the degree of superheat is 4 °C. The reason for that R134a is a wet fluid and it needed to be superheated around 4 °C in order to be still at vapor phase at the expander outlet.

T-s diagram of R134a is indicated in Figure 2.22. Here, both isentropic and non-isentropic expansion show why R134a is needed to be superheated.

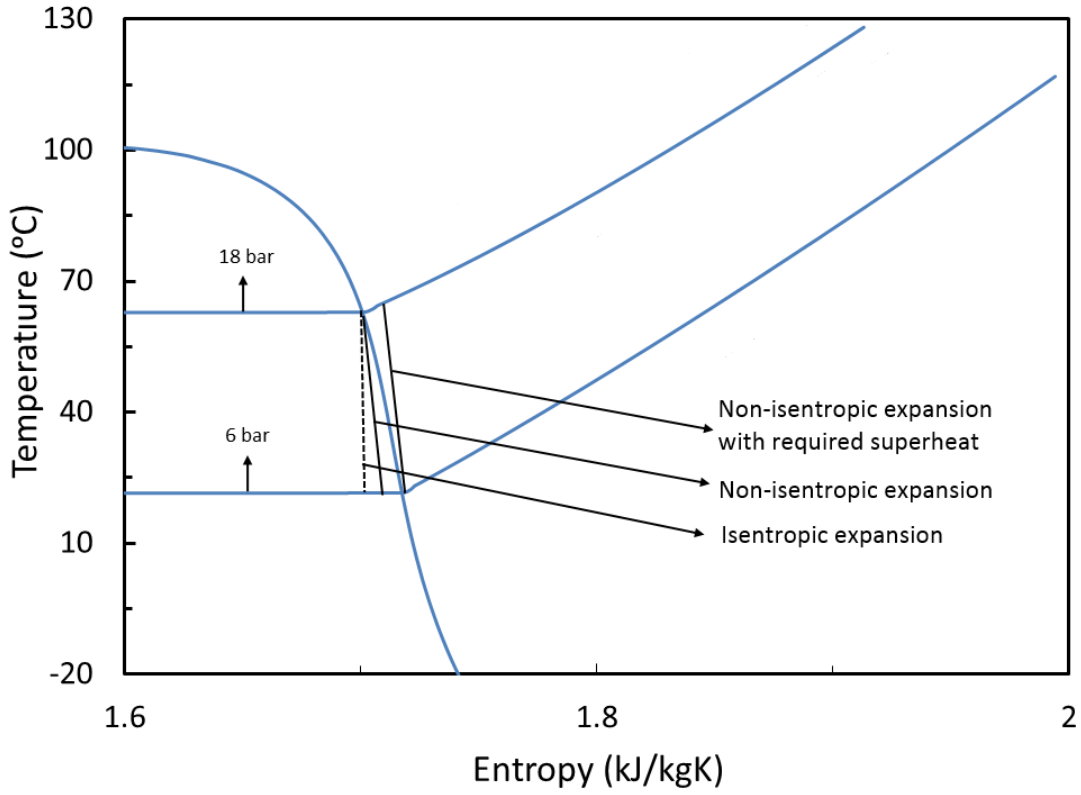


Figure 2.22. T-s diagram of R134a with two different pressure and two different temperature states.

If R134a is operated with the saturation vapor at expander inlet, the expander outlet will be liquid-vapor mixture. Therefore, it requires a superheat which is defined by the operating pressure.

### 2.2.4. Selection of state points

From the net power output and cycle efficiency graphics, it can be seen that maximum net power output and maximum cycle efficiency does not correspond to the same expander inlet pressure. There is an optimum operating pressure at the expander inlet where the net power output reaches its peak and then it reduces dramatically. Likewise, regarding cycle efficiency, it improves with the increasing expander inlet pressure for all investigated working fluids at some point between 4 to 30 bar expander inlet pressure and then it starts to decrease.

On one hand, net power output improves with increasing the degree of superheat at the evaporator. The reason is that the area enclosed by cycle state points in the T-s diagram increases with the increasing superheating. On the other hand, that is not the same case for cycle efficiency which shows various trends for different working fluid types. For wet fluids, in that case R134a, it keeps constant with increasing the degree of superheat; however, for dry fluids namely R245ca and R245fa, cycle efficiency reaches their maximum at the saturation points in terms of simple ORC. For isentropic fluids such as R141b, superheating does not have a big impact on the cycle efficiency.

Table 2.4. Max. net power output and cycle efficiency conditions for simple ORC.

| Fluid Type | Max. Net Power Output Conditions | Max. Cycle Efficiency Conditions |
|---|---|---|
| R134a | Expander inlet pressure: 8 bar<br>Degree of superheating: 15°C<br>Required heat input: 59.28 kW<br>Mass flow rate: 0.25 kg/s | Expander inlet pressure: 18 bar<br>Degree of superheating: 15°C<br>Required heat input: 60 kW<br>Mass flow rate: 0.274 kg/s |
| R141b | Expander inlet pressure: 9 bar<br>Degree of superheating: 15°C<br>Required heat input: 62.61 kW<br>Mass flow rate: 0.25 kg/s | Expander inlet pressure: 17 bar<br>Degree of superheating: 15°C<br>Required heat input: 60 kW<br>Mass flow rate: 0.251 kg/s |
| R245ca | Expander inlet pressure: 8 bar<br>Degree of superheating: 15°C<br>Required heat input: 59.35 kW<br>Mass flow rate: 0.25 kg/s | Expander inlet pressure: 13 bar<br>Degree of superheating: 0°C<br>Required heat input: 60 kW<br>Mass flow rate: 0.282 kg/s |
| R245fa | Expander inlet pressure: 7 bar<br>Degree of superheating: 15°C<br>Required heat input: 56.80 kW<br>Mass flow rate: 0.25 kg/s | Expander inlet pressure: 13 bar<br>Degree of superheating: 0°C<br>Required heat input: 60 kW<br>Mass flow rate: 0.298 kg/s |

When considering regenerative ORC, cycle efficiency improves with the degree of superheat for all investigated fluids. The reason is that the recuperator is identified as there will be 5 °C difference between the hot fluid inlet temperature and the cold fluid outlet temperature. Depend on the fixed temperature difference, the heat duty of the recuperator is kept increasing; therefore, the heat duty of the evaporator is decreased. Since the net power output is constant, the cycle efficiency is increased gradually.

Table 2.5. Max. net power output and cycle efficiency conditions for regenerative ORC.

| Fluid Type | Max. Net Power Output Conditions | Max. Cycle Efficiency Conditions |
|---|---|---|
| R134a | Expander inlet pressure: 8 bar<br>Degree of superheating: 15°C<br>Required heat input: 56.27 kW<br>Mass flow rate: 0.25 kg/s | Expander inlet pressure: 18 bar<br>Degree of superheating: 15°C<br>Required heat input: 60 kW<br>Mass flow rate: 0.291 kg/s |
| R141b | Expander inlet pressure: 9 bar<br>Degree of superheating: 15°C<br>Required heat input: 57.25 kW<br>Mass flow rate: 0.25 kg/s | Expander inlet pressure: 19 bar<br>Degree of superheating: 15°C<br>Required heat input: 60 kW<br>Mass flow rate: 0.283 kg/s |
| R245ca | Expander inlet pressure: 8 bar<br>Degree of superheating: 15°C<br>Required heat input: 52.24 kW<br>Mass flow rate: 0.25 kg/s | Expander inlet pressure: 18 bar<br>Degree of superheating: 15°C<br>Required heat input: 60 kW<br>Mass flow rate: 0.313 kg/s |
| R245fa | Expander inlet pressure: 7 bar<br>Degree of superheating: 15°C<br>Required heat input: 50.87 kW<br>Mass flow rate: 0.25 kg/s | Expander inlet pressure: 17 bar<br>Degree of superheating: 15°C<br>Required heat input: 60 kW<br>Mass flow rate: 0.324 kg/s |

Design points of the simple and regenerative ORC for each working fluid is indicated in Tables 2.4 and 2.5. It can be seen that max. net power output conditions are the same for simple and regenerative ORC. Regeneration does not affect the obtainable power but only cycle efficiency. They all need highest superheating as explained before. Regarding these four fluids, R245fa needs lowest maximum cycle pressure, which is 7 bar, to provide maximum power output condition. R134a and R245ca need 8 bar pressure while R141b needs 9 at the expander.

However, maximum cycle efficiency conditions are different considering simple and regenerative ORC. Generally, in regenerative ORC, these fluids need higher maximum cycle pressure values. R245fa and R245ca need 13 bar maximum cycle pressure while R141b needs 17 and R134a needs 18 bar for simple ORC.

Regarding regenerative ORC, R245a has a maximum cycle pressure of 17 bar while R134a and R245ca have 18 and R141b has 19. Additionally, superheating effect improves the regenerative cycle efficiency because of the recuperator design.

Maximum net power output and maximum cycle efficiency values for all investigated fluids are indicated in Table 2.6 for both simple and regenerative ORC.

Table 2.6. Max. net power output and maximum cycle efficiency values for each working fluid.

| Fluid Type | Max. Net Power Out. for simp. and reg. ORC (kW) | Max. Cycle Eff. for simple ORC (%) | Max. Cycle Eff. for regenerative ORC (%) |
|---|---|---|---|
| R134a | 4.13 | 7.18 | 7.64 |
| R141b | 4.52 | 7.34 | 8.19 |
| R245ca | 3.84 | 6.63 | 7.66 |
| R245fa | 3.68 | 6.64 | 7.55 |

When looking at the maximum efficiency values, recuperator contributes slightly on the cycle performance; therefore, it seems that it may not be used for this application especially for R134a. However, for a better judgement, a recuperator is integrated into the test rig to compare the difference in the experimental investigation.

As it mentioned before, R134a is selected as the working fluid for experimental investigation. It must be emphasized that R134a is a wet fluid and it should be superheated in order to obtain vapor phase at the expander outlet. To be able to do that, instead of saturation point at the expander inlet pressure, minimum degree of superheat at the evaporator is considered just enough to obtain vapor refrigerant at the expander outlet.

# 3. HEAT EXCHANGER DESIGN

This proposed ORC system consists of four heat exchangers as evaporator, condenser, recuperator and pre-cooler. The evaporator is used to vaporize the liquid working fluid while absorbing heat from the heater via heat transfer fluid before it enters the expander. Condenser, on the other hand, is used to cool down and condense the expanded working fluid at the expander outlet via cooling water before it enters the pump.

A recuperator is integrated into the system to decrease the heat duty of the evaporator; hence increasing the cycle efficiency since the power output is constant. One inlet port of the recuperator is occupied by expanded vapor at the expander outlet, the other one is occupied by pressurized working fluid at the pump outlet. Pressurized working fluid absorbs the heat of the expanded vapor and therefore decreases the required enthalpy difference at the evaporator.

Pre-cooler is a part of the expander simulator which enables to bypass the expander in the commissioning process. When operating the cycle with expander simulator, throttle valves use to decrease the pressure of the working fluid likewise the expander; however, the enthalpy of the fluid stays the same since the process is isenthalpic. In that case, pre-cooler is used to cool down the vaporized fluid and then, it enters the condenser in order to condense.

As mentioned earlier, heat duties of the heat exchangers are predetermined in Aspen Plus cycle simulation. However, to select the proper heat exchangers, heat exchanger design and rating with respect to exchanger geometry is also necessary. In order to achieve a proper design and rating of heat exchangers, heat transfer and pressure drop calculations must be performed. Aspen Exchanger Design and Rating (EDR) module is used to determine the exchanger performance and geometries. Since the design temperature and pressure values are relatively low comparing to the industrial processes, plate type heat exchangers are adopted for the proposed ORC test rig.

Since heat duties and the temperature differences are determined, effective heat transfer area needs to be specified with using the heat transfer calculations. In order to achieve this, a plate geometry must be defined. At the final stage, required effective heat transfer area and therefore required plate number can be calculated. In the case of the evaporator, when considering the working fluid side, mass flow rate and the temperature difference between inlet and outlet ports are defined. Heat transfer fluid side, on the other hand, mass flow rate and only the inlet temperature is defined. By using the heat balance equation, outlet temperature of the heat transfer fluid is determined. With respect to condenser, same steps are followed only, this time, the other fluid is water rather than heat transfer oil. However, in case of recuperator, since the outlet temperatures of both sides are not known, pinch point approach is used to calculate heat duty for predetermined temperature difference. Then, required effective heat transfer area and required plate number can be calculated. As for the pre-cooler, expander outlet temperature is considered as the hot side outlet temperature.

## 3.1. Heat Transfer Calculations

Heat transfer calculations are mainly included heat duty, heat transfer coefficients, and heat transfer area. Heat duty of an exchanger can be expressed for both hot and cold sides as:

$$\dot{Q}_h = \dot{m}_h c_{p,h}(T_{h,in} - T_{h,out}) \tag{3.1a}$$

$$\dot{Q}_c = \dot{m}_c c_{p,c}(T_{c,out} - T_{c,in}) \tag{3.1b}$$

and through a phase change:

$$\dot{Q_p}h = \dot{m}\Delta h_{pc} \tag{3.1c}$$

Also, the amount of transferred heat can be expressed with respect to overall heat transfer coefficient, effective surface area and logarithmic mean temperature difference as follows:

$$\dot{Q} = U_f A_e \Delta T_{lm} \tag{3.2}$$

The overall heat transfer coefficient under fouling conditions and logarithmic mean temperature difference can be written as:

$$U_f = \frac{1}{\frac{1}{\left(\frac{1}{\alpha_h} + \frac{t}{k_w} + \frac{1}{\alpha_c}\right)} + R_{fh} + R_{fc}} \tag{3.3}$$

$$\Delta T_{lm} = \frac{(T_{h,in} - T_{c,out}) - (T_{h,out} - T_{c,in})}{ln\left(\frac{T_{h,in} - T_{c,out}}{T_{h,out} - T_{c,in}}\right)} \tag{3.4}$$

Nusselt Number depends on the heat transfer coefficient, hydraulic diameter and thermal conductivity of fluid and it can be defined by:

$$Nu = \frac{\alpha D_h}{k} \tag{3.5}$$

Nusselt number is also a function of Reynolds number, Prandtl number and dynamic viscosity and can be expressed by:

$$Nu = CRe^n Pr^{1/3} \left(\frac{\mu}{\mu_w}\right)^{0.17} \tag{3.6}$$

where constants of C and n are indicated in Table 3.1 depending on the Re and chevron angles($\beta$). Chevron angle is defined as the angle of the triangular pattern of the heat transfer area. By using Eq.(3.5) and Eq.(3.6), heat transfer coefficient is obtained and given in Eq.(3.7) for single phase heat transfer.

$$\alpha = \left(\frac{k}{D_h}\right) C Re^n Pr^{1/3} \left(\frac{\mu}{\mu_w}\right)^{0.17} \tag{3.7}$$

Reynolds number gives the information about if the flow is laminar or turbulent. Laminar flow occurs at low Reynolds numbers which mean the flow is relatively regular compared to turbulent flow, occurs at high Reynolds numbers. The Prandtl number, on the other hand, is a dimensionless number and depend on the type and state of the fluid. Reynolds and Prandtl number can be obtained from:

$$Re = \frac{G_c D_h}{\mu} \tag{3.8}$$

$$Pr = \frac{c_p \mu}{k} \tag{3.9}$$

where $G_e$ is the channel mass velocity, $D_h$ is the hydraulic diameter, $\mu$ is the dynamic viscosity and $c_p$ is the specific heat. The channel mass velocity and the hydraulic diameter are expressed as:

$$G_c = \frac{\dot{m}}{N_{cp} b L_w} \tag{3.10}$$

$$D_h = \frac{4A_c}{P_w} = \frac{4bL_w}{2(b + L_w \phi)} \approx \frac{2b}{\phi} \tag{3.11}$$

where $N_{cp}$ is the number of channel per pass, b is the mean channel spacing, $L_w$ is the summation of the port distance and port diameter obtained from the exchanger geometry, $A_c$ is the channel flow area, $P_w$ is the wetted surface and $\phi$ is the surface enlargement factor which is specified by the manufacturer to calculate effective flow path. The number of channel per pass is defined as:

$$N_{cp} = \frac{N_t - 1}{2N_p} \tag{3.12}$$

where $N_t$ and $N_p$ are the total number of plates and the number of passes. Mean channel spacing is directly affects the Reynolds number, therefore it is important. It is given by:

$$b = \frac{p}{t} \tag{3.13}$$

where p denotes the plate pitch and t denotes the plate thickness. Plate pitch also is given by:

$$p = \frac{L_c}{N_t} \tag{3.14}$$

where $L_c$ is the distance between the head plates. On the other hand, in order to find the hydraulic diameter, the surface enlargement factor must be known. The surface enlargement factor is defined by:

$$\phi = \frac{A_1}{A_{1p}} \tag{3.15}$$

where $A_1$ is the actual effective area which is usually given by the manufacturer and $A_{1p}$ is the projected plate area and it can be written as:

$$A_{1p} = L_p \cdot L_w \tag{3.16}$$

and $L_p$ and $L_w$ can be written as:

$$L_p \approx L_v - D_p \tag{3.17}$$

$$L_w \approx L_h + D_p \tag{3.18}$$

Parameters with regard to exchanger geometry are indicated in Figure 3.1.

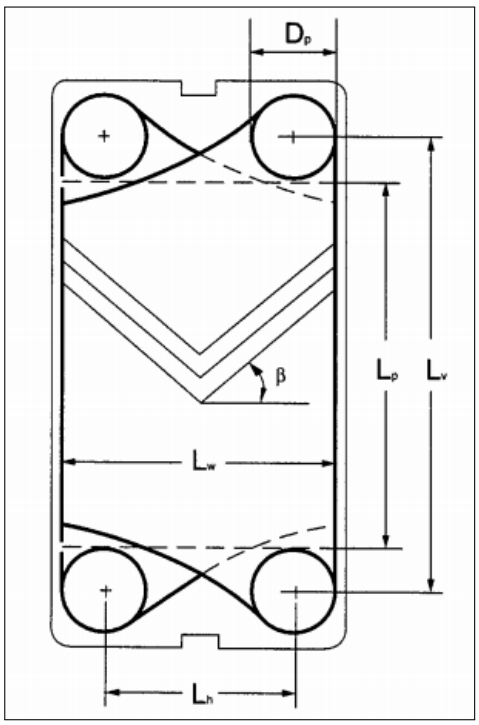


Figure 3.1. Section drawing of a plate type heat exchanger [64].

However, there is a phase changing process at the evaporator and condenser and therefore, two-phase flow calculations should be taken into account. Yan and Lin correlations [65, 66] are given in Eq.(3.19) and Eq.(3.20) in order to calculate evaporation and condensation heat transfer.

$$\alpha_e = 1.926 \left( \frac{Re_{eq}}{Re^{0.5}} \right) \left( \frac{Pr^{1/3} Bo_{eq}^{0.3} k_l}{D_h} \right) \tag{3.19}$$

$$\alpha_c = 4.118 \frac{Re_{eq}^{0.4} Pr^{1/3} k_l}{D_h} \tag{3.20}$$

where;

$$Re_{eq} = \frac{G_{eq} D_h}{\mu_l} \tag{3.21}$$

$$Bo_{eq} = \frac{q"_w}{G_{eq} h_{lv}} \tag{3.22}$$

$$G_{eq} = G_c \left[ (1 - x_m) + x_m \left( \frac{\rho_l}{\rho_g} \right)^{0.5} \right] \tag{3.23}$$

### 3.2. Pressure Drop Calculations

There are two main parts namely channels and ports where pressure drops occur in a plate type heat exchanger. A two-phase pressure drop calculation is necessary with regard to exchanger channels since phase-change occurs at the evaporator and condenser models. Channel pressure drop is calculated by:

$$\Delta p_c = 4f \frac{L_v N_p}{D_e} \frac{{G_c}^2}{2\rho} \left( \frac{\mu}{\mu_w} \right)^{-0.17} \tag{3.24}$$

where $f$ is the friction factor that includes enlargement factor $\phi$ and given by:

$$f = \frac{K_p}{Re^m} \tag{3.25}$$

The density of the fluid in two-phase flow can be calculated from:

$$\rho = (1 - X)\rho_l + X\rho_v \tag{3.26}$$

where X is the vapor quality of the fluid. The constants of $K_p$ and $m$ are the functions of Re and chevron angles and they are given in Table 3.1.

Port pressure drop is given by:

$$\Delta p_p = 1.4 N_p \left( \frac{{G_p}^2}{2\rho} \right) \tag{3.27}$$

where;

$$G_p = \frac{\dot{m}}{\left(\frac{\pi {D_p}^2}{4}\right)} \tag{3.28}$$

On the other hand, the total pressure drop can be calculated by:

$$\Delta p_t = \Delta p_c + \Delta p_p \tag{3.29}$$

Table 3.1. Heat transfer and pressure drop equation constants [64].

| | Heat Transfer | | | Pressure Loss | | |
|---|---|---|---|---|---|---|
| Chevron Angle (degree) | Reynolds Number | $C$ | n | Reynolds Number | $K_p$ | m |
| $\leq 30$ | $\leq 10$ | 0.718 | 0.349 | 10 | 50 | 1 |
| | >10 | 0.348 | 0.663 | 10-100 | 19.4 | 0.589 |
| 45 | <10 | 0.718 | 0.349 | <15 | 47 | 1 |
| | 10-100 | 0.4 | 0.598 | 15-300 | 18.29 | 0.652 |
| | >100 | 0.3 | 0.663 | >300 | 1.441 | 0.206 |
| 50 | <20 | 0.63 | 0.333 | <20 | 34 | 1 |
| | 20-300 | 0.291 | 0.591 | 20-300 | 11.25 | 0.631 |
| | >300 | 0.13 | 0.732 | >300 | 0.772 | 0.161 |
| 60 | <20 | 0.562 | 0.326 | <40 | 24 | 1 |
| | 20-400 | 0.306 | 0.529 | 40-400 | 3.24 | 0.457 |
| | >400 | 0.108 | 0.703 | >40 | 0.76 | 0.215 |
| $\geq 65$ | <20 | 0.562 | 0.326 | 50 | 24 | 1 |
| | 20-500 | 0.331 | 0.503 | 50-500 | 2.8 | 0.451 |
| | >500 | 0.087 | 0.718 | >500 | 0.639 | 0.213 |

# 4. ORC Test Rig

The ORC test rig at the BURET Laboratory consists of both on-skid and off-skid equipment. On-skid equipment consists of two pumps, four heat exchangers, two throttle valves, a liquid collector, complete with interconnection piping, valves and instrumentation. Off-skid equipment mainly consists of a scroll type expander, a chiller, an electric heater, an expansion vessel and a fluid recovery heat exchanger. Components of the system are listed below:

- Scroll type expander
- Process pumps
  - (i) Feed pump
  - (ii) Heat transfer oil pump
- Heat exchangers
  - (i) Evaporator
  - (ii) Condenser
  - (iii) Recuperator
  - (iv) Pre-cooler
- Throttle valves
- Heater
- Chiller
- Dynamometer
- Pressure vessels
  - (i) Liquid collector
  - (ii) Expansion vessel
- Fluid recovery heat exchanger
- Sensors

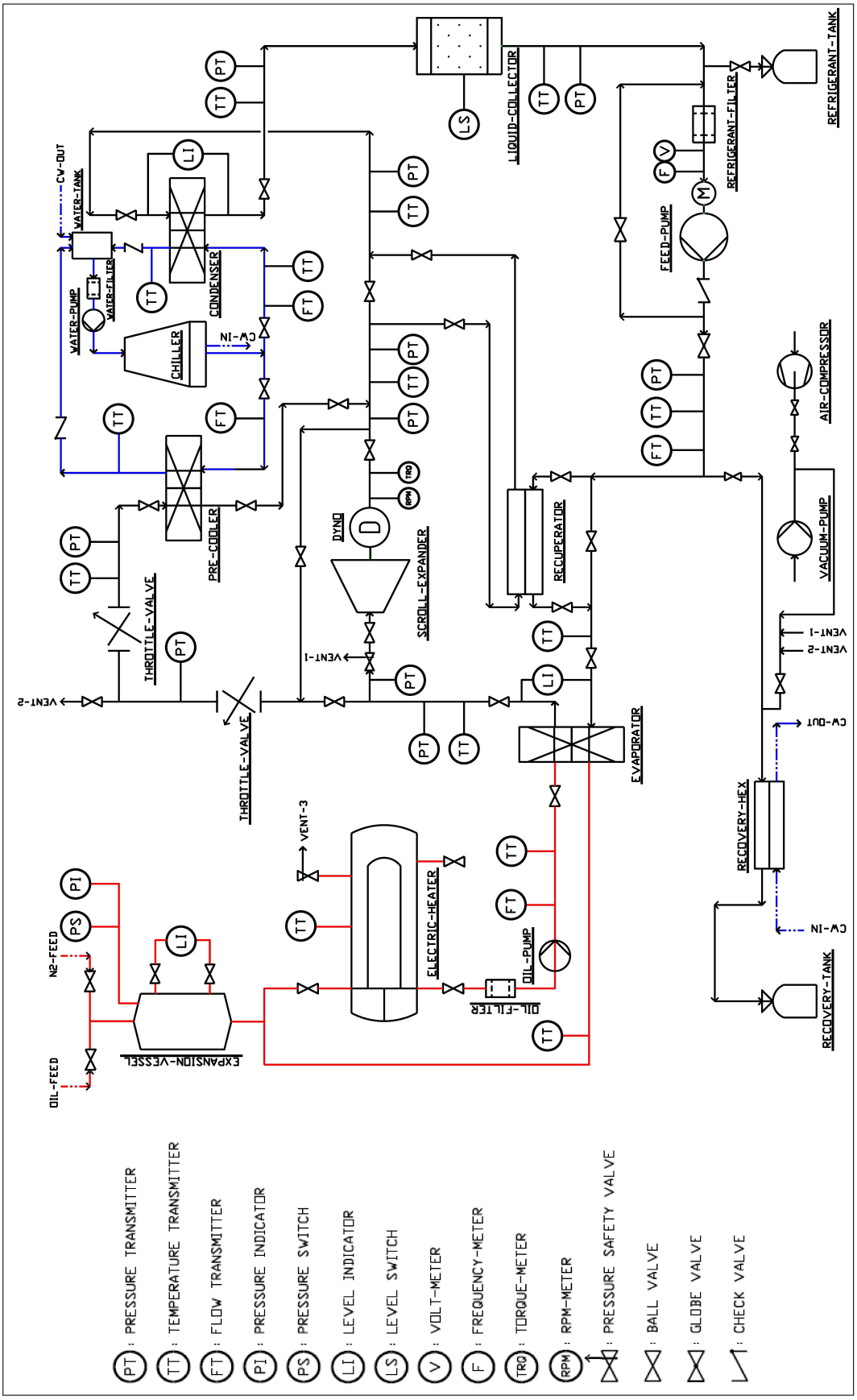


Figure 4.1. P&ID of the ORC.

Components of the system are divided into three groups namely main equipment, balance of plant, and sensors & data acquisition. After performance analyses of the proposed ORC and heat exchangers are completed, piping and instrumentation diagram (P& ID) of the cycle is drawn and indicated in Figure 4.1. Here, the process starts with the feed pump that pressurizes the liquid working fluid and transfers it to the evaporator. At the evaporator, liquid working fluid turns into vapor and goes into expander in order to expand and lose its enthalpy. A expander simulator, which consists of two throttle valves and a heat exchanger called pre-cooler, is designed and implemented on the skid to simulate the expander. Expanded vapor goes into the condenser to create a liquid phase at the pump suction and forms a closed-loop system.

## 4.1. Main Equipment

Main equipment basically consists of a scroll expander, a feed pump, throttle valves and heat exchangers such as evaporator, condenser, recuperator and pre-cooler.

### 4.1.1. Scroll expander

A scroll expander is a positive displacement machine that expansion is achieved by relative contact between two spiral curves. The gap between two curves starts to decrease as one curve moves relative to the other. As it mentioned before, scroll type expanders are widely used in small scale power generation cycles, because of its lower rotational speed, lower flow rate, proportionally less windage loss, and potentially lower cost due to the availability.

E25H074A-SH coded semi-hermetic oil-free scroll expander is purchased from a company named Air Squared, Inc. in the United States. Specifications of the scroll type expander are given in Table 4.1. Installed scroll type expander is shown in Figure 4.2 and section drawing of the expander is given in Appendix A.

Table 4.1. Specifications of the scroll type expander.

| Fluid Type | Working Fluid |
|---|---|
| Mass Flow Rate (kg/s) | 0.45 |
| Maximum Pressure (bar) | 10 |
| Maximum Temperature (°C) | 160 |
| Vapor Quality (inlet/outlet) | 1/1 |
| Maximum Shaft Speed (rpm) | 2600 |
| Nominal Power Output (kW) | 10 |
| Volume Ratio (Outlet/Inlet) | 2 |
| Displacement ($cm^3$/rev.) | 420 |
| Nominal Sound Level (dB(A)) | 65 |

Figure 4.2. Installed scroll type expander on ORC test rig.

### 4.1.2. Feed pump

Feed pump pressurizes and transfers the working fluid from the condenser outlet to the evaporator inlet through a pipe structure. Speck Pumpen SK 2007-LL model side channel pump is selected for this closed-loop cycle. Side channel pump is a combination of positive displacement and centrifugal types that enables to pressurize both liquids and little amount of gasses. At the start-up process, the pump acts like a positive displacement pump because of its self-priming capability; however, then it shows the characteristics of a centrifugal pump when the channels are filled with liquid.

The advantage of the side channel pump is that it can transfer both gas and fluid without damaging the bearings due to dry running, which makes them favorable. Although they can transfer both phases of a fluid from a particular time, liquid collector is designed and mounted on the pump suction pipeline to prevent damage due to dry running for a long time.

A by-pass line with a globe valve is added at the discharge of the pump to adjust the mass flow rate. Additionally, a frequency converter is installed on the cycles control panel to be able to vary the rotational speed by varying the AC motor input frequency for possible future experiments. Specifications and the image of the installed side channel pump is given in Table 4.2 and Figure 4.3. Section drawing of the side channel pump is given in Appendix B.

Table 4.2. Specifications of the feed pump.

| | |
|---|---|
| Fluid Type | R134a |
| Mass Flow Rate (kg/s) | 0.45 |
| Operational Pressure (bar) | 19 |
| Operational Temperature (°C) | 14 |
| Vapor Quality (inlet/outlet) | 0/0 |
| Required Shaft Speed (rpm) | 1450 |
| Nominal Power (kW) | 1.8 |
| Total Efficiency (%) | 23 |
| NPSH (m) | 1.6 |

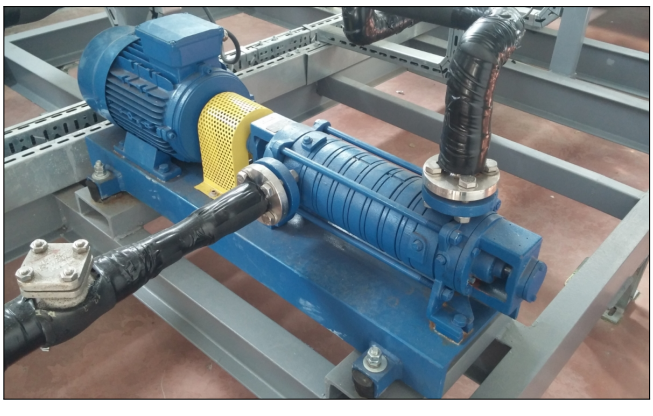

Figure 4.3. Installed side channel pump on ORC test rig.

### 4.1.3. Evaporator

Evaporator is a basic heat exchanger that enables heat transfer one medium to another in order to change the liquid phase into gaseous of a fluid. Plate type heat exchanger is used to evaporate the working fluid in this proposed ORC. They are formed of thin plates which are made of sheet metals with flow channels and widely used in low operating pressure and temperature applications. Besides high availability and economic to purchase, the most important factor for taking into consideration of a plate type heat exchanger is that they supply more heat transfer area than the others.

MB-09-80-H coded brazed type heat exchanger is acquired for this process. It has 80 plates which correspond to 7.4 $m^2$ total heat transfer area. One region of the evaporator is the working fluid side where the working fluid is heated and vaporized. On the other hand, another region is the heat transfer fluid side where the heat transfer oil is cooled down. Counter-flow is selected as the flow type to increase exchanger efficiency. Specifications of the evaporator for simple ORC are listed below in Table 4.3. Image of the installed brazed type heat exchangers is shown in Figure 4.5 and section drawing of the acquired heat exchangers is shown in Appendix D.

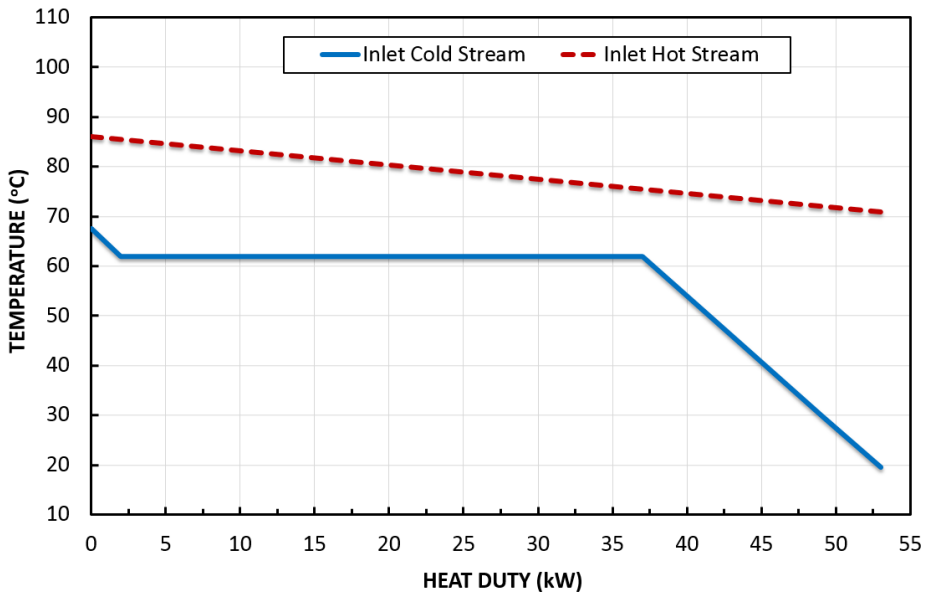


Figure 4.4. T-Q curves of the evaporator.

Table 4.3. Evaporator performance and geometry results.

| | Hot Side (Inlet-Outlet) | | Cold Side (Inlet-Outlet) | |
|---|---|---|---|---|
| Total mass flow rate (kg/s) | 1.6 | | 0.25 | |
| Vapor mass flow rate (kg/s) | 0 | 0 | 0 | 0.25 |
| Liquid mass flow rate (kg/s) | 1.6 | 1.6 | 0.25 | 0 |
| Vapor mass quality | 0 | 0 | 0 | 1 |
| Temperature (°C) | 86 | 70.9 | 19.5 | 67.5 |
| Pressure (bar) | 2 | 1.90 | 18 | 17.99 |
| Heat transfer coeff. (mean) ($W/m^2K$) | 654.5 | | 1301.6 | |
| Overall coeff. (dirty/clean) ($W/m^2K$) | 374.4 / 429.7 | | | |
| Prandtl Numbers | 141.48 | 215.26 | 3.61 | 1.05 |
| Reynolds Numbers | 47.19 | 29.84 | 270.63 | 3894.56 |
| Fouling resistance ($m^2K/W$) | 0.00017 | | 0.00017 | |
| Velocity (Port/Plate) (m/s) | 0.99 / 0.14 | | 1.42 / 0.2 | |
| Wall shear stress (mean) ($N/m^2$) | 22.34 | | 0.14 | |
| Port Pressure drop (bar) | 0.0055 | | 0.00067 | |
| Channel Pressure drop (bar) | 0.0966 | | 0.00307 | |
| Total Pressure drop (bar) | 0.1021 | | 0.00374 | |
| Residence volume ($m^3$) | 0.0064 | | 0.0065 | |
| Residence time (s) | 3.33 | | 4.37 | |
| Total heat exchanged (kW) | 53 | | | |
| Effective surface area ($m^2$) | 7.4 | | | |
| Effective MTD (°C) | 19.18 | | | |
| Total plate number | 80 | | | |
| Plate length / width (mm) | 615 / 188 | | | |
| Plate pitch / thickness (mm) | 2.4 / 0.5 | | | |
| Port diameter (mm) | 50 | | 50 | |
| Chevron angle (Degrees) | 30 | | 30 | |

### 4.1.4. Condenser

Condenser is a heat exchanger that enables heat transfer one medium to another in order to change the gaseous phase into liquid phase of the working fluid. Similarly to evaporator, plate type heat exchanger is used to condensate the working fluid.

Figure 4.5. Installed brazed type heat exchanger on ORC test rig.

MB-09-66-H coded brazed type heat exchanger is selected to condense the expanded vapor at the expander outlet. It has 66 plates which correspond to 6.1 $m^2$ total heat transfer area. Cooling water mass flow rate is specified as 3 kg/s with the temperature difference of 6.5 °C. One region is the working fluid side where working fluid is cooled and condensed, on the other hand, another region is the cooling water side where cooling water is heated up. Counter-flow is selected as the flow type to increase exchanger efficiency. Specifications of the condenser for simple ORC are listed below in Table 4.4.

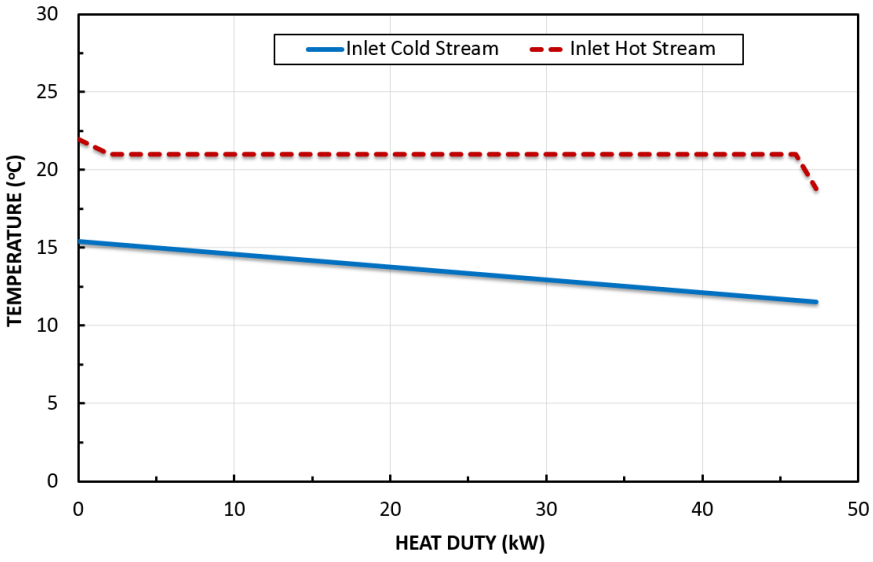


Figure 4.6. T-Q curves of the condenser.

Table 4.4. Condenser performance and geometry results.

| | Hot Side (Inlet-Outlet) | | Cold Side (Inlet-Outlet) | |
|---|---|---|---|---|
| Total mass flow rate (kg/s) | 0.25 | | 2.7 | |
| Vapor mass flow rate (kg/s) | 0.25 | 0 | 0 | 0 |
| Liquid mass flow rate (kg/s) | 0 | 0.25 | 2.7 | 2.7 |
| Vapor mass quality | 1 | 0 | 0 | 0 |
| Temperature (°C) | 22 | 18.8 | 11.5 | 15.37 |
| Pressure (bar) | 6 | 5.99 | 2 | 1.85 |
| Heat transfer coeff. (mean) ($W/m^2K$) | 1946.5 | | 7749.7 | |
| Overall coeff. (dirty/clean) ($W/m^2K$) | 973.4/ 1481.3 | | | |
| Prandtl Numbers | 0.84 | 3.67 | 9.69 | 8.72 |
| Reynolds Numbers | 5999.1 | 335.4 | 609.6 | 670.5 |
| Fouling resistance ($m^2K/W$) | 0.00018 | | 0.00018 | |
| Velocity (Port/Plate) (m/s) | 4.45 / 0.76 | | 1.37 / 0.23 | |
| Wall shear stress (mean) ($N/m^2$) | 5.3 | | 25.9 | |
| Port Pressure drop (bar) | 0.00189 | | 0.01238 | |
| Channel Pressure drop (bar) | 0.0104 | | 0.13883 | |
| Total Pressure drop (bar) | 0.01229 | | 0.15121 | |
| Residence volume ($m^3$) | 0.0053 | | 0.0054 | |
| Residence time (s) | 1.18 | | 2.01 | |
| Total heat exchanged (kW) | 47.3 | | | |
| Effective surface area ($m^2$) | 6.1 | | | |
| Effective MTD (°C) | 8.03 | | | |
| Total plate number | 66 | | | |
| Plate length / width (mm) | 615 / 188 | | | |
| Plate pitch / thickness (mm) | 2.4 / 0.5 | | | |
| Port diameter (mm) | 50 | | 50 | |
| Chevron angle (Degrees) | 30 | | 30 | |

### 4.1.5. Recuperator

A recuperator is used to increase the efficiency of the cycle by decreasing evaporators heat duty. At first, the working fluid is pressurized by the feed pump as usual. Then, before it gets into the evaporator, working fluid is preheated by the waste heat of the expanded vapor. The expanded vapor is cooled by losing its enthalpy. Besides, the recuperator increases the cycle performance, it also decreases the heat duty of the condenser as well.

MB-09-66-H coded brazed type heat exchanger with 66 plates, which correspond to 6.08 $m^2$ total heat transfer area, is acquired likewise condenser. Specifications of the recuperator are listed below in Table 4.5.

The cold fluid inlet and the hot fluid outlet are closed to each other for two reasons. Former one is that hot fluid has vapor phase while cold fluid has liquid phase. Latter one is that the recuperator is designed to supply 5 °C temperature difference between cold fluid outlet and hot fluid inlet.

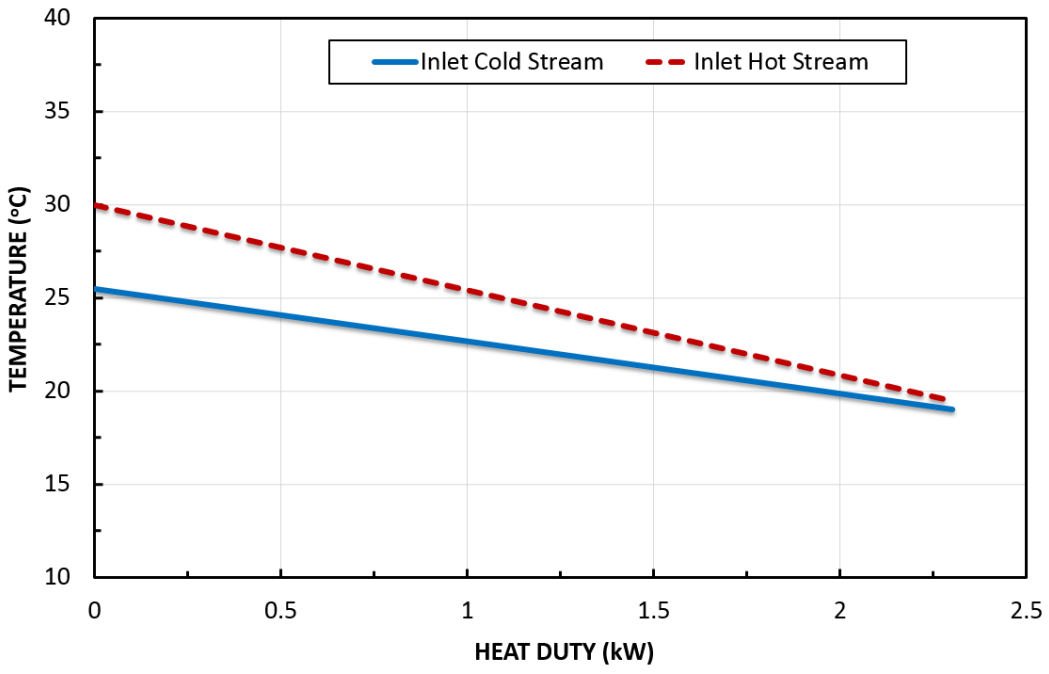


Figure 4.7. T-Q curves of the recuperator.

Table 4.5. Recuperator performance and geometry results.

| | Hot Side (Inlet-Outlet) | | Cold Side (Inlet-Outlet) | |
|---|---|---|---|---|
| Total mass flow rate (kg/s) | 0.25 | | 0.25 | |
| Vapor mass flow rate (kg/s) | 0.25 | 0.25 | 0 | 0 |
| Liquid mass flow rate (kg/s) | 0 | 0 | 0.25 | 0.25 |
| Vapor mass quality | 1 | 1 | 0 | 0 |
| Temperature (°C) | 30 | 19.5 | 19 | 25.5 |
| Pressure (bar) | 6 | 5.97 | 18 | 17.99 |
| Heat transfer coeff. (mean) ($W/m^2K$) | 414.1 | | 502.9 | |
| Overall coeff. (dirty/clean) ($W/m^2K$) | 208.9 / 225.5 | | | |
| Prandtl Numbers | 0.83 | 0.84 | 3.62 | 3.55 |
| Reynolds Numbers | 5854.8 | 6045.1 | 326 | 353.2 |
| Fouling resistance ($m^2K/W$) | 0.00018 | | 0.00018 | |
| Velocity (Port/Plate) (m/s) | 4.63 / 0.8 | | 0.11 / 0.02 | |
| Wall shear stress (mean) ($N/m^2$) | 5.6 | | 0.2 | |
| Port Pressure drop (bar) | 0.00376 | | 0.00009 | |
| Channel Pressure drop (bar) | 0.02895 | | 0.00112 | |
| Total Pressure drop (bar) | 0.03271 | | 0.00121 | |
| Residence volume ($m^3$) | 0.0053 | | 0.0054 | |
| Residence time (s) | 0.6 | | 26.3 | |
| Total heat exchanged (kW) | 2.3 | | | |
| Effective surface area ($m^2$) | 6.1 | | | |
| Effective MTD (°C) | 1.85 | | | |
| Total plate number | 66 | | | |
| Plate length / width (mm) | 615 / 188 | | | |
| Plate pitch / thickness (mm) | 2.4 / 0.5 | | | |
| Port diameter (mm) | 50 | | 50 | |
| Chevron angle (Degrees) | 30 | | 30 | |

### 4.1.6. Expander simulator

A expander simulator which consists of two throttle valves and a pre-cooler is designed and implemented to the cycle to simulate the expander in the commissioning process and to protect expander from running with vapor and liquid states together.

Figure 4.8. Installed throttle valve on ORC test rig.

Throttles are pressure regulating valves that reduce the pressure of a fluid regardless of changing the mass flow rate and/or varying inlet pressure. Pressure drop through a throttle valve is an isenthalpic process since the enthalpy difference between inlet and outlet is the same and there is no work done on the control volume. Two different models in terms of pressure grades (high pressure to middle pressure and middle pressure to low pressure) are used to regulate the pressure before the working fluid goes into pre-cooler, hence controlling the pressure drop without any oscillation would be accomplished. Depend on the desired outlet pressure, they can be used together or separately. The image of a throttle valve is shown in Figure 4.8.

Pre-cooler is used to cool the working fluid only in case of the throttles are operating. Outlet nozzle of the pre-cooler is attached to the inlet nozzle of the condenser where the condensation process occurs.

Table 4.6. Pre-cooler performance and geometry results.

| | Hot Side (Inlet-Outlet) | | Cold Side (Inlet-Outlet) | |
|---|---|---|---|---|
| Total mass flow rate (kg/s) | 0.25 | | 0.02 | |
| Vapor mass flow rate (kg/s) | 0.25 | 0.25 | 0 | 0 |
| Liquid mass flow rate (kg/s) | 0 | 0 | 0.02 | 0.02 |
| Vapor mass quality | 1 | 1 | 0 | 0 |
| Temperature (°C) | 30 | 22.5 | 11.5 | 29.9 |
| Pressure (bar) | 6 | 5.95 | 2 | 1.99 |
| Heat transfer coeff. (mean) ($W/m^2K$) | 524 | | 540.6 | |
| Overall coeff. (dirty/clean) ($W/m^2K$) | 241.4/ 263.8 | | | |
| Prandtl Numbers | 0.83 | 0.84 | 9.69 | 6.05 |
| Reynolds Numbers | 7806.4 | 7985.6 | 5.9 | 9.1 |
| Fouling resistance ($m^2K/W$) | 0.00018 | | 0.00018 | |
| Velocity (Port/Plate) (m/s) | 4.63 / 1.06 | | 0.01 / 0.01 | |
| Wall shear stress (mean) ($N/m^2$) | 9.4 | | 0.1 | |
| Port Pressure drop (bar) | 0.00357 | | 0 | |
| Channel Pressure drop (bar) | 0.04907 | | 0.00011 | |
| Total Pressure drop (bar) | 0.05263 | | 0.00011 | |
| Residence volume ($m^3$) | 0.004 | | 0.004 | |
| Residence time (s) | 0.44 | | 203.9 | |
| Total heat exchanged (kW) | 1.7 | | | |
| Effective surface area ($m^2$) | 4.6 | | | |
| Effective MTD (°C) | 1.53 | | | |
| Total plate number | 50 | | | |
| Plate length / width (mm) | 615 / 188 | | | |
| Plate pitch / thickness (mm) | 2.4 / 0.5 | | | |
| Port diameter (mm) | 50 | | 50 | |
| Chevron angle (Degrees) | 30 | | 30 | |

MB-09-50-H coded brazed type heat exchanger with 50 plates which correspond to 4.6 $m^2$ total heat transfer area is selected for application. Specifications of the pre-cooler are listed below in Table 4.6.

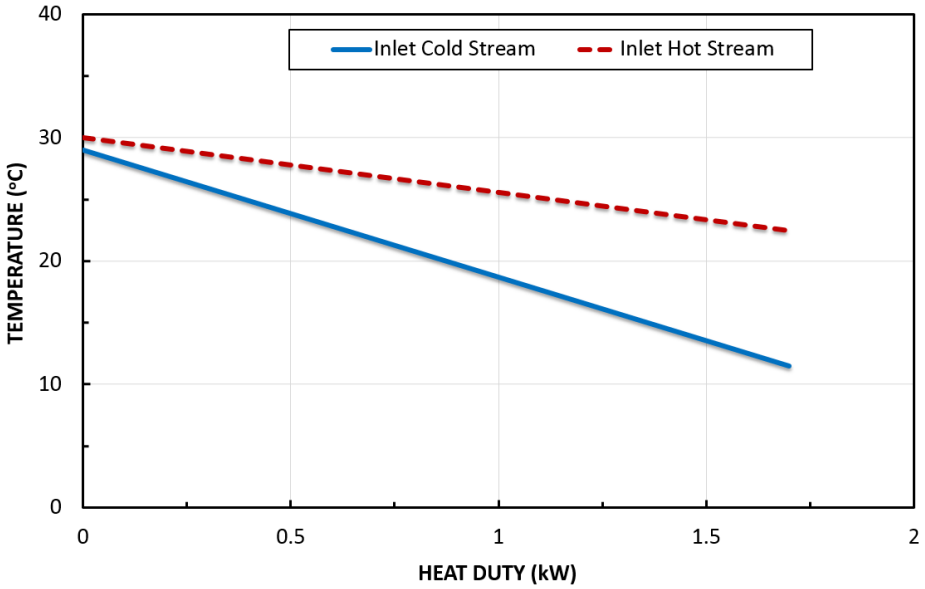


Figure 4.9. T-Q curves of the pre-cooler.

## 4.2. Balance of Plant

### 4.2.1. Heater

The cycle needs a heat source to increase the temperature of the liquid working fluid above its boiling point for corresponding pressure. Generally, in organic Rankine cycle applications; solar, waste heat, biomass or geothermal sources are used for heating up the medium through a heat exchanger unit. Although a parabolic trough collector is established in the BURET Laboratory's open front area, an electric heater is used as the heat source for the commissioning process.

The electric heater on the ORC setup has a maximum capacity of 107 kW. It consists of a boiler vessel which has 'U' shape stainless steel rods inside covered with baffles. The heat transfer fluid runs through the boiler vessel and heats up via these rods. A K-type thermocouple and a relief valve were located on the pre-decided shell surface. To control the heater system, three-phase power unit with PID control is integrated. The image of the heater is shown in Figure 4.10. Datasheet of the heater and section drawing of the designed boiler vessel are indicated in Appendix E and F.


Figure 4.10. Installed heater on ORC test rig.

### 4.2.2. Heat transfer oil pump

Heat transfer oil pump is used for transferring heat transfer oil from the electrical heater towards the evaporator. King Integral CC-2214 model gear pump is selected for circulating the oil at a specified constant pressure.

Gear pumps are positive displacement rotary pumps that transport liquids using rotating gears. They consist of a couple of external and internal spur gears to move constant amount of fluid for each revolution. Gear pumps are compact and high-pressure pumps which provide a steady and pulseless flow. They are generally used with high viscosity fluids. Specifications of the internal gear pump are given in Table 4.7. Image of the installed internal gear pump is given in Figure 4.11 and the section drawing of the internal gear pump is given in Appendix C.

Table 4.7. Specifications of the internal gear pump.

| Fluid Type | Heat Transfer Oil |
|---|---|
| Mass Flow Rate (kg/s) | 1 |
| Operational Pressure (bar) | 2 |
| Operational Temperature (°C) | 155 |
| Vapor Quality (inlet/outlet) | 0/0 |
| Required Shaft Speed (rpm) | 1140 |
| Nominal Power (kW) | 0.6 |
| Isentropic Efficiency (%) | 93 |
| Mechanical Efficiency (%) | 32 |
| NPSH (m) | 1.85 |

Figure 4.11. Installed internal gear pump on ORC test rig.

### 4.2.3. Expansion Vessel

An expansion vessel is installed on the heat transfer oil process line to take the expansion of hot oil caused by the temperature increase between start-up and steady-state conditions. It protects the pipelines and components from being failed by over pressurization. A level gauge is installed to monitor the expanded heat transfer oil amount. The tank is filled with nitrogen with approximately 4 bar pressure. A pressure switch is also installed to control the pressure inside the tank. If the pressure exceeds the design pressure which is 5 bar, pressure switch will be activated, hence the heater and the heat transfer oil pump will be turned off as a safety precaution.

The image of the expansion vessel is given in Figure 4.12 and section drawing of the expansion vessel is indicated in Appendix H.

Figure 4.12. Installed expansion vessel on ORC test rig.

### 4.2.4. Chiller

Vaporization and condensation of the working fluids are indispensable for ORCs. The cycle needs a cooling source to reject the heat of the expanded vapor, therefore, supply liquid for the feed pump so it can operate properly. An air cooled chiller which had two hermetic scroll-type compressors inside was integrated into the system to supply cooled water for both condenser and pre-cooler.

A chiller with a maximum heat load of 107 kW is selected based on the thermodynamic analysis. Specifications of the chiller are listed below in Table 4.8 and the image of the chiller alone is shown in Figure 4.13.

Table 4.8. Specifications of the chiller.

| | |
|---|---|
| Maximum cooling capacity (kW) | 107 |
| Compressor type | Hermetic scroll |
| Number of compressors | 2 |
| Evaporator type | Shell & tube |
| Water volumetric flow rate in evaporator ($m^3/h$) | 18.5 |
| Power supply | 400 V/3 phz/50 Hz |
| Number of fans | 2 |
| Air volumetric flow rate at fans ($m^3/h$) | 34500 |
| Pump nominal power (kW) | 4 |
| Water tank volume (lt) | 350 |

Figure 4.13. Installed chiller on ORC test rig.

### 4.2.5. Dynamometer

A dynamometer is used for measuring the obtainable power from expander with simultaneous torque and angular velocity data processing from installed sensors. Dynamometer and expander are connected via magnetic coupling. Since the power equals to torque times angular velocity, net power output can be found.

With a software integrated into the expander & dynamometer control unit, rotational speed can be adjusted constantly. The image of the dynamometer is shown in Figure 4.14.

Figure 4.14. Installed dynamometer on ORC test rig.

### 4.2.6. Liquid collector

A liquid collector is designed to prevent gaseous phase at the suction line of the feed pump. Even the side channel type feed pump can work with relatively low vapor and liquid mixtures, it is better to use liquid collector to extend the impellers operating life. Additionally, a vibronic type level switch is installed on the liquid collector to shut down the feed pump if any vapor phase is occurred. Section drawing of the liquid collector is indicated in Appendix G.

Figure 4.15. Installed liquid collector on ORC test rig.

### 4.2.7. Fluid recovery exchanger

Fluid recovery exchanger is designed to prevent the vapor working fluid releasing into atmosphere through a pressure safety valve. With the opening of the safety valve, over pressurized working fluid flows through the fluid recovery exchanger, which is mounted outside of the laboratory. Here, the fluid is cooled, changed its vapor phase into liquid and collected into an accumulation tank. In order to cool down the fluid, cooling water supplied by the chiller is used. Section drawing of the fluid recovery exchanger is indicated in Appendix I.

Figure 4.16. Installed fluid recovery exchanger on ORC test rig.

## 4.3. Sensors and Data Acquisition

Sensors supply not only diagnostic data from the cycle, but also give some control parameters. Via the data acquisition system, all sensor outputs can be measured, read, and saved. In this cycle, ten pressure and thirteen temperature sensors are installed. Four flowmeters of which two of them are electromagnetic type for the cooling circuit, one vortex-type for the heating circuit and one coriolis-type for the working fluid circuit is acquired. They measure volumetric flow rate except coriolis, which measures mass flow rate, instead. There is a vibronic type level switch installed on the liquid collector in order to stop the working fluid pump when there is a gas phase. Additionally, a pressure switch is installed on the expansion vessel in order to shut down the heater and the heat transfer oil pump, thus keep the cycle in safe region if the heat transfer oil temperature rises above the design temperature.

Pressure and temperature transmitters are mounted on the pre-decided locations along the process lines with tee connections as shown in P&ID. With regard to temperature transmitter installation, the immersion length of the transmitter is taken into consideration for the best accuracy. On the flowmeter side, electromagnetic and vortex types have some restrictions regarding the pipe sections. When installing a vortex-type flowmeter, particular dimensions must be supplied. Besides, these required dimensions vary from the pipe section whether straight or elbowed. Installation of electromagnetic flowmeters also requires some specifications but only for the pipe sections with elbows. However, coriolis flowmeter does not require any installation specifications since it measures mass flow rate instead of volumetric flow rate. Figures 4.17 to 4.19 show the recommended installation procedures for electromagnetic and vortex flowmeters.

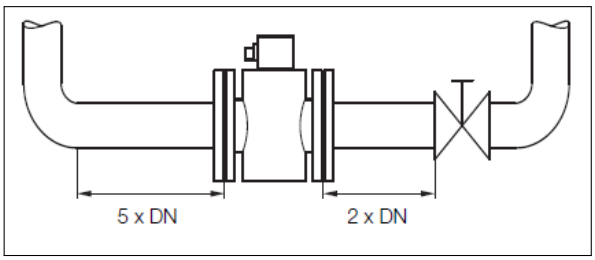


Figure 4.17. Installation specifications of electromagnetic flowmeter for pipe sections with elbows.

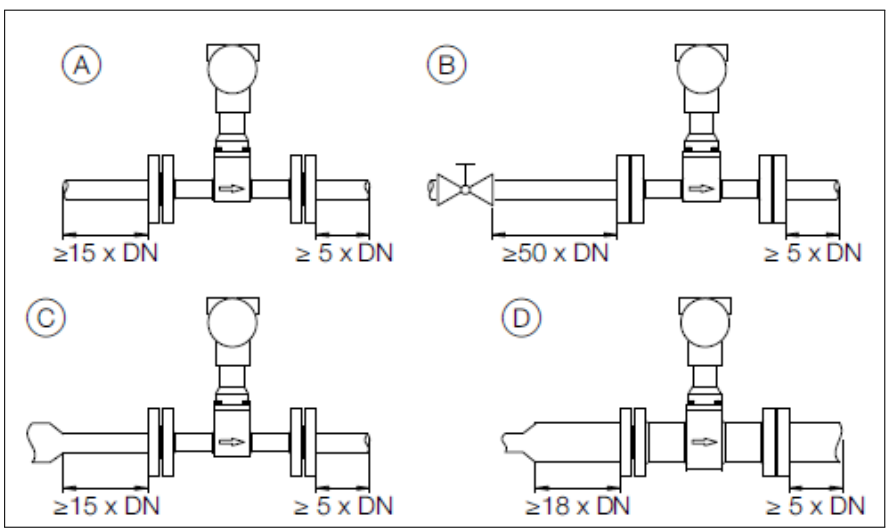


Figure 4.18. Installation specifications of vortex flowmeter for straight pipe sections.

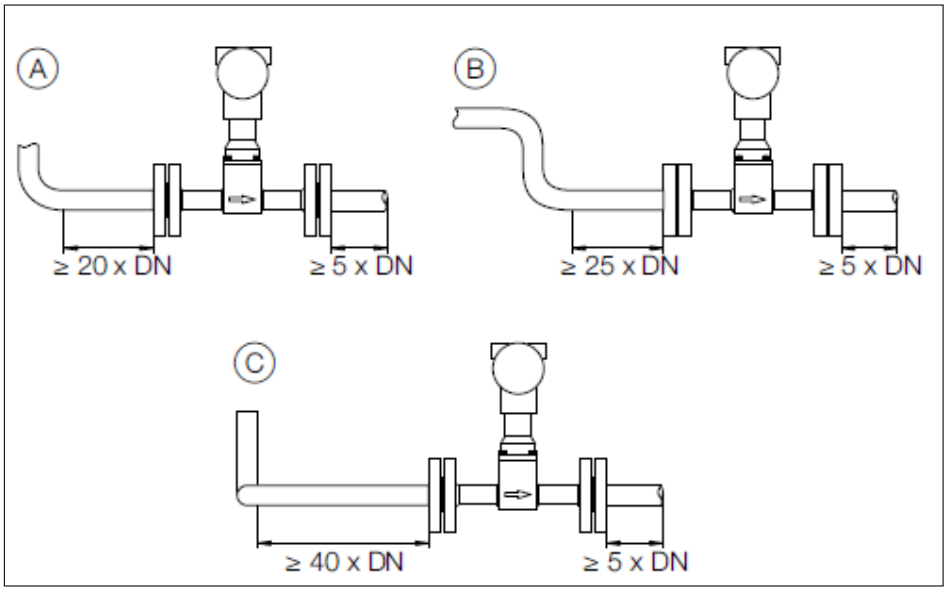


Figure 4.19. Installation specifications of vortex flowmeter for pipe sections with elbows.

Specifications of the sensors are listed below in Table 4.9. Images of pressure and temperature transmitters, electromagnetic, vortex and coriolis flowmeters are shown in Figure 4.20.

Table 4.9. Specifications of the sensors.

| | Temperature transmitters | Pressure transmitters | Flowmeters | Level switch | Pressure switch |
|---|---|---|---|---|---|
| Quantity | 10 | 13 | 4 | 1 | 1 |
| Type | RTD | Piezoresistive | Coriolis: 1<br>Electromagnetic: 2<br>Vortex: 1 | Vibronic | - |
| Range of measurement | 0-60°C for 7 transmitter<br>(Low-temperature pipelines)<br>0-250°C for 6 transmitter<br>(High-temperature pipelines) | 0-10 bar for 6 transmitter<br>(Low-pressure pipelines)<br>0-40 bar for 4 transmitter<br>(High-pressure pipelines) | Coriolis: 0-3600 kg/h<br>Electromagnetic 1: 0-25 $dm^3/s$<br>Electromagnetic 2: 0-75 $dm^3/s$<br>Vortex: 0-125 $m^3/h$ | - | - |
| Accuracy of measurement | ±0.3 | ±0.1% | Coriolis: ±0.4%<br>Electromagnetic 1,2: ±0.4%<br>Vortex: ±0.65% | - | - |
| Fluid type | WF, HTO, CW | WF | Coriolis: WF<br>Electromagnetic 1,2: CW<br>Vortex: HTO | WF | HTO |
| Desing Pressure (bar) | 40 | 0-30 bar for 6 transmitter<br>0-100 bar for 4 transmitter | Coriolis: 40<br>Electromagnetic: 10<br>Vortex: 10 | 40 | 10 |
| Desing Temperature (°C) | 250 | 150 | 160 | 100 | 170 |

(a) Temperature (left) and pressure (right) transmitters


(b) Coriolis flowmeter


(c) Electromagnetic flowmeter

(d) Vortex flowmeter


(e) Pressure switch

(f) Level switch

Figure 4.20. Installed transmitters and flowmeters.

Data Acquisition system is integrated into the ORC setup to monitor and save the data acquired from the measurement devices. Moreover, a basic control algorithm is added inside the modules that enables to shut down the components such as heater, feed pump, and heat transfer pump; and to vary the shaft rotational speed of the feed pump through changing its AC motor input frequency by an installed frequency converter. All the data is transferred via four IPETRONIK 'M-SENS 8' and one 'M-SENS 4' modules to a data acquisition computer.

Specifications of the M-SENS module is given in Table 4.10 and image of the M-SENS module is indicated in Figure 4.21.

Table 4.10. Specifications of the data acquisition modules.

| | |
|---|---|
| Measurement ranges | Covering input signals 0.1 V to 100 V |
| Input voltage (IN+ $\leftrightarrow$ IN−) | max. ± 100 V, short time (1 ms) ± 200 V |
| Channel sample rates | 1/ 2/ 5/ 10/ 50/ 100/ 200/ 500/ 1000/ 2000 Hz |
| Voltage supply | 12, 24, 36 $V_{DC}$ automotive power supply systems<br>Switch-off for voltage <6 V |
| Power consumption | 3.5 W |
| Working temperature range | -40 °C ... +125 °C |
| Storage temperature range | -55 °C ... +150 °C |
| IP-code | IP 67 (ISO 20653 - 2013) |
| Dimensions | W204 mm x H41 mm x D55 mm |

Figure 4.21. Installed M-SENS module on ORC test rig.

After performance analyses of the proposed ORC and heat exchangers are completed, piping and instrumentation diagram (P& ID) of the cycle is drawn and the 3D modeling of the system is generated. 3D layout model of the ORC is shown in Figure 4.22 and image of the proposed ORC system is indicated in Figure 4.23.

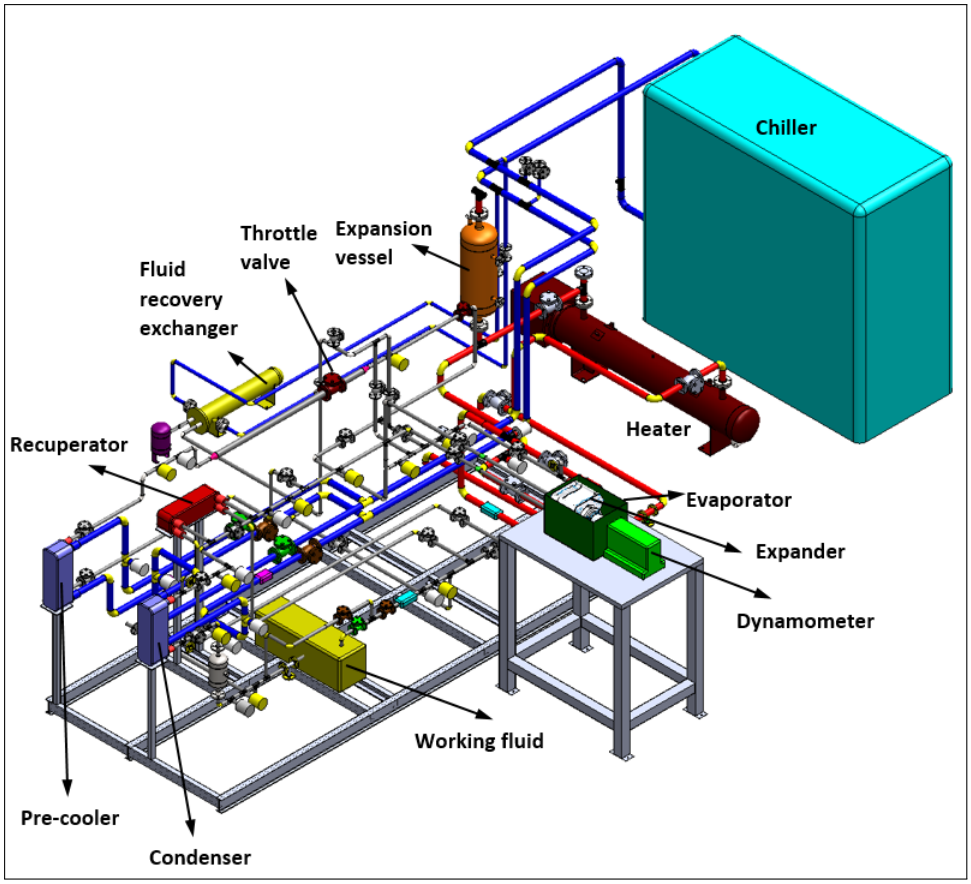


Figure 4.22. 3D model of the proposed ORC.

Figure 4.23. Image of the proposed ORC.

# 5. COMMISSIONING AND PRELIMINARY TESTING

Commissioning procedures are vital since the reaction of the process of disturbances is unknown due to unsteady-state conditions. A well-prepared commissioning can save time and minimize the capital cost; however, the most important outcome is the reduction of risk of unplanned outages. In organic Rankine cycle applications, it is even more significant since it involves an organic fluid in the process. After the ORC test rig is manufactured, commissioning procedures are prepared in order to conduct preliminary tests for pre-determined cycle points indicated in the cycle analyses.

## 5.1. Procedures

At the beginning of the the commissioning procedures, the test rig was divided into three parts namely working fluid circuit, heating circuit, and cooling circuit. At first, a pre-commissioning procedure was prepared. All electrical and mechanical connections were supervised through this procedure. The pre-commissioning procedure is indicated in Table 5.1.

When all the requirements were fulfilled with regard to the pre-commissioning procedure, commissioning procedures were implemented afterwards. All divided three parts are examined, separately. Working fluid circuit procedure involves seventeen steps including hydrostatic pressure testing, drying, nitrogen pressure testing, vacuum testing, refrigerant filling, feed pump cold running, and draining some of the refrigerant for normal operation. Tables 5.2 to 5.4 shows the commissioning procedures regarding the working fluid, heating, and cooling circuits.

Hydrostatic pressure testing must be conducted to find out the leakages and eliminate them. A hand water pump is used to supply water to the working fluid circuit. After the leakages are eliminated, water is drained and air is supplied for drying. The reason is to create water-free volume for the working fluid. Because of the pipe pockets, the water could not be drained completely.

Table 5.1. Pre-commissioning procedure of the proposed ORC test rig.

| Step | Actions |
|---|---|
| 1 | Check grounding for skid-mounted equipment |
| 2 | Check electrical connections |
| 3 | Check pump rotations |
| 4 | Check piping connections |
| 5 | Check insulation |
| 6 | Check instrument signals |
| 7 | Check all valves to be in open position |
| 8 | Check level gauge valves to be in open position |
| 9 | Check direction of the check valves |
| 10 | Check relief valves cracking pressure adjustment |
| 11 | Check the emergency shut down |
| 12 | Check water level inside the water tank* |
| 13 | Put some anti-freeze inside of the water tank as corrosion inhibitor* |

*Only valid for cooling circuit.

Therefore, drying with compressed air shall be carried out in three different routes. After drying is completed, system is tested with pressurized nitrogen. The reason is to ensure there will not be any leakage issues since some of the working fluid circuit will be operated at gaseous phase. When the pressure test with nitrogen is completed, the nitrogen is vented and air vacuuming is conducted. The vacuum pump is connected to the ORC test rig via a ball valve, thus vacuuming is completed.

Fluid filling is the most important and challenging part of all because the amount of refrigerant must be adjusted properly. Additionally, there are certain pipelines that must involve certain phases such as at the pump suction; there must be liquid refrigerant while at the expander inlet and outlet; there must be vapor refrigerant. Testing will be carried out at different cycle design points for a given flow rate. Frequency inverter can change the revolution of the process pump, thus vary the head and flow rate. To supply constant flow rate, a by-pass line is created with two globe valves integrated into the system.

During the cold run process, all parts of the system should be full of liquid phase except pre-cooler, which will be kept half liquid phase as the precaution since it can act as a buffer for volume changes due to small temperature rises caused by environmental effects. Recuperator shall be completely isolated by surrounded valves. During the initial phase of the filling process, cooling water should not be circulated through pre-cooler. The aim is to carry out condensation solely in the condenser and fill the evaporator completely liquid. Meanwhile, level switch onto the liquid collector should be checked. The evaporator is filled with liquid refrigerant by using the elevation difference. Once the evaporator is fully filled, cooling water is permitted to flow through pre-cooler.

Table 5.2. Commissioning procedure of the working fluid circuit.

| Step | Actions |
|---|---|
| 1 | Fill water into the system and pressurize until the system reaches the design pressure |
| 2 | Observe and prevent the leakages |
| 3 | Dry the system with air |
| 4 | Pressurize the system with nitrogen |
| 5 | Observe and prevent the leakages |
| 6 | Vent the nitrogen and vacuum the system |
| 7 | Fill the refrigerant into the system |
| 8 | Start the feed pump cold run |
| 9 | Vary and adjust the frequency inverter |
| 10 | Check the coriolis flowmeter |
| 11 | Check the level on the level switch |
| 12 | Check the relief valve |
| 13 | Cross-check the indicators & computer readings |
| 14 | Determine feed pump performance by using frequency inverter and globe valves |
| 15 | Drain and recover some of the refrigerant |
| 16 | Start the feed pump for normal operation |
| 17 | Check the control module |

Following the cold run, some of the liquid phases should be drained and recovered since some parts of the cycle should be in gaseous phase during hot operation. Drain process is conducted with using two different valves that can allow recovering; one from the suction and the other from the discharge line of the feed pump.

Table 5.3. Commissioning procedure of the heating circuit.

| Step | Actions |
|---|---|
| 1 | Dry the system with air |
| 2 | Fill the heat transfer oil into the system |
| 3 | Vent the air from the highest elevation |
| 4 | Check oil level on the level switch |
| 5 | Check pressure in the expansion tank |
| 6 | Drain suction line and check & clean strainer filter |
| 7 | Fill oil enough to compensate drained amount |
| 8 | Set temperature of the heater resistance |
| 9 | Start the heat transfer oil hot run |
| 10 | Check oil level on the level switch |
| 11 | Check pressure in the expansion tank |
| 12 | Check the vortex flowmeter |
| 13 | Cross-check the indicators & computer readings |
| 14 | Check the control module |

Table 5.4. Commissioning procedure of the cooling circuit.

| Step | Actions |
|---|---|
| 1 | Dry the system with air |
| 2 | Check the water level inside at the water tank |
| 3 | Vent the air from the highest elevation |
| 4 | Set suction and discharge temperatures |
| 5 | Check electromagnetic flowmeters |
| 6 | Cross-check the indicators & computer readings |

Again, a part of liquid will be left in some parts due to piping pockets. Before starting the feed pump circulation, it is necessary to transfer this liquid phase to the suction line and fill the condenser with the liquid phase. In order to achieve this, gradual heating of the evaporator is carried out by circulating warm oil through the heat transfer oil side of the evaporator.

This will result in evaporation of the liquid inside the evaporator and thus push the liquid inside of the pre-cooler where cooling process drops the pressure and condenses the incoming gas. Inlet and outlet valves of the recuperator are opened so that it can operate. During normal operation, working fluid sides of the evaporator and pre-cooler shall be half liquid and half gaseous phase. Working fluid side of the condenser shall be almost full of liquid and regarding the recuperator, low temperature side shall be full of liquid and high temperature side shall be full of vapor phase only.

## 5.2. Cold Run of the System

Before the experiments were started, an error analysis is conducted. Enthalpy of R134a is directly calculated from REFPROP. Temprerature, pressure and mass flow rate values are measured via sensors and their accuracy is indicated Table 4.9. Heat input rate, net power output and cycle efficiency uncertainties are calculated via these related variables.

Table 5.5. Error analysis parameters.

| Parameter | Related variables | Average uncertainty |
|---|---|---|
| Enthalpy (h) | T, P | 1.7 % |
| Mass flow rate ($\dot{m}$) | * | 0.4 % |
| Heat input rate (kW) | $\dot{m}$, h | 3.8 % |
| Net power output (kW) | $\dot{m}$, h | 3.8 % |
| Cycle efficiency (%) | $\dot{W}_{net}$, $\dot{Q}_{in}$ | 7.6 % |

* : Depend on measurement accuracy.

In the testing process, each circuit was commissioned separately. Chiller system has a centrifugal type circulation pump. Therefore, it pressurizes the water only to overcome the piping structure friction and to circulate the close loop water cycle. In the water circuit, water outlet temperature can be set via chiller control unit and water flow rate can be adjusted via globe valves on the water pipeline. During the cooling circuit commissioning, obtained minimum water temperature was 0 °C with using ethylene glycol concentration as antifreeze material.

Heater system has a similar structure to chiller. Heat transfer oil outlet temperature can be set via heater control unit. A gear pump is used to pressurize the heat transfer oil. Since the gear pump supplies constant discharge pressure, outlet pressure is already set. There are globe valves on the heating circuit to adjust the flow rate. During the heating circuit commissioning, obtained maximum heat transfer oil temperature was 160 °C.

Working fluid circuit has a feed pump which works like centrifugal pumps most of the time. A by-pass line with a by-pass valve and a globe valve is mounted on the discharge line of the feed pump and a frequency inverter is installed inside the heater control unit to be able to adjust the flow rate. In any case, working fluid temperature is depend on the heater and chiller temperature.

Cold run of the working fluid circuit was conducted within a limited range. Mass flow rate can be adjusted between 0 to 0.45 kg/s; while, feed pump discharge pressure can be adjusted between 12 to 22 bar. The reason is that high pressure values are required at the expander inlet to obtain maximum obtainable power and cycle efficiency as predetermined in the selection of the cycle points section in Chapter 2.

Adjusting mass flow rate is the most challenging factor. By using globe valve on by-pass process line and by varying frequency inverter of the feed pump, mass flow rate was adjusted. Minimum pressure of the cycle is another challenging factor. By adjusting the throttle valve, minimum cycle pressure was adjusted. There are two throttle valves that can be used in the process depend on the process type. At high pressures, only one throttle valve should be used since it has a specific outlet pressure value which is 4. When low pressure operation is conducted, both of the throttle valves must be used to obtain low pressures lower than 4. Second throttle can decrease the pressure down to 0.8 bar. Cold run of the working fluid is shown in Figure 5.1

Feed pump motor frequency is varied in two case, %100 and %90 to obtain discharge pressure and mass flow rate values. Obtained data is indicated in Tables 5.6 and 5.7.

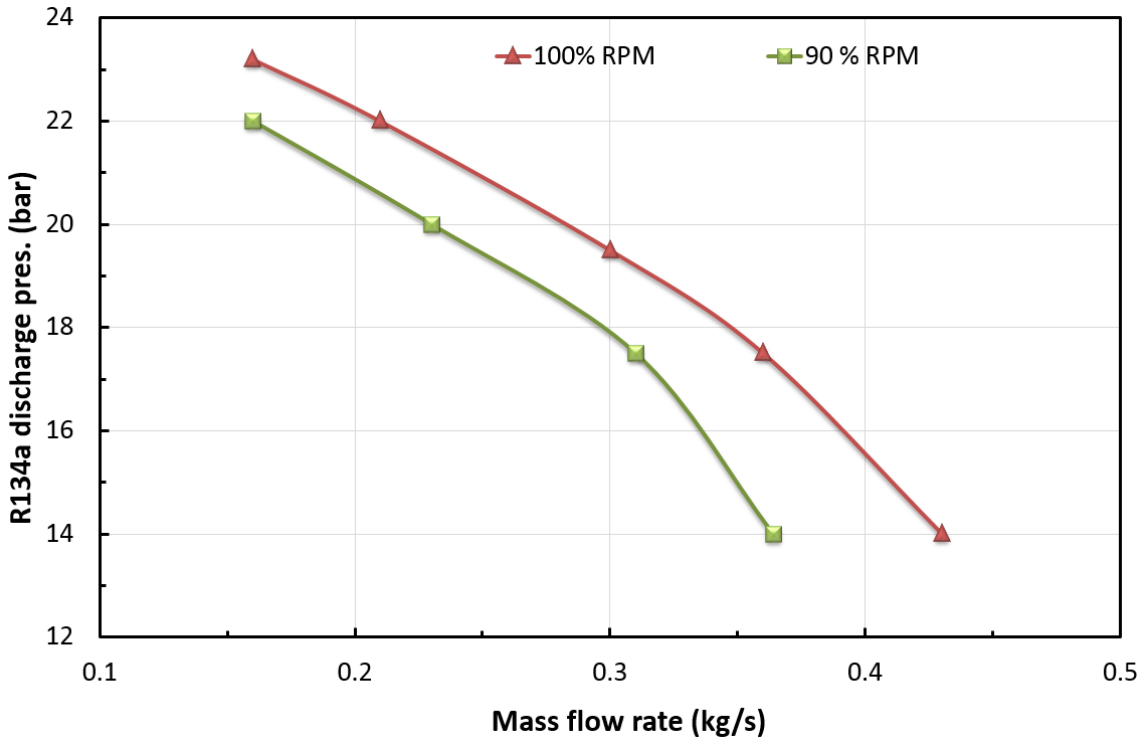


Figure 5.1. Feed pump cold run testing.

Table 5.6. Cold run testing with 100% pump motor frequency.

| Discharge pressure (bar) | Suction pressure (bar) | Temperature (°C) | Density (kg/m$^3$) | Mass flow rate (kg/s) | Shaft speed (rpm) |
|---|---|---|---|---|---|
| 14 | 7.1 | 22 | 1222 | 0.43 | 1426 |
| 17.5 | 7.8 | 32 | 1185 | 0.36 | 1426 |
| 19.5 | 7.6 | 32 | 1185 | 0.3 | 1426 |
| 22 | 7.3 | 22 | 1226 | 0.21 | 1426 |
| 23.2 | 7.3 | 22 | 1227 | 0.16 | 1426 |

Table 5.7. Cold run testing with 90% pump motor frequency.

| Discharge pressure (bar) | Suction pressure (bar) | Temperature (°C) | Density (kg/m$^3$) | Mass flow rate (kg/s) | Shaft speed (rpm) |
|---|---|---|---|---|---|
| 14 | 8.1 | 32 | 1184 | 0.38 | 1330 |
| 17.5 | 8.2 | 33 | 1181 | 0.31 | 1330 |
| 20 | 7.3 | 33 | 1183 | 0.23 | 1330 |
| 22 | 7.4 | 35 | 1176 | 0.16 | 1330 |

Tables 5.6 and 5.7 show that 0.25 kg/s mass flow rate is reachable up to 21 bar with 100 % feed pump motor frequency. In order to reach higher flow rate values, discharge pressure must be decreased. Likewise, in order to reach higher discharge pressures than 21 bar, working fluid mass flow rate must be decreased.

With respect to feed pump capability, three cases are prepared for detailed experimental investigation. Maximum pressure values are determined as 15, 18 and 21. In the start-up process, expander, one throttle valve, recuperator and simulator is isolated.

Detailed experimental procedure is prepared for start-up, actual testing and shut-down processes. Due to a filtration problem with the side channel pump, actual testing process cannot be completed on time. When the problem is solved, detailed experiments will be conducted. Experimental procedure and the testing simulation is indicated in Appendix J.

# 6. CONCLUSION

In this research, a laboratory scale ORC system was designed and constructed in Boğaziçi University's Renewable Energy Technologies Laboratory (BURET) in İstanbul, Turkey. An electric heater was considered as a simulation of renewable energy source and scroll-type expander was selected due to the small scale power requirement of the system. Environmental and safety characteristics are considered as the first step of the fluid selection; therefore, four fluids; R134a, R141b, R245ca and R245fa, are taken into consideration. R134a is adopted as the working fluid because of its good performance in small heat inputs, broad availability, and cost-effectiveness. A recuperator was implemented on the cycle to examine its effects on the ORC performance.

Steady-state analyses were conducted for the ORC system. A complete cycle simulation was run by modeling each component. Two different case results, simple and regenerative ORC, were obtained and compared in this study. Expander inlet pressure and the degree of superheat at the evaporator were the two main variables. Net power output and first law efficiency (cycle efficiency) were the two performance indicators. Theoretical results showed that cycle with recuperator gives higher maximum efficiency value than the simple ORC by 0.46% with respect to the same power output for R134a. Maximum power output, simple cycle and regenerative cycle efficiency were found to be 4.13 kW, 7.18% and 7.64%, respectively.

After the thermodynamic analysis, Piping and Instrumentation Diagram (P&ID) was created and 3D layout of the test rig was generated. Pressure vessels namely Boiler Vessel, Liquid Collector, Expansion Vessel and Fluid Recovery Exchanger were designed and manufactured. A data acquisition system to monitor and save the obtained data was integrated into the test rig. Additionally, a basic control algorithm was generated to shut down the equipment to emergency site protection if needed and control the frequency inverter of the feed pump motor. A fully instrumented test rig, which will be used for testing different fluids, was designed and constructed.

After the test rig was constructed, pre-commissioning, commissioning and experiment procedures were created. Hydrostatic pressure testing, drying, nitrogen pressure testing, vacuum testing, refrigerant filling, feed pump cold running, and draining some of the refrigerant for normal operation processes were conducted. Heating, cooling and working fluid circuits were commissioned separately. During the preliminary tests, throttle valve was used as the expander simulator. Recuperator was isolated from the system.

Due to a filtration problem with the feed pump, actual testing process cannot be completed. When the problem with the feed pump is solved, detailed experiments, which were defined in the Appendix J, will be conducted.

A 10 kW capacity scroll-type expander was installed on the system but it was not used during the preliminary tests due to the leakage issues. As a future work, the scroll-type expander would be integrated into the system. As another future work, recuperator effect would be analyzed and a comparison between regenerative and simple ORC would be made. Additionally, there is a parabolic trough collector, which has a 10 kW heat rate capacity, already installed next to the laboratory building and it is planned to be used afterwards as an additional heat source for the system.

# REFERENCES


1. "World Energy Resources: 2013 Survey", https://www.worldenergy.org/wp-content/uploads/2013/09/Complete_WER_2013_Survey.pdf, accessed at December 2016.

2. "Global Electricity Initiative: 2014 Report", https://www.worldenergy.org/wp-content/uploads/2014/12/Global_Electricity_Initiative_WEB.pdf, accessed at December 2016.

3. "Republic of Turkey Ministry of Energy and Natural Resources: Electricity Generation by Source in Turkey", http://www.mfa.gov.tr/turkeys-energy-strategy.en.mfa, accessed at December 2016.

4. Peris, B., J. Navarro-Esbrí, F. Molés and A. Mota-Babiloni, "Experimental study of an ORC (organic Rankine cycle) for low grade waste heat recovery in a ceramic industry", *Energy*, Vol. 85, pp. 534–542, 2015.

5. Hung, T.-C., "Waste heat recovery of organic Rankine cycle using dry fluids", *Energy Conversion and Management*, Vol. 42, No. 5, pp. 539–553, 2001.

6. Chinese, D., A. Meneghetti and G. Nardin, "Diffused introduction of Organic Rankine Cycle for biomass-based power generation in an industrial district: a systems analysis", *International Journal of Energy Research*, Vol. 28, No. 11, pp. 1003–1021, 2004.

7. Maraver, D., A. Sin, J. Royo and F. Sebastián, "Assessment of CCHP systems based on biomass combustion for small-scale applications through a review of the technology and analysis of energy efficiency parameters", *Applied Energy*, Vol. 102, pp. 1303–1313, 2013.

8. Mertoglu, O., S. Simsek and N. Basarir, "Geothermal Country Update Report of

Turkey (2010-2015)", *World geothermal congress*, 2015.

9. Yamamoto, T., T. Furuhata, N. Arai and K. Mori, "Design and testing of the organic Rankine cycle", *Energy*, Vol. 26, No. 3, pp. 239–251, 2001.

10. Cirincione, N., *Design, construction and commissioning of an Organic Rankine Cycle waste heat recovery system with a Tesla-hybrid turbine expander*, Ph.D. Thesis, Colorado State University, 2011.

11. Algieri, A. and P. Morrone, "Energy analysis of Organic Rankine Cycles for biomass applications", *Thermal Science*, Vol. 19, No. 1, pp. 193–205, 2015.

12. Quoilin, S., S. Declaye, B. F. Tchanche and V. Lemort, "Thermo-economic optimization of waste heat recovery Organic Rankine Cycles", *Applied Thermal Engineering*, Vol. 31, No. 14, pp. 2885–2893, 2011.

13. Obernberger, I., P. Thonhofer and E. Reisenhofer, "Description and evaluation of the new 1000 kWel Organic Rankine Cycle process integrated in the biomass CHP plant in Lienz, Austria", *Euroheat & Power*, Vol. 10, pp. 1–17, 2002.

14. Rahbar, K., S. Mahmoud, R. K. Al-Dadah and N. Moazami, "Modelling and optimization of organic Rankine cycle based on a small-scale radial inflow turbine", *Energy Conversion and Management*, Vol. 91, pp. 186–198, 2015.

15. Pei, G., J. Li, Y. Li, D. Wang and J. Ji, "Construction and dynamic test of a small-scale organic rankine cycle", *Energy*, Vol. 36, No. 5, pp. 3215–3223, 2011.

16. Farrokhi, M., S. Noie and A. Akbarzadeh, "Preliminary experimental investigation of a natural gas-fired ORC-based micro-CHP system for residential buildings", *Applied thermal engineering*, Vol. 69, No. 1, pp. 221–229, 2014.

17. Kang, S. H., "Design and experimental study of ORC (organic Rankine cycle) and radial turbine using R245fa working fluid", *Energy*, Vol. 41, No. 1, pp. 514–524,

2012.

18. Wei, D., X. Lu, Z. Lu and J. Gu, "Performance analysis and optimization of organic Rankine cycle (ORC) for waste heat recovery", *Energy conversion and Management*, Vol. 48, No. 4, pp. 1113–1119, 2007.

19. Chen, H., D. Y. Goswami and E. K. Stefanakos, "A review of thermodynamic cycles and working fluids for the conversion of low-grade heat", *Renewable and sustainable energy reviews*, Vol. 14, No. 9, pp. 3059–3067, 2010.

20. Chang, J.-C., T.-C. Hung, Y.-L. He and W. Zhang, "Experimental study on low-temperature organic Rankine cycle utilizing scroll type expander", *Applied Energy*, Vol. 155, pp. 150–159, 2015.

21. Hung, T.-C., T. Shai and S. Wang, "A review of organic Rankine cycles (ORCs) for the recovery of low-grade waste heat", *Energy*, Vol. 22, No. 7, pp. 661–667, 1997.

22. Dai, Y., J. Wang and L. Gao, "Parametric optimization and comparative study of organic Rankine cycle (ORC) for low grade waste heat recovery", *Energy Conversion and Management*, Vol. 50, No. 3, pp. 576–582, 2009.

23. Ma, X. L., X. R. Meng, X. L. Wei, J. Chang and H. Li, "Analysis and Optimization of ORC for Low-Temperature Waste Heat Power Generation", *Advanced Materials Research*, Vol. 383, pp. 6614–6620, Trans Tech Publ, 2012.

24. Astolfi, M., M. C. Romano, P. Bombarda and E. Macchi, "Binary ORC (Organic Rankine Cycles) power plants for the exploitation of medium–low temperature geothermal sources–Part A: Thermodynamic optimization", *Energy*, Vol. 66, pp. 423–434, 2014.

25. Galanis, N., E. Cayer, P. Roy, E. Denis and M. Desilets, "Electricity generation from low temperature sources", *Journal of Applied Fluid Mechanics*, Vol. 2, No. 2,

pp. 55–67, 2009.

26. Hettiarachchi, H. M., M. Golubovic, W. M. Worek and Y. Ikegami, "Optimum design criteria for an organic Rankine cycle using low-temperature geothermal heat sources", *Energy*, Vol. 32, No. 9, pp. 1698–1706, 2007.

27. Meyer, D., C. Wong, F. Engel and S. Krumdieck, "Design and build of a 1 kilowatt organic Rankine cycle power generator", *35th New Zealand Geothermal Workshop*, pp. 17–20, 2013.

28. Li, M., J. Wang, W. He, L. Gao, B. Wang, S. Ma and Y. Dai, "Construction and preliminary test of a low-temperature regenerative Organic Rankine Cycle (ORC) using R123", *Renewable Energy*, Vol. 57, pp. 216–222, 2013.

29. Nikolskiy, A. I., A. A. Shipkov, V. N. Semenov, G. V. Tomarov and B. E. Parshin, "Russian Geothermal Power Plants Equipped with ORC-units", *World Geothermal Congress, Melbourne, Australia*, 2015.

30. El-Emam, R. S. and I. Dincer, "Exergy and exergoeconomic analyses and optimization of geothermal organic Rankine cycle", *Applied Thermal Engineering*, Vol. 59, No. 1, pp. 435–444, 2013.

31. Zhou, N., X. Wang, Z. Chen and Z. Wang, "Experimental study on organic Rankine cycle for waste heat recovery from low-temperature flue gas", *Energy*, Vol. 55, pp. 216–225, 2013.

32. Cohen, G., R. Cable, D. Brosseau and H. Price, "Parabolic trough organic Rankine cycle solar power plant", *Golden, Colorado: National Renewable Energy Laboratory*, 2005.

33. Quoilin, S., M. Orosz, H. Hemond and V. Lemort, "Performance and design optimization of a low-cost solar organic Rankine cycle for remote power generation", *Solar Energy*, Vol. 85, No. 5, pp. 955–966, 2011.

34. Tchanche, B. F., G. Papadakis, G. Lambrinos and A. Frangoudakis, "Fluid selection for a low-temperature solar organic Rankine cycle", *Applied Thermal Engineering*, Vol. 29, No. 11, pp. 2468–2476, 2009.

35. Twomey, B., P. Jacobs and H. Gurgenci, "Dynamic performance estimation of small-scale solar cogeneration with an organic Rankine cycle using a scroll expander", *Applied Thermal Engineering*, Vol. 51, No. 1, pp. 1307–1316, 2013.

36. Saitoh, T., N. Yamada and S.-I. Wakashima, "Solar Rankine cycle system using scroll expander", *Journal of Environment and Engineering*, Vol. 2, No. 4, pp. 708–719, 2007.

37. Dong, L., H. Liu and S. Riffat, "Development of small-scale and micro-scale biomass-fuelled CHP systems–A literature review", *Applied thermal engineering*, Vol. 29, No. 11, pp. 2119–2126, 2009.

38. Obernberger, I., "Biomass CHP Plant Based on an ORC Process-Realized EU-Demonstration Project in Admont/Austria", *Meeting of IEA Bionergy, TASK*, Vol. 19.

39. Perilhon, C., D. Alkadee, G. Descombes and S. Lacour, "Life cycle assessment applied to electricity generation from renewable biomass", *Energy Procedia*, Vol. 18, pp. 165–176, 2012.

40. Huang, Y., Y. Wang, S. Rezvani, D. McIlveen-Wright, M. Anderson, J. Mondol, A. Zacharopolous and N. Hewitt, "A techno-economic assessment of biomass fuelled trigeneration system integrated with organic Rankine cycle", *Applied Thermal Engineering*, Vol. 53, No. 2, pp. 325–331, 2013.

41. Vélez, F., J. J. Segovia, M. C. Martín, G. Antolín, F. Chejne and A. Quijano, "A technical, economical and market review of organic Rankine cycles for the conversion of low-grade heat for power generation", *Renewable and Sustainable Energy Reviews*, Vol. 16, No. 6, pp. 4175–4189, 2012.

42. Delgado-Torres, A. M. and L. García-Rodríguez, "Design recommendations for solar organic Rankine cycle (ORC)–powered reverse osmosis (RO) desalination", *Renewable and Sustainable Energy Reviews*, Vol. 16, No. 1, pp. 44–53, 2012.

43. Manolakos, D., G. Papadakis, S. Kyritsis and K. Bouzianas, "Experimental evaluation of an autonomous low-temperature solar Rankine cycle system for reverse osmosis desalination", *Desalination*, Vol. 203, No. 1, pp. 366–374, 2007.

44. Tchanche, B. F., G. Lambrinos, A. Frangoudakis and G. Papadakis, "Low-grade heat conversion into power using organic Rankine cycles–a review of various applications", *Renewable and Sustainable Energy Reviews*, Vol. 15, No. 8, pp. 3963–3979, 2011.

45. "ORMAT Inc. Web Site", `http://www.ormat.com/`, accessed at December 2016.

46. "Turboden Web Site", `http://www.turboden.eu/`, accessed at December 2016.

47. "Exergy Web Site", `http://www.exergy-orc.com/`, accessed at December 2016.

48. Song, P., M. Wei, L. Shi, S. N. Danish and C. Ma, "A review of scroll expanders for organic Rankine cycle systems", *Applied Thermal Engineering*, Vol. 75, pp. 54–64, 2015.

49. Bao, J. and L. Zhao, "A review of working fluid and expander selections for organic Rankine cycle", *Renewable and Sustainable Energy Reviews*, Vol. 24, pp. 325–342, 2013.

50. Lemort, V., S. Quoilin, C. Cuevas and J. Lebrun, "Testing and modeling a scroll expander integrated into an Organic Rankine Cycle", *Applied Thermal Engineering*, Vol. 29, No. 14, pp. 3094–3102, 2009.

51. Orosz, M. S., A. V. Mueller, B. J. Dechesne and H. F. Hemond, "Geometric design of scroll expanders optimized for small Organic Rankine Cycles", *Journal of*

*Engineering for Gas Turbines and Power*, Vol. 135, No. 4, p. 042303, 2013.

52. Schuster, A., S. Karellas, E. Kakaras and H. Spliethoff, "Energetic and economic investigation of Organic Rankine Cycle applications", *Applied thermal engineering*, Vol. 29, No. 8, pp. 1809–1817, 2009.

53. Quoilin, S., V. Lemort and J. Lebrun, "Experimental study and modeling of an Organic Rankine Cycle using scroll expander", *Applied energy*, Vol. 87, No. 4, pp. 1260–1268, 2010.

54. Nguyen, V., P. Doherty and S. Riffat, "Development of a prototype low-temperature Rankine cycle electricity generation system", *Applied Thermal Engineering*, Vol. 21, No. 2, pp. 169–181, 2001.

55. Tarique, A., I. Dincer, C. Zamfirescu *et al.*, "Experimental investigation of a scroll expander for an organic Rankine cycle", *International Journal of Energy Research*, Vol. 38, No. 14, pp. 1825–1834, 2014.

56. Lemmon, E., M. Huber and M. McLinden, "REFPROP: Reference fluid thermodynamic and transport properties", *NIST standard reference database*, Vol. 23, No. 8.0, 2007.

57. Abdulkadirova, K. S., C. Peters, J. Sengers and M. Anisimov, "An isomorphic Peng–Robinson equation for phase-equilibria properties of hydrocarbon mixtures in the critical region", *The Journal of Supercritical Fluids*, Vol. 55, No. 2, pp. 594–602, 2010.

58. Peng, D.-Y. and D. B. Robinson, "A new two-constant equation of state", *Industrial & Engineering Chemistry Fundamentals*, Vol. 15, No. 1, pp. 59–64, 1976.

59. Qiu, G., "Selection of working fluids for micro-CHP systems with ORC", *Renewable Energy*, Vol. 48, pp. 565–570, 2012.

60. Papadopoulos, A. I., M. Stijepovic and P. Linke, "On the systematic design and selection of optimal working fluids for Organic Rankine Cycles", *Applied Thermal Engineering*, Vol. 30, No. 6, pp. 760–769, 2010.

61. Wang, D., X. Ling, H. Peng, L. Liu and L. Tao, "Efficiency and optimal performance evaluation of organic Rankine cycle for low grade waste heat power generation", *Energy*, Vol. 50, pp. 343–352, 2013.

62. Calm, J. M. and G. C. Hourahan, "Refrigerant data summary", *Engineered Systems*, Vol. 18, No. 11, pp. 74–88, 2001.

63. Zyhowski, G. and A. Brown, "Low global warming fluids for replacement of HFC-245fa and HFC-134a in ORC applications", *Proceedings of First International Seminar on ORC systems, Delft, The Netherlands*, pp. 22–23, 2011.

64. Kakac, S., H. Liu and A. Pramuanjaroenkij, *Heat exchangers: selection, rating, and thermal design*, CRC press, 2012.

65. Yan, Y.-Y. and T.-F. Lin, "Evaporation heat transfer and pressure drop of refrigerant R-134a in a plate heat exchanger", *Journal of Heat Transfer*, Vol. 121, No. 1, pp. 118–127, 1999.

66. Yan, Y.-Y., H.-C. Lio and T.-F. Lin, "Condensation heat transfer and pressure drop of refrigerant R-134a in a plate heat exchanger", *International Journal of Heat and Mass Transfer*, Vol. 42, No. 6, pp. 993–1006, 1999.

# APPENDIX A: SECTION DRAWING OF THE SCROLL EXPANDER

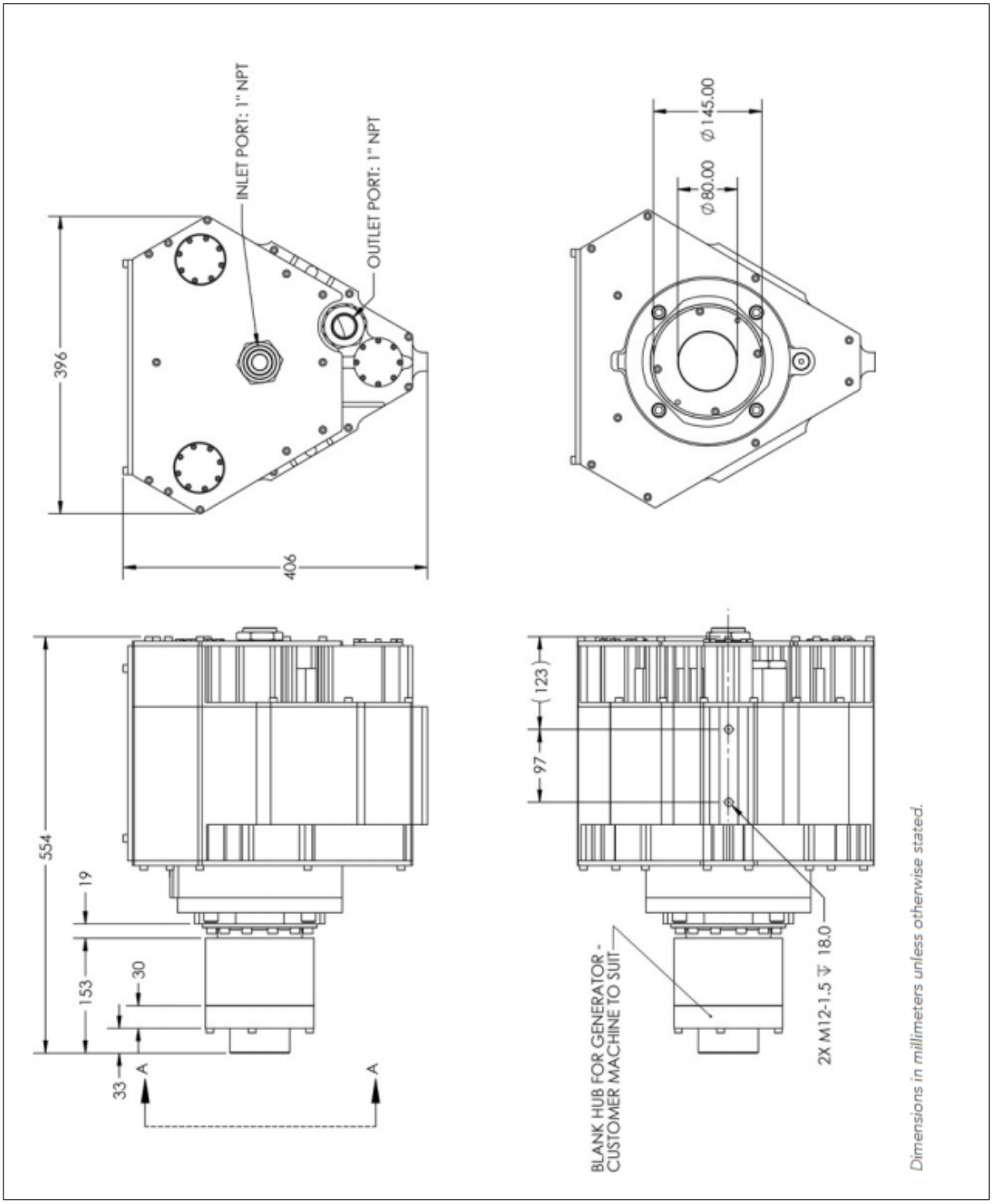


Figure A.1. Section drawing of the scroll expander.

# APPENDIX B: SECTION DRAWING OF THE SIDE CHANNEL PUMP

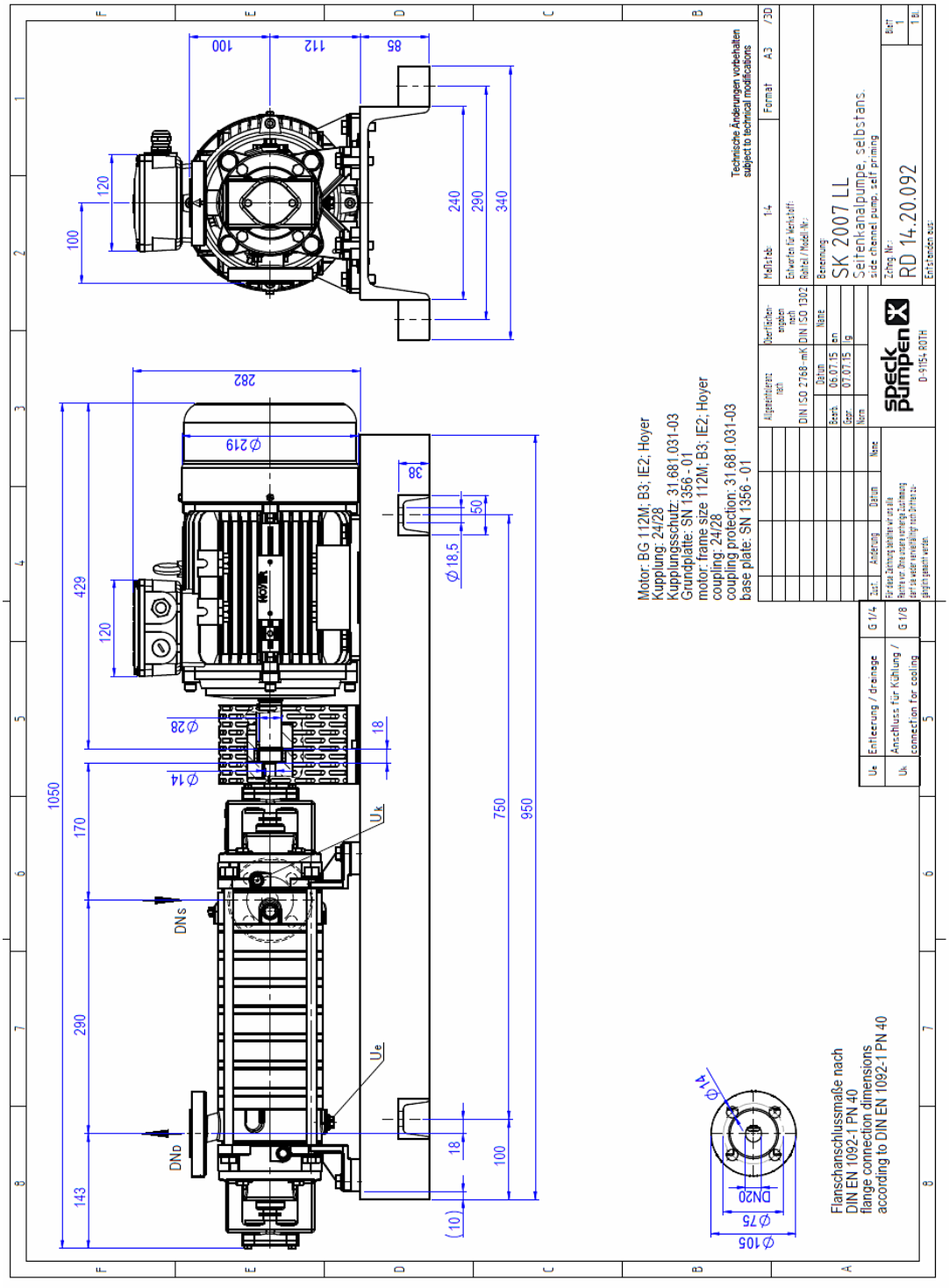


Figure B.1. Section drawing of the side channel pump.

# APPENDIX C: SECTION DRAWING OF THE INTERNAL GEAR PUMP

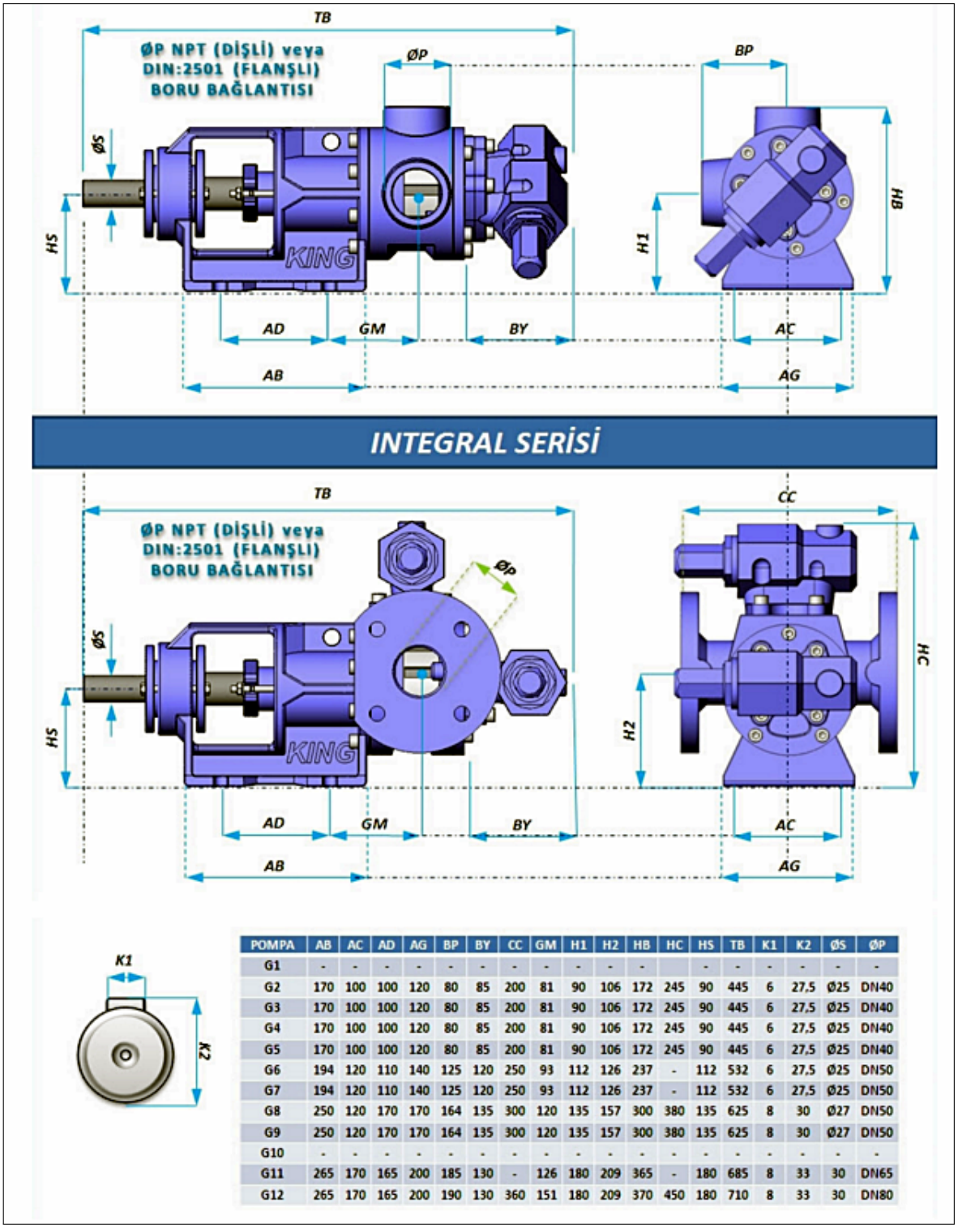


| POMPA | AB | AC | AD | AG | BP | BY | CC | GM | H1 | H2 | HB | HC | HS | TB | K1 | K2 | ØS | ØP |
|---|---|---|---|---|---|---|---|---|---|---|---|---|---|---|---|---|---|---|
| G1 | - | - | - | - | - | - | - | - | - | - | - | | - | - | - | - | - | - |
| G2 | 170 | 100 | 100 | 120 | 80 | 85 | 200 | 81 | 90 | 106 | 172 | 245 | 90 | 445 | 6 | 27,5 | Ø25 | DN40 |
| G3 | 170 | 100 | 100 | 120 | 80 | 85 | 200 | 81 | 90 | 106 | 172 | 245 | 90 | 445 | 6 | 27,5 | Ø25 | DN40 |
| G4 | 170 | 100 | 100 | 120 | 80 | 85 | 200 | 81 | 90 | 106 | 172 | 245 | 90 | 445 | 6 | 27,5 | Ø25 | DN40 |
| G5 | 170 | 100 | 100 | 120 | 80 | 85 | 200 | 81 | 90 | 106 | 172 | 245 | 90 | 445 | 6 | 27,5 | Ø25 | DN40 |
| G6 | 194 | 120 | 110 | 140 | 125 | 120 | 250 | 93 | 112 | 126 | 237 | - | 112 | 532 | 6 | 27,5 | Ø25 | DN50 |
| G7 | 194 | 120 | 110 | 140 | 125 | 120 | 250 | 93 | 112 | 126 | 237 | - | 112 | 532 | 6 | 27,5 | Ø25 | DN50 |
| G8 | 250 | 120 | 170 | 170 | 164 | 135 | 300 | 120 | 135 | 157 | 300 | 380 | 135 | 625 | 8 | 30 | Ø27 | DN50 |
| G9 | 250 | 120 | 170 | 170 | 164 | 135 | 300 | 120 | 135 | 157 | 300 | 380 | 135 | 625 | 8 | 30 | Ø27 | DN50 |
| G10 | - | - | - | - | - | - | - | - | - | - | - | - | - | - | - | - | - | - |
| G11 | 265 | 170 | 165 | 200 | 185 | 130 | - | 126 | 180 | 209 | 365 | - | 180 | 685 | 8 | 33 | 30 | DN65 |
| G12 | 265 | 170 | 165 | 200 | 190 | 130 | 360 | 151 | 180 | 209 | 370 | 450 | 180 | 710 | 8 | 33 | 30 | DN80 |

Figure C.1. Section drawing of the internal gear pump.

# APPENDIX D: SECTION DRAWING OF THE HEAT EXCHANGERS

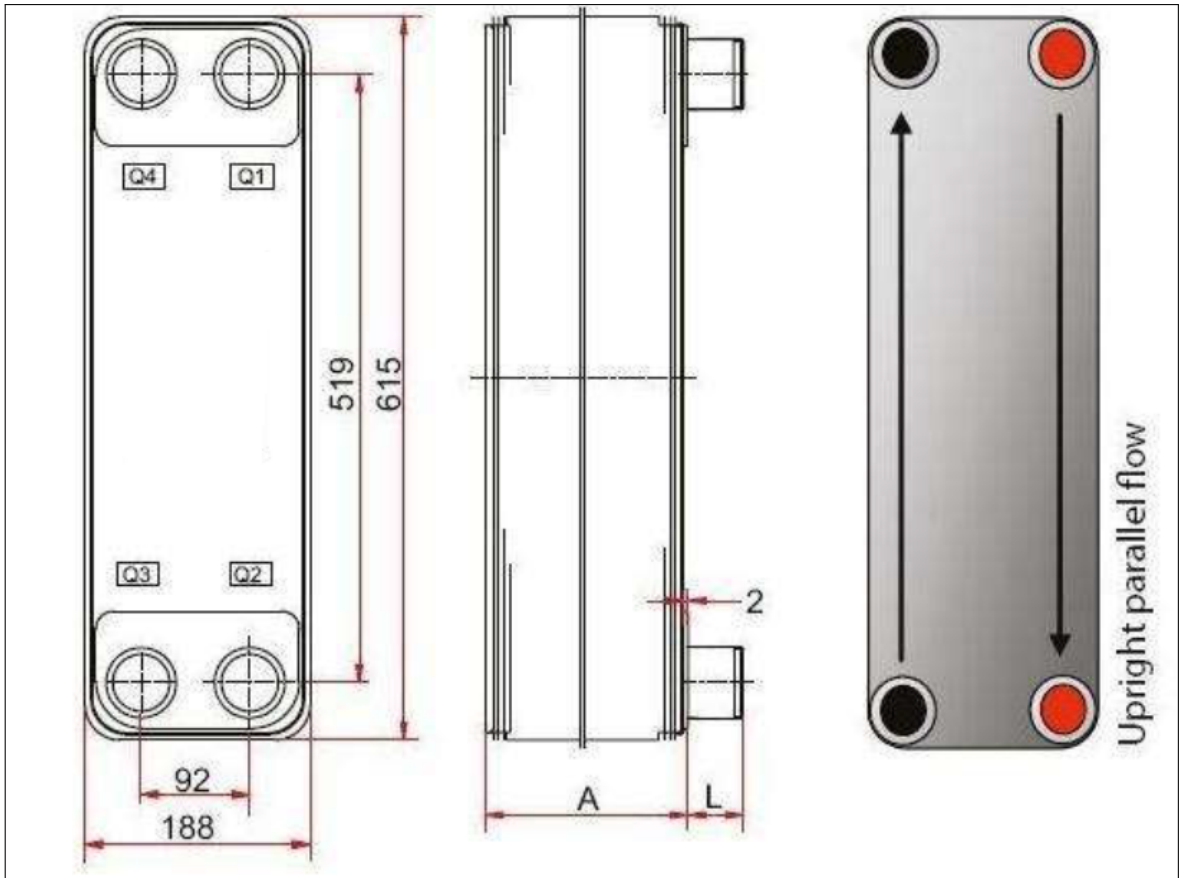


| | |
|---|---|
| Number of plates | 80 |
| A (mm) | 204 |
| L (mm) | 25 |
| Weight (kg) | 38,44 |
| Channel volume (L) | Q1 Q2 side: 8,04 / Q3 Q4 side: 7,839 |
| Design Pressure(Max) (bar) | 30 |
| Test pressure (bar) | 45 |
| Design Temp. (Max/Min) (°C) | -196 / +200 |

Figure D.1. Section drawing of the heat exchangers.

# APPENDIX E: DATASHEET OF THE HEATER

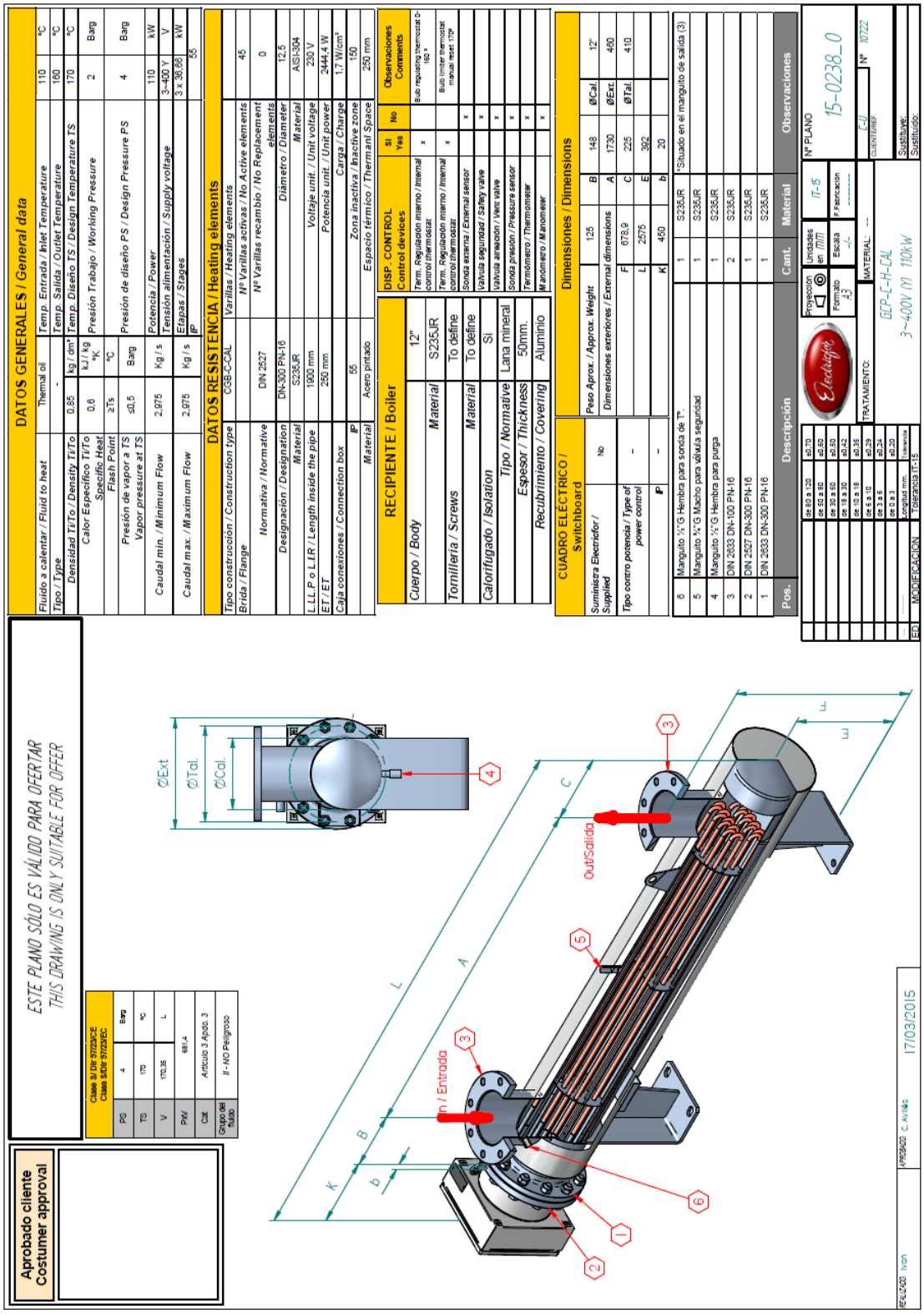


Figure E.1. Datasheet of the heater.

# APPENDIX F: SECTION DRAWING OF THE BOILER VESSEL

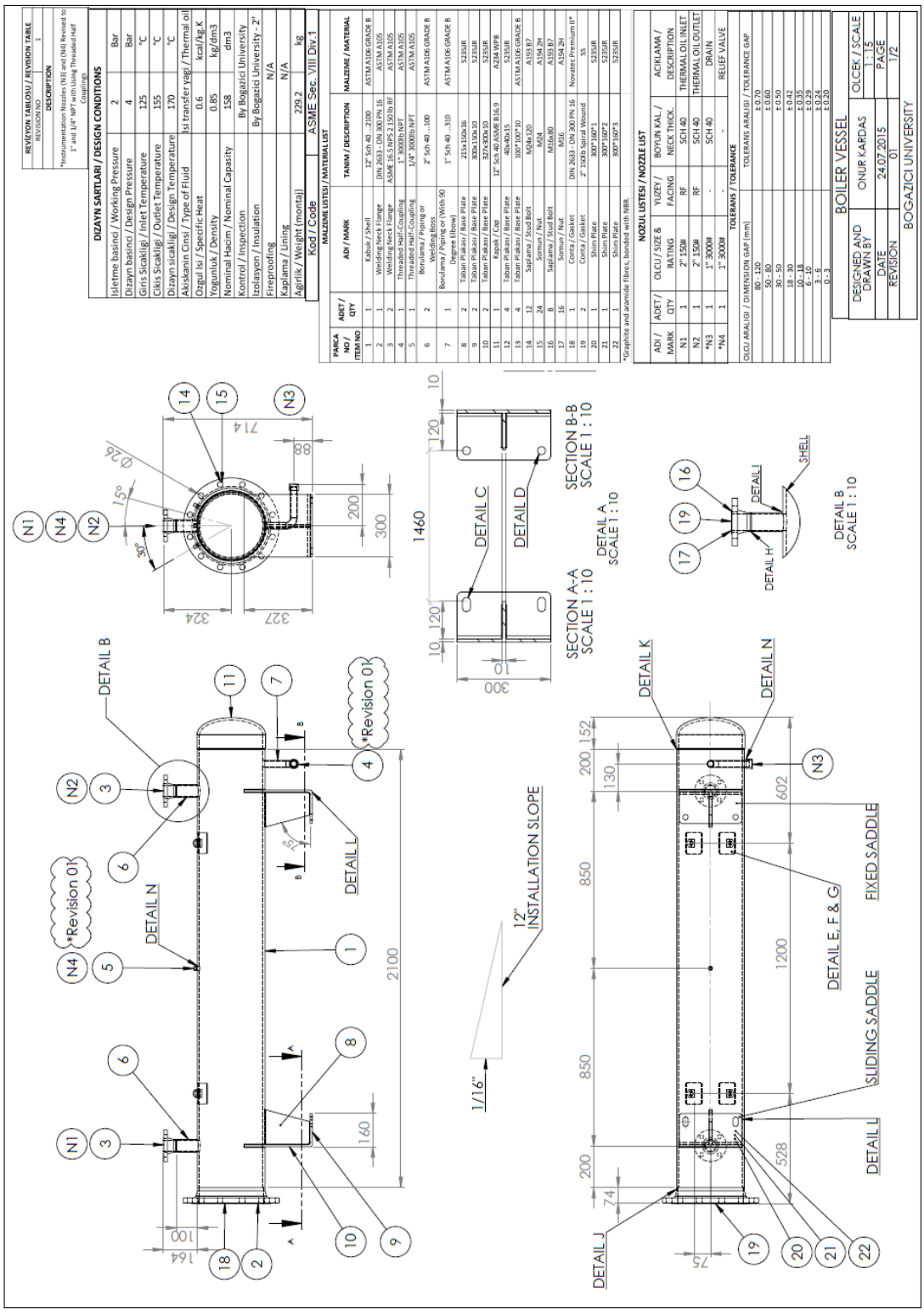


Figure F.1. Section drawing of the boiler vessel.

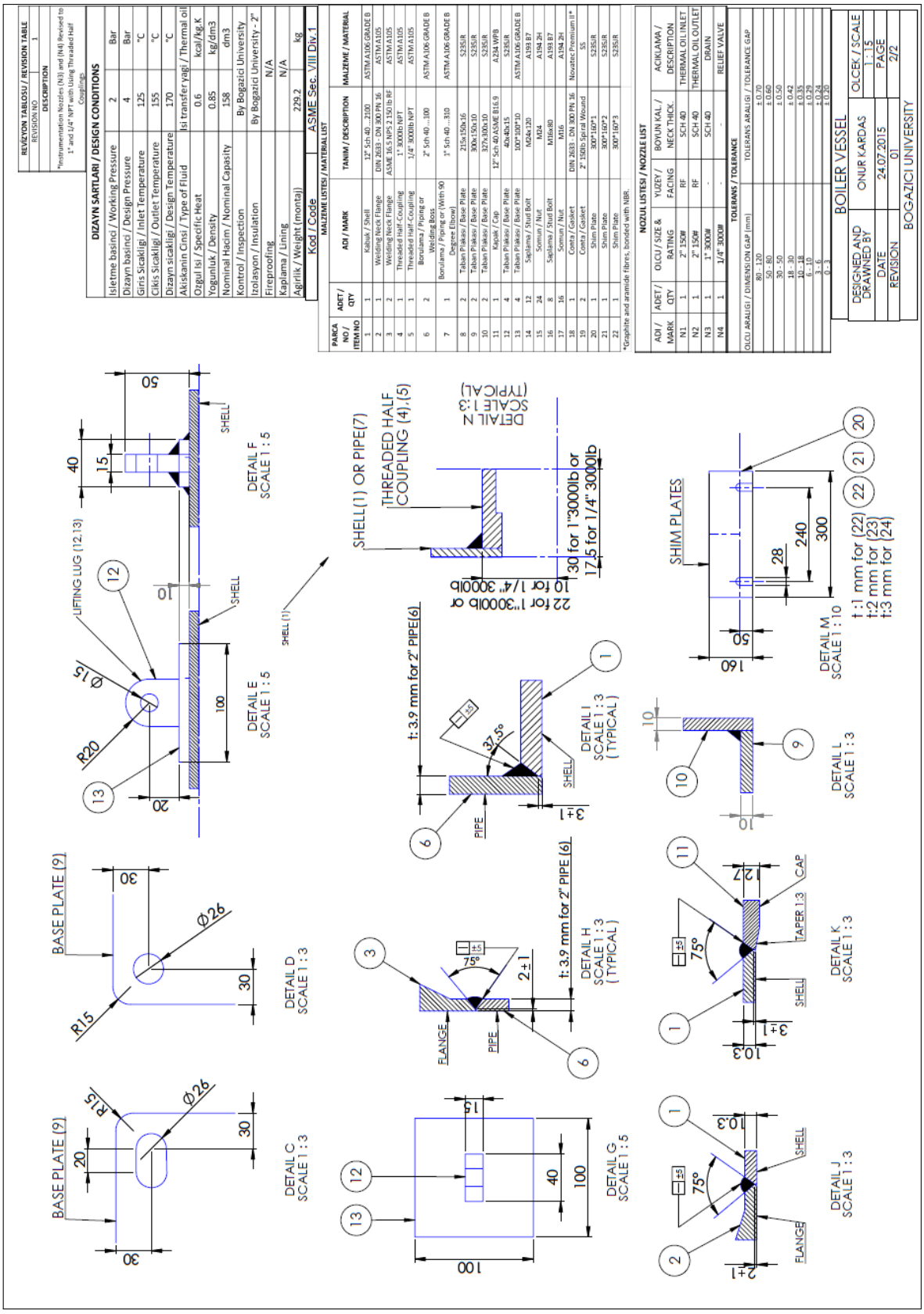


Figure F.1. Section drawing of the boiler vessel (cont.).

# APPENDIX G: SECTION DRAWING OF THE LIQUID COLLECTOR

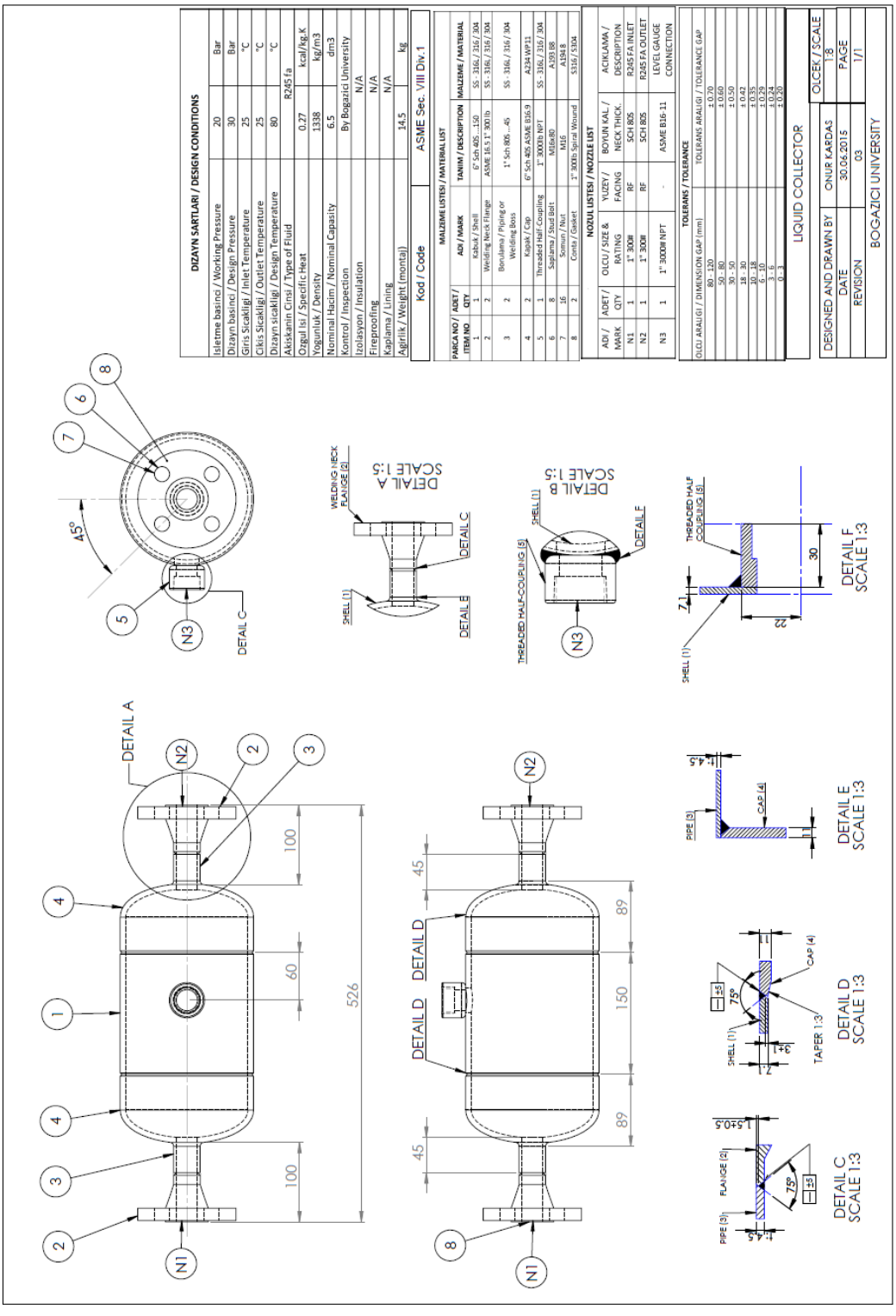


Figure G.1. Section drawing of the liquid collector.

# APPENDIX H: SECTION DRAWING OF THE EXPANSION VESSEL

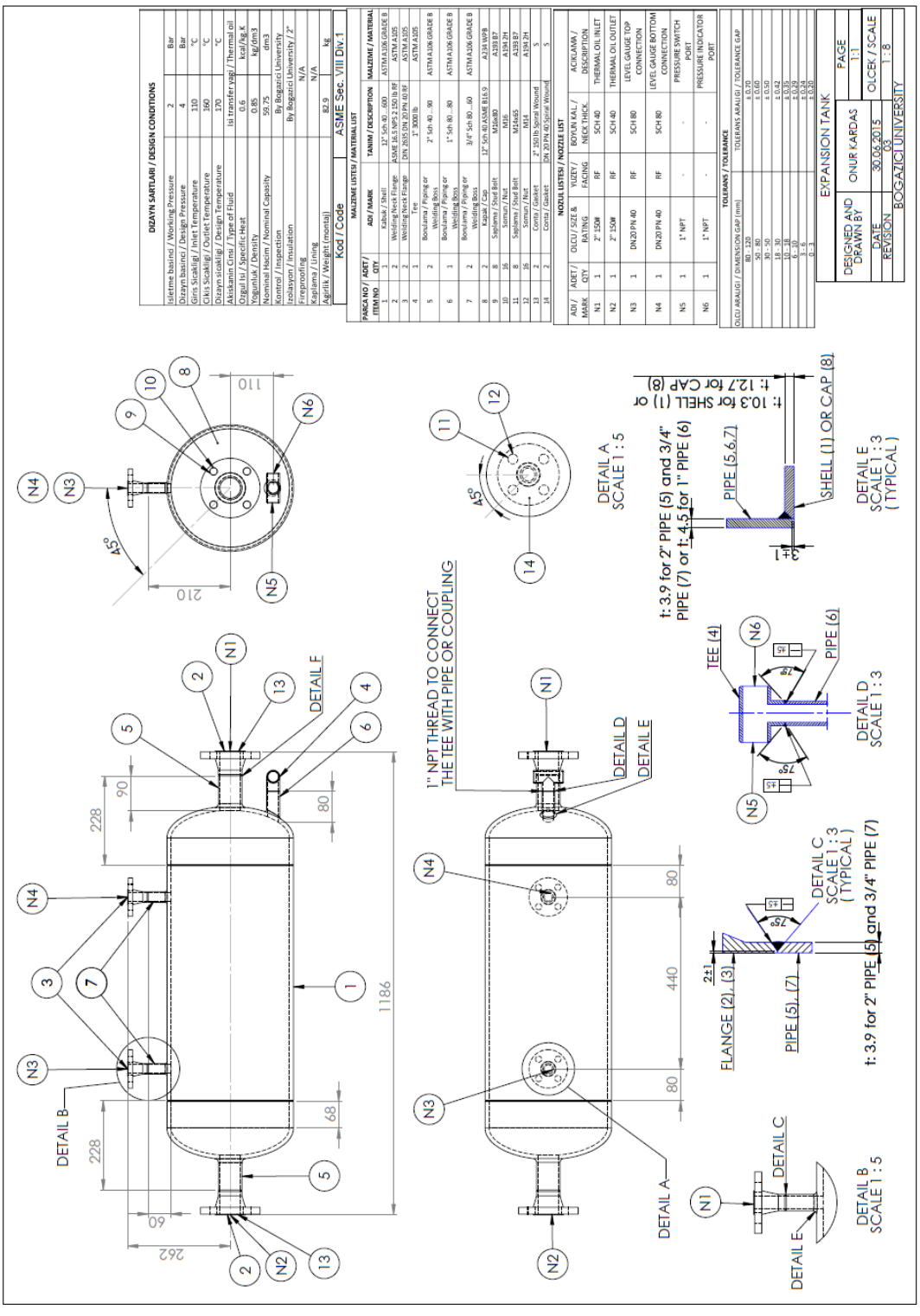


Figure H.1. Section drawing of the expansion vessel.

# APPENDIX I: SECTION DRAWING OF THE FLUID RECOVERY HEX

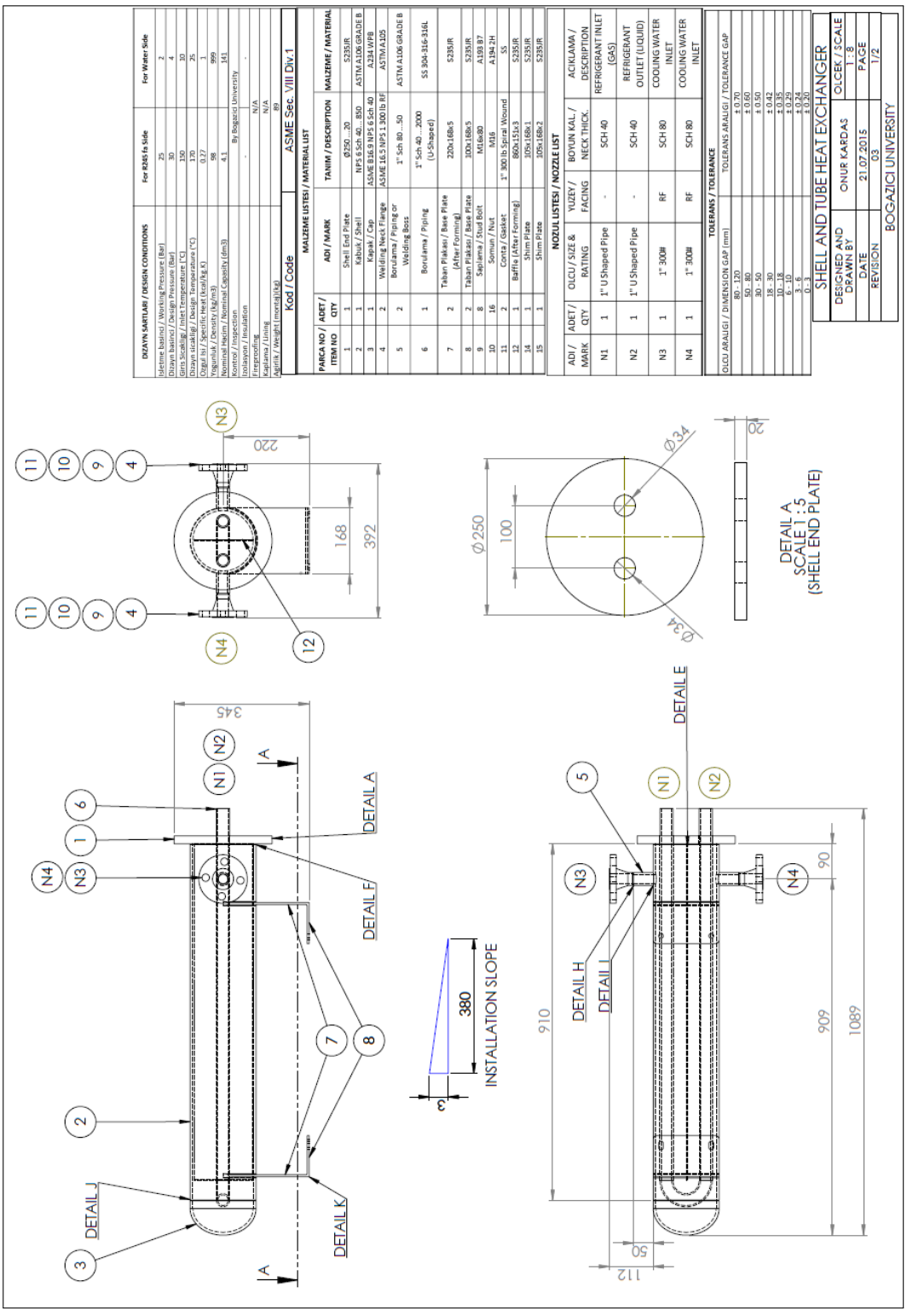


Figure I.1. Section drawing of the fluid recovery hex.

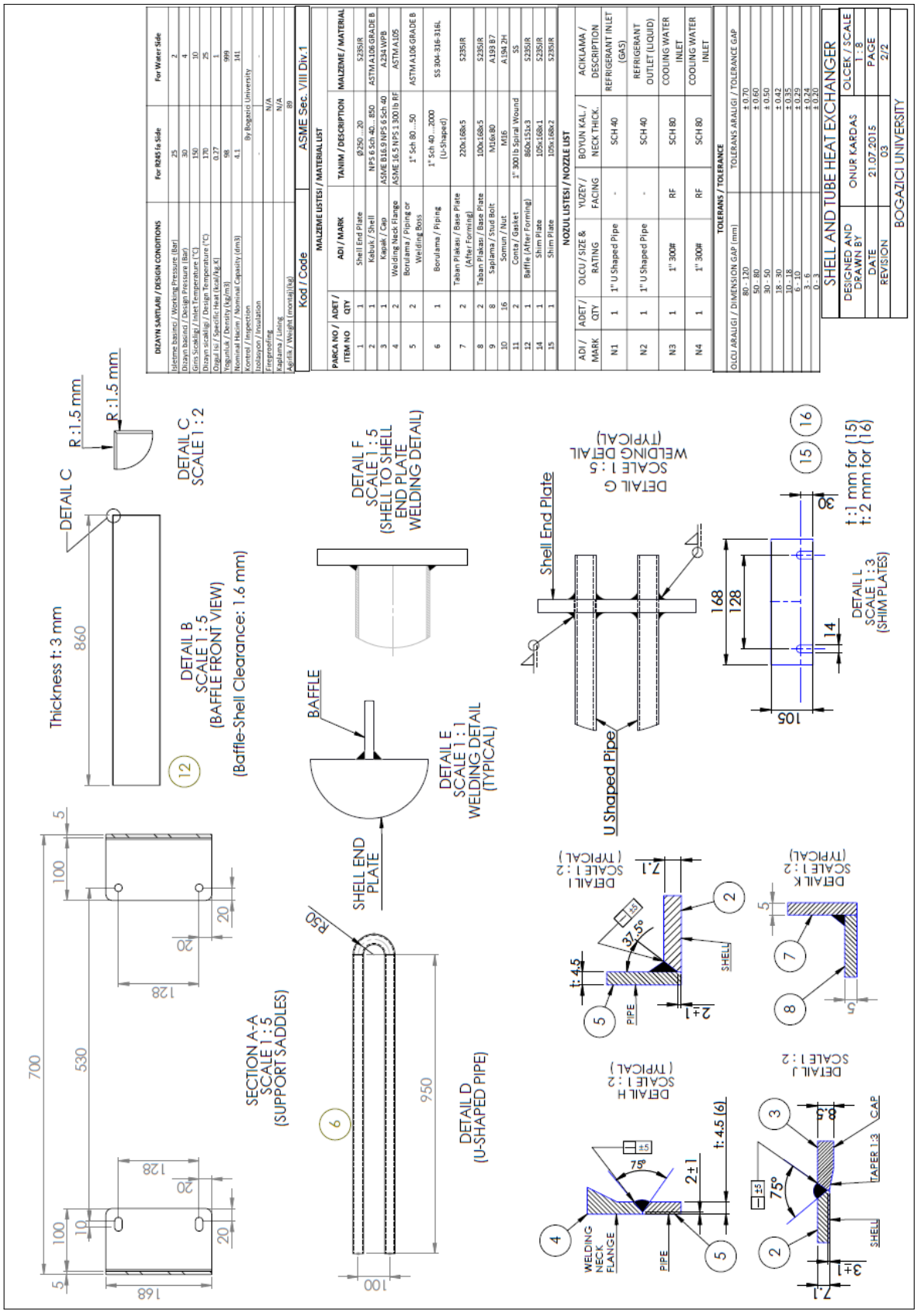


| DIZAYN SARTLARI / DESIGN CONDITIONS | For R245 fa Side | For Water Side |
|---|---|---|
| Isletme basinci / Working Pressure (Bar) | 25 | 2 |
| Dizayn basinci / Design Pressure (Bar) | 30 | 4 |
| Giris Sicakligi / Inlet Temperature (°C) | 150 | 10 |
| Dizayn sicakligi / Design Temperature (°C) | 170 | 25 |
| Ozgul Isi / Specific Heat (kcal/kg.K) | 0.27 | 1 |
| Yogunluk / Density (kg/m3) | 98 | 999 |
| Nominal Hacim / Nominal Capasity (dm3) | 4.1 | 141 |
| Kontrol / Inspection | By Bogazici University | |
| Izolasyon / Insulation | - | - |
| Fireproofing | N/A | |
| Kaplama / Lining | N/A | |
| Agirlik / Weight (montaj) (kg) | 89 | |

MALZEME LISTESI / MATERIAL LIST

| PARCA NO / ITEM NO | ADET / QTY | ADI / MARK | TANIM / DESCRIPTION | MALZEME / MATERIAL |
|---|---|---|---|---|
| 1 | 1 | Shell End Plate | Ø250 ... 20 | S235JR |
| 2 | 1 | Kabuk / Shell | NPS 6 Sch 40 ... 850 | ASTM A106 GRADE B |
| 3 | 1 | Kapak / Cap | ASME B16.9 NPS 6 Sch 40 | A234 WPB |
| 4 | 2 | Welding Neck Flange | ASME 16.5 NPS 1 300 lb RF | ASTM A105 |
| 5 | 2 | Borulama / Piping or Welding Boss | 1" Sch 80 ...50 | ASTM A106 GRADE B |
| 6 | 1 | Borulama / Piping | 1" Sch 40 ...2000 (U-Shaped) | SS 304-316-316L |
| 7 | 2 | Taban Plakasi / Base Plate (After Forming) | 220x168x5 | S235JR |
| 8 | 2 | Taban Plakasi / Base Plate | 100x168x5 | S235JR |
| 9 | 8 | Saplama / Stud Bolt | M16x80 | A193 B7 |
| 10 | 16 | Somun / Nut | M16 | A194 2H |
| 11 | 2 | Conta / Gasket | 1" 300 lb Spiral Wound | SS |
| 12 | 1 | Baffle (After Forming) | 860x153x3 | S235JR |
| 14 | 1 | Shim Plate | 105x168x1 | S235JR |
| 15 | 1 | Shim Plate | 105x168x2 | S235JR |

NOZUL LISTESI / NOZZLE LIST

| ADI / MARK | ADET / QTY | OLCU / SIZE & RATING | YUZEY / FACING | BOYUN KAL. / NECK THICK. | ACIKLAMA / DESCRIPTION |
|---|---|---|---|---|---|
| N1 | 1 | 1" U Shaped Pipe | - | SCH 40 | REFRIGERANT INLET (GAS) |
| N2 | 1 | 1" U Shaped Pipe | - | SCH 40 | REFRIGERANT OUTLET (LIQUID) |
| N3 | 1 | 1" 300# | RF | SCH 80 | COOLING WATER INLET |
| N4 | 1 | 1" 300# | RF | SCH 80 | COOLING WATER INLET |

TOLERANS / TOLERANCE

| OLCU ARALIGI / DIMENSION GAP (mm) | TOLERANS ARALIGI / TOLERANCE GAP |
|---|---|
| 80 - 120 | ± 0.70 |
| 50 - 80 | ± 0.60 |
| 30 - 50 | ± 0.50 |
| 18 - 30 | ± 0.42 |
| 10 - 18 | ± 0.35 |
| 6 - 10 | ± 0.29 |
| 3 - 6 | ± 0.24 |
| 0 - 3 | ± 0.20 |

Figure I.1. Section drawing of the fluid recovery hex (cont.).

# APPENDIX J: EXPERIMENTAL PROCEDURE

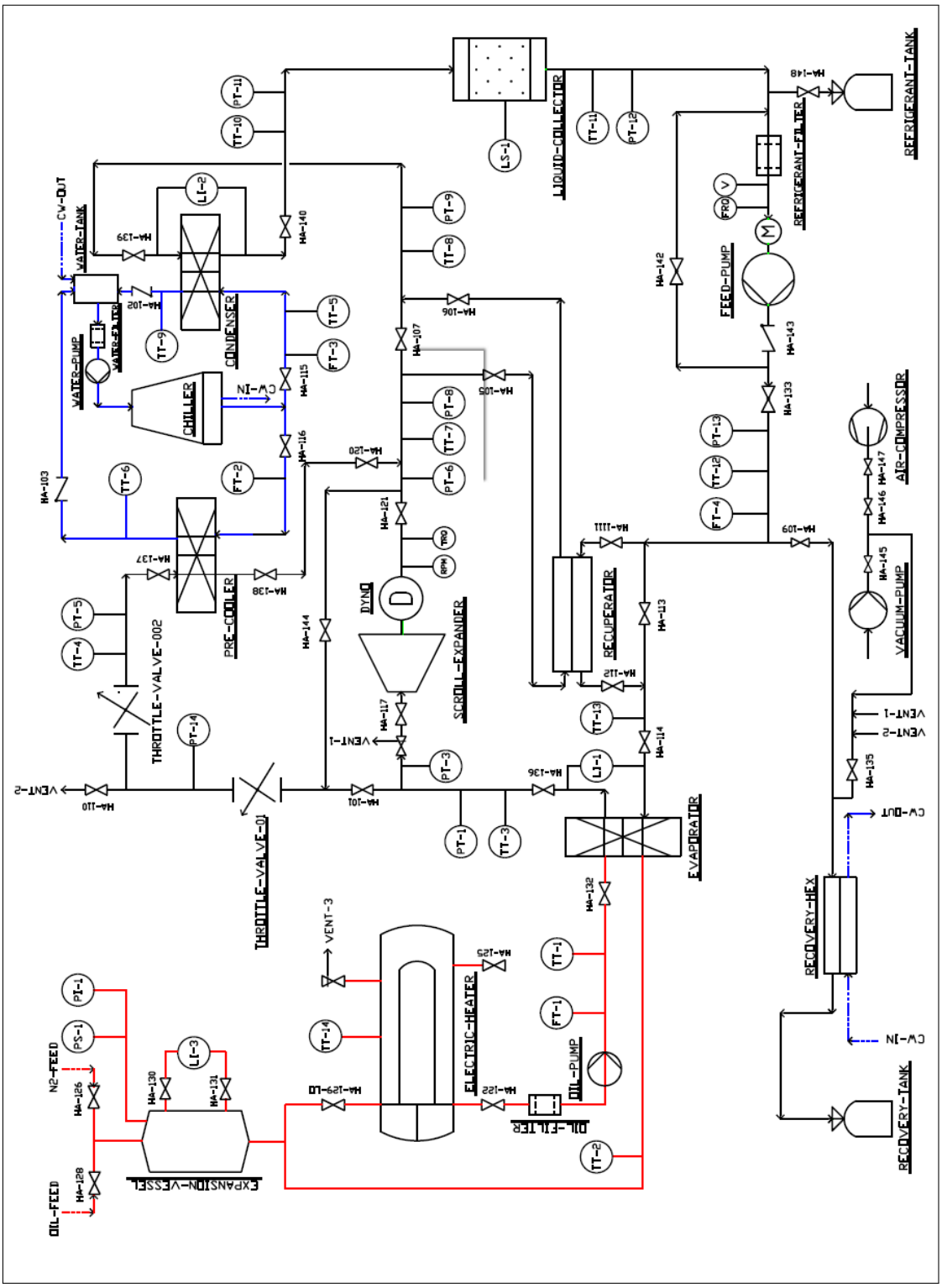


Figure J.1. Piping and instrumentation diagram of the proposed ORC with valve and sensor numbers.

Experimental procedure consists of checking of safety valve and adjusting pressure reducing valve, vacuuming, filling, putting heater and chiller into operation, start-up, testing and shut-down operations and actions to be taken parts.

## J.1. Checking of Safety Valve and Adjusting Pressure Reducing Valve

1. Pressurize the system with nitrogen up to 25 bar via HA-135 and HA-110. Valves HA-101, HA-134, HA-109, HA-144 and HA-137 should be closed.
2. When pressurizing is complete, close valve HA-135.
3. Adjust pressure reducing Valve (Throttle-01) to 4 barg.
4. Remove the nitrogen hose and keep that end open to atmosphere. When removing, do it slowly so that the pressure in the line up to HA-109 is gradually released.
5. Make sure that the outlet of the safety valve is open. One person shall be near valve Ha-110. If there is an excess pressure and safety valve fails to operate, he/she will open the valve HA-110. HA-135 should be in opened position.

## J.2. Vacuuming

6. Vacuum pump is connected to the nozzle via valve HA-145 as shown on the P&ID.
7. HA-145 is opened prior to vacuuming. Valves HA-135, HA-148, HA-109, HA-117, HA-121 are kept in closed position in order to avoid air entering the system. All other valves are in opened position.

## J.3. Filling

8. Start refrigerant filling. During filling process, weight of R134 shall be measured.
9. Liquid phase shall be present in the pipeline that connects condenser with the evaporator. The evaporator shall be full with liquid and condenser shall be empty. Level gauges shall be marked so that the level can be monitored. All other parts shall be filled with gaseous phase.

10. During filling process, monitor the level gage of the evaporator which is filling with liquid. As soon as the evaporator is filled completely, the outlet valve (HA-136) shall be closed so that liquid phase do not move further.
11. Ambient temperature is assumed as 15 °C. Pressure will be the saturation pressure at this temperature. All pressures mentioned in this procedure are measured locally and recorded in the data acquisition system with a unit of barg.
12. At the end of the filling process, all PT's shall show 3.9 barg (at 15 °C). Condenser, simulator, both sides of the PRV up to top of evaporator are full of vapor phase.

### J.4. Putting Heater and Chiller into Operation

At this stage evaporation shall not start. Process Pump is not working.

13. Data acquisition system must be opened. Make sure that the sensor board is enpowered and "Ipetronik Ipemotion" software is working. Open "ORC data acquisition" folder and then "ORC data acquisition" Ipemotion workspace file. Make sure that Ipemotion, NI card and modbus modules are working. Click display and read sensor data. Then, click store. At the end of the experiments, click stop. Now, all the data is restored in an excel file.
14. Regarding heater adjustment, turn on the power switch of the heater. At the touch screen, click on "kızgın yağ sıc. in the white area". Set kızgın yağ sıc. and resistans sıc. to predetermined oil temperature.
15. One person shall be near valve HA-110. If there is an excess pressure and safety valve is not adequate or fails to operate, he/she has to open the valve HA-110 manually. Check safety valve discharge pipeline to be opened to atmosphere. HA-135 should be in opened position.
16. Check oil level in the tank.
17. Adjust pressure reducing valve (throttle-01) set value to 4 barg.
18. Start chiller.
19. Set only chiller's water supply temperature to 10 °C.
20. Adjust water flow rate to 0 $m^3/h$ for the simulator and maximum for the condenser (9.8 $m^3/h$) by globe valves. Cooling water shall only flow through the condenser.

21. Since oil pump is a positive displacement type, flow adjustment is not possible. Mass flow rate is considered as constant and heater temperature will be the only variable for heat transfer oil circuit.
22. Make sure that valves HA-133, HA-142, HA-111, HA-112 and HA-136 are closed. Valves HA-101, HA-137, HA-138, HA-120, HA-107, HA-139 and HA-140 are opened. Recuperator is isolated. At this stage, evaporation shall start. Feed pump is not working.
23. Evaporator needs to be heated so that two phases exist in the evaporator. This will allow the control of the system.
24. At the beginning, set heater temperature to 16 °C with assuming the ambient temperature is 15 °C. Allow only a small temperature difference between condenser and evaporator. As the process fluid heats up, the evaporation begins and the liquid level starts to drop in the evaporator.
25. Monitor the pressure increase in the evaporator. Don't let the pressure to exceed 4 barg.
26. When the pressure reaches 4 barg, the valve at the outlet of the evaporator (HA-136) shall be gradually opened so that the discharge section up to the condenser is fully connected. This will allow expanded gas volume to find required space once evaporation starts. Monitor the level and make sure it approaches mid-level.
27. The temperature in the condenser shall be approximately 10 °C which corresponds to 3.2 barg. Due to the pressure difference, there will be a flow from evaporator to condenser. When mid-level is reached, turn off the oil pump.
28. Since there is no more heat transfer in the evaporator, the pressure difference between the two sides of the PRV decreases. Make sure that evaporator and condenser are half-filled with refrigerant R134a.
29. Since start-up is the next step, there is no need to turn off the cooling water circulation.

### J.5. Start-up, Testing and Shut-down Operations

Please refer to Table J.1 for start-up, testing and shut down processes. Pressure vales are given in gage pressure (barg) because of the sensor types.

Table J.1. Start-up, testing and shut-down conditions

| | | $\dot{m}_{R134a}$ (kg/s) | Max. pres. (barg) | Estimated inverter (%) | Oil temp. (°C) | TT-3 temp. (°C) | Water temp. (°C) | TT-10 temp. (°C) | $\dot{Q}_{water}$ ($m^3$/h) | Throttle outlet pres. (barg) |
|---|---|---|---|---|---|---|---|---|---|---|
| START UP | A | 0.1 | 6 | 30 | 40 | 29 | 10 | 13 | 9.8 | 4 |
| | B | 0.1 | 10 | 40 | 55 | 45 | 10 | 13 | 9.8 | 4 |
| | C | 0.1 | 14 | 50 | 65 | 57 | 10 | 13 | 9.8 | 4 |
| | D | 0.15 | 14 | 60 | 70 | 57 | 8 | 13 | 9.8 | 4 |
| | E | 0.2 | 14 | 70 | 70 | 57 | 5 | 13 | 9.8 | 4 |
| TESTING | A | 0.25 | 14 | 80 | 73 | 57 | 5 | 13 | 9.8 | 4 |
| | B | 0.25 | 17 | 90 | 79.5 | 65 | 11 | 19.5 | 9.8 | 5 |
| | C | 0.25 | 20 | 100 | 85 | 72 | 14 | 24.5 | 7.5 | 6 |
| SHUT DOWN | A | 0.25 | 14 | 80 | 73 | 57 | 5 | 13 | 9.8 | 4 |
| | B | 0.25 | 6 | 60 | 60 | 29 | 5 | 13 | 9.8 | 4 |
| | C | 0.1 | 6 | 30 | 40 | 29 | 10 | 13 | 9.8 | 4 |

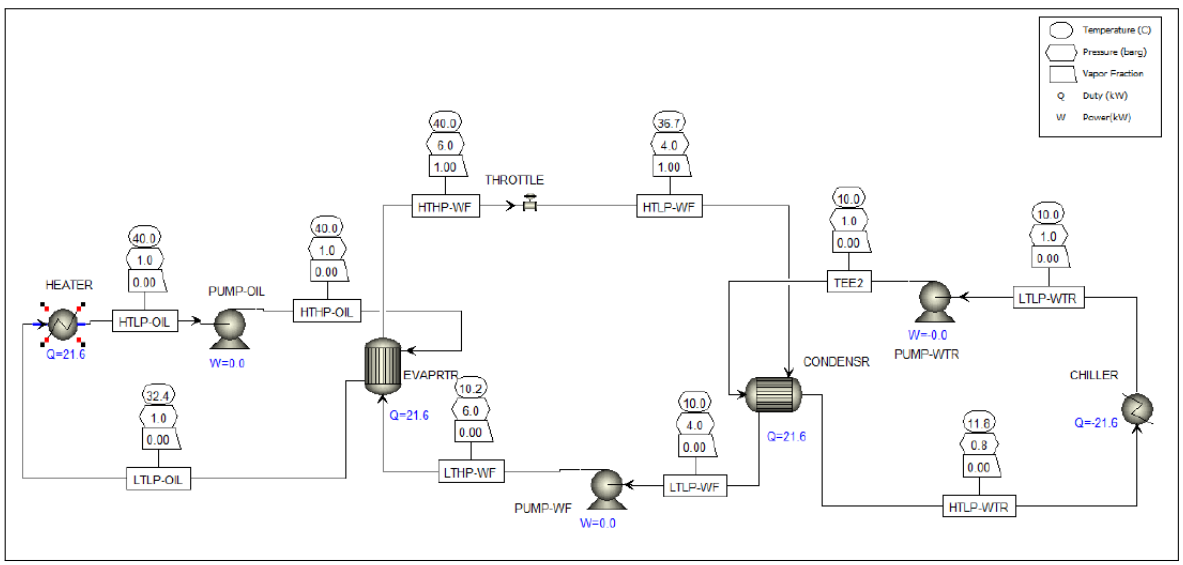


Figure J.2. Start-up A operation conditions.

30. Adjust the cooling water flow rate to 9.8 $m^3$/h.
31. All test crew shall be in their positions.
32. Close valve HA-114 and set the frequency inverter to 30 %.
33. Start process pump (Pump-01) and find the shut off pressure.
34. Set shut off pressure 6 barg via adjusting frequency inverter.
35. When 6 barg is obtained, close Pump-01.
36. Set oil temperature to 40 °C and wait until oil temperature reaches to the set value.

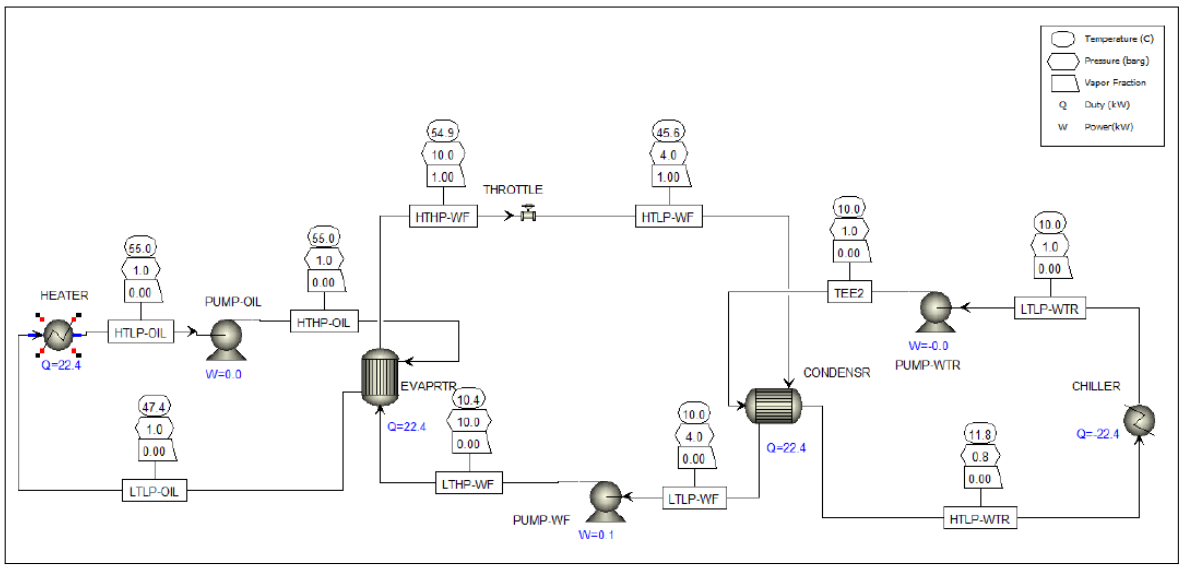


Figure J.3. Start-up B operation conditions.

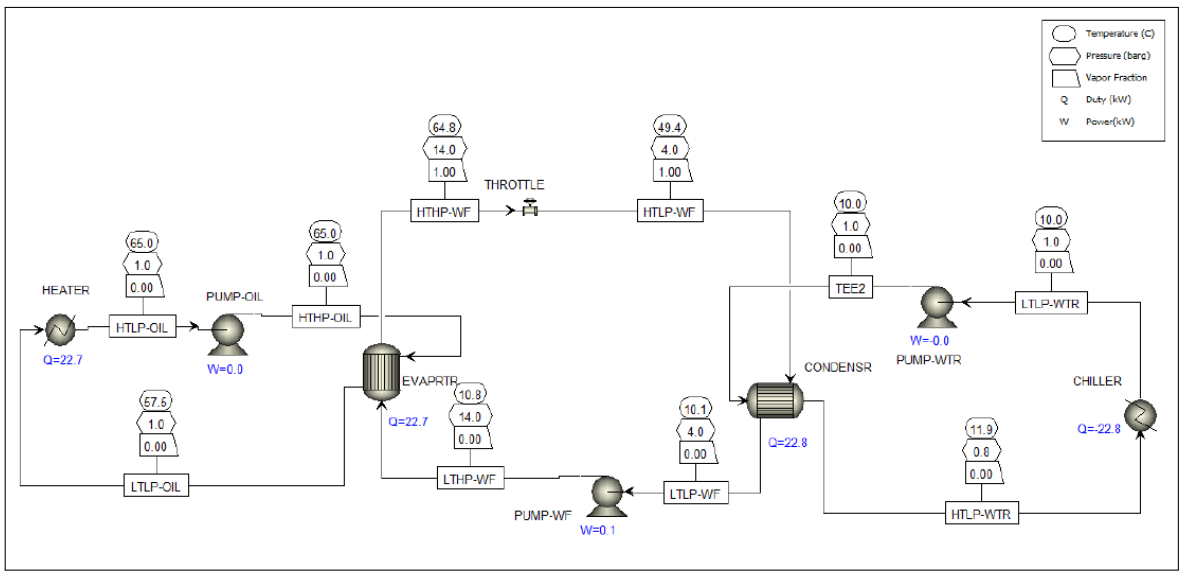


Figure J.4. Start-up C operation conditions.

37. Set water temperature to 10 °C. (It is already set to 10 °C).
38. Adjust valve HA-115 to set water flow rate which is 9.8 $m^3$/h.
39. Set pressure reducing valve (Throttle-01) to 4 barg. (It is already set to 4 barg).
40. Turn on the oil pump.
41. Start Pump-01 and adjust mass flow rate to 0.1 kg/s via HA-133 (globe valve) and HA-142 (by-pass valve).
42. Check process pump discharge pressure. If it is different from 6 barg, adjust frequency inverter.

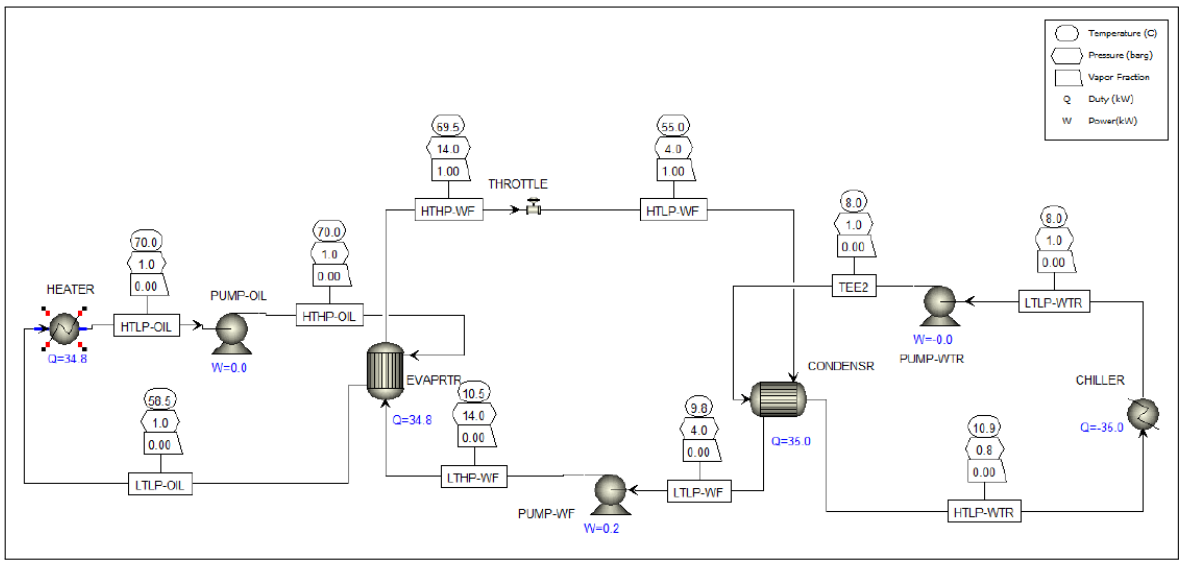


Figure J.5. Start-up D operation conditions.

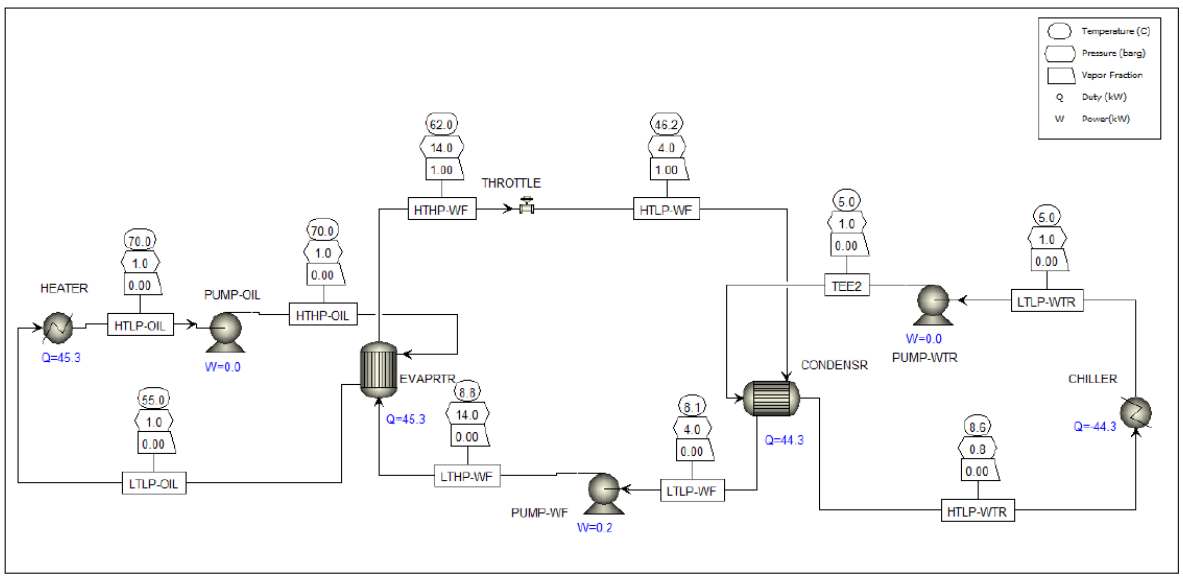


Figure J.6. Start-up E operation conditions.

43. Check level gages and take actions if levels are not equal. Refer “Actions to be taken” at the end of the document.
44. Under steady state conditions, it is expected that TT-3 is 29 °C and TT-10 is 13 °C. Process circulation is going on without interruption.
45. When “Start-up A” conditions are fulfilled, pass to the next step “Start-up B” conditions.
46. Set water temperature to 10 °C. (It is already set to 10 °C). Adjust valve HA-115 to set water flow rate which is 9.8 $m^3/h$. (It is already set to 9.8 $m^3/h$).

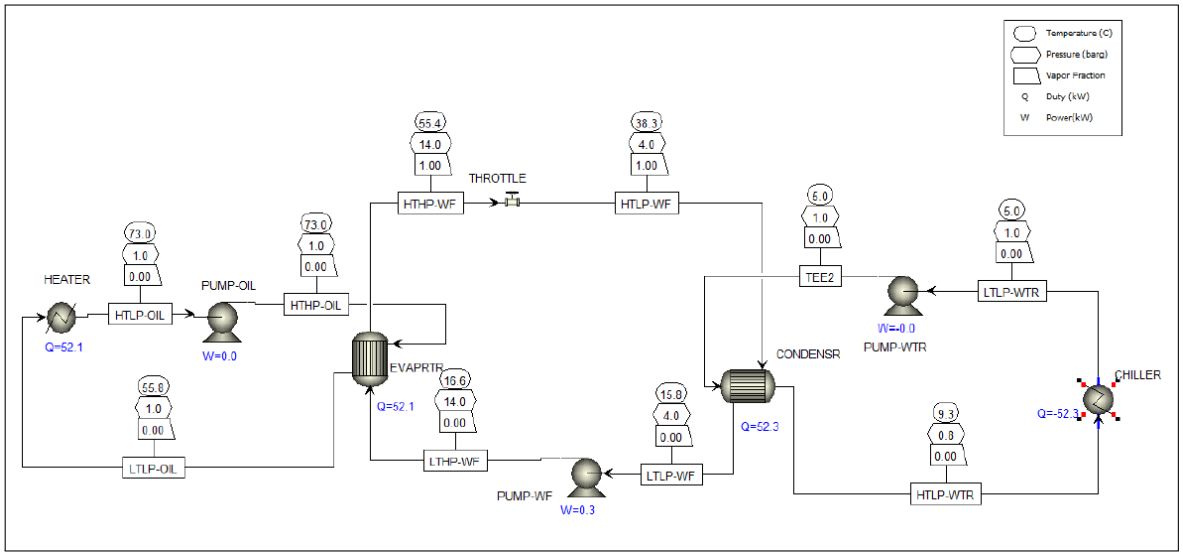


Figure J.7. Testing A operation conditions.

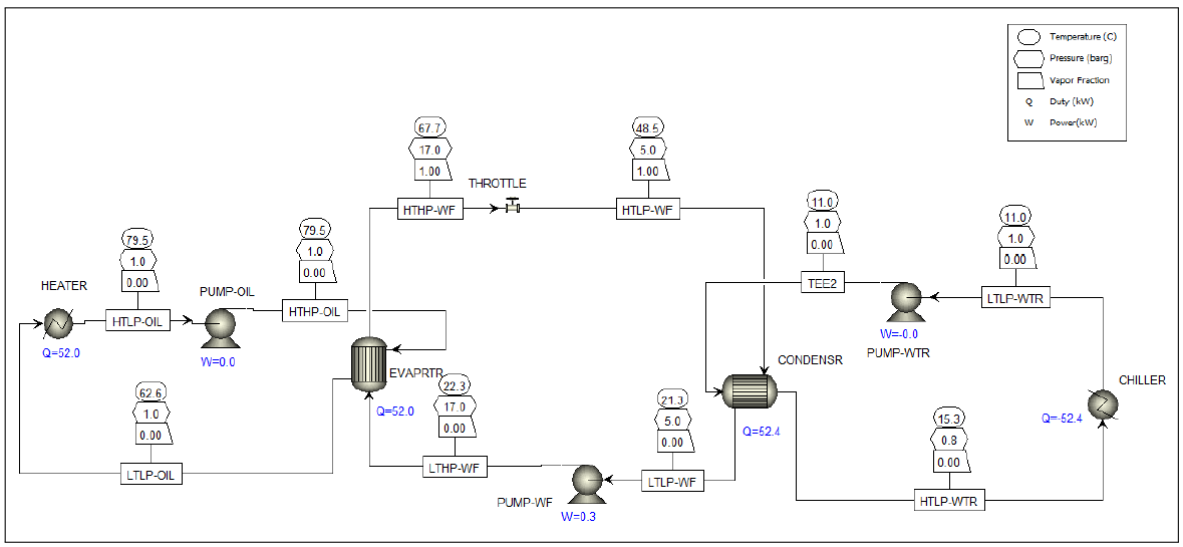


Figure J.8. Testing B operation conditions.

47. Set pressure reducing valve (Throttle-01) to 4 barg. (It is already set 4 to barg).
48. Set oil temperature to 55 °C.
49. Gradually increase frequency inverter to a percentage that gives 10 barg pump discharge pressure. (Should be above the value of case “Start-up A”).
50. Adjust Pump-01 mass flow rate to 0.1 kg/s via HA-133 (globe valve) and HA-142 (by-pass valve). (It is already set to 0.1 kg/s).
51. Check level gages and take actions if levels are both not around mid-level. Refer “Actions to be taken” at the end of the document.

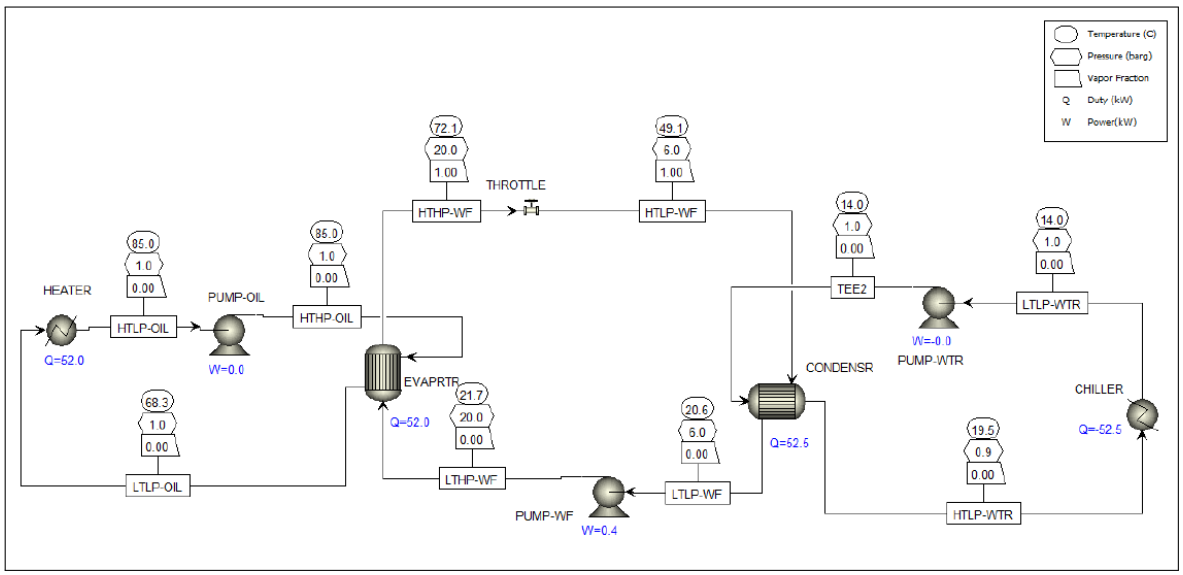


Figure J.9. Testing C operation conditions.

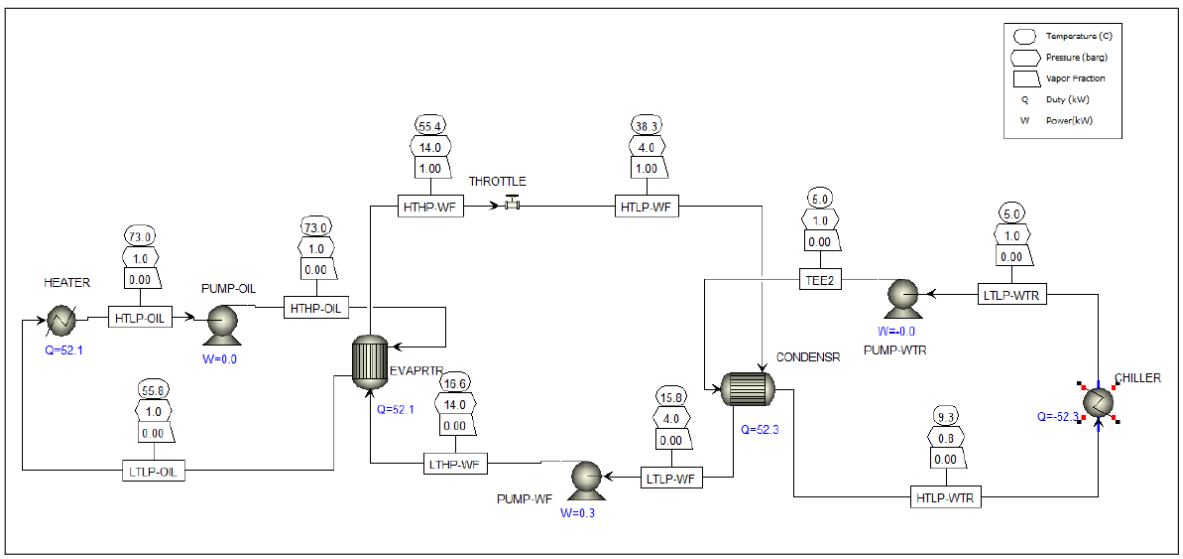


Figure J.10. Shut-down A operation conditions.

52. Under steady state conditions, it is expected that TT-3 is 45 °C and TT-10 is 13 °C. Process circulation is going on without interruption.
53. When "Start-up B" conditions are fulfilled, skip to the "Start-up C" conditions.
54. Set water temperature to 10 °C. (It is already set to 10 °C).
55. Adjust valve HA-115 to set water flow rate which is 9.8 $m^3$/h. (It is already set to 9.8 $m^3$/h).
56. Set pressure reducing valve (Throttle-01) to 4 barg (It is already set to 4 barg).
57. Set oil temperature to 65 °C.

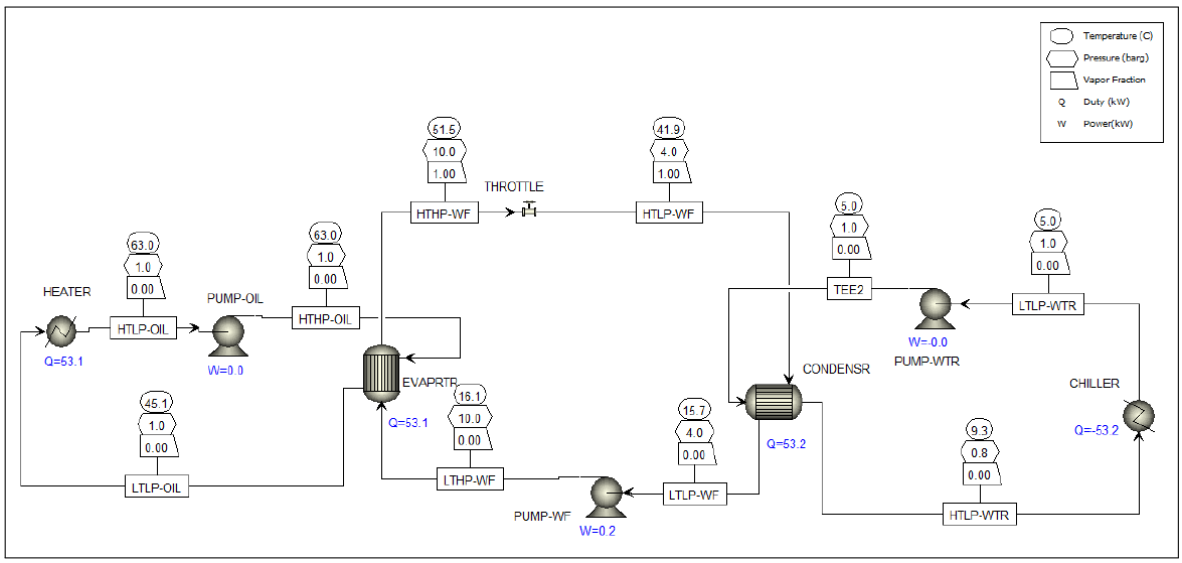


Figure J.11. Shut-down B operation conditions.

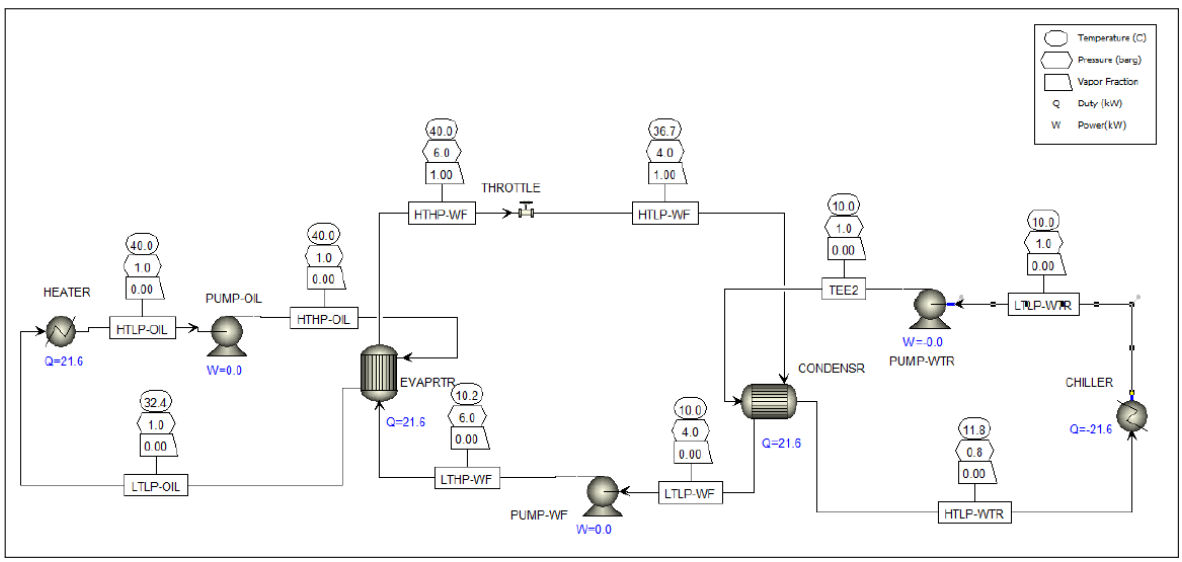


Figure J.12. Shut-down C operation conditions.

58. Adjust frequency inverter to a percentage that gives 14 barg pump discharge pressure. (Should be above the value of case “Start-up B”).
59. Adjust Pump-01 mass flow rate to 0.1 kg/s via HA-133 (globe valve) and HA-142 (by-pass valve). (It is already set to 0.1 kg/s).
60. Check level gages and take actions if levels are both not around mid-level. Refer “Actions to be taken” at the end of the document.
61. Under steady state conditions, it is expected that TT-3 is 57 °C and TT-10 is 13 °C. Process circulation is going on without interruption.
62. When “Start-up C” conditions are fulfilled, skip to the “Start-up D” conditions.

63. Set oil temperature to 70 °C. (It is already set to 70 °C).
64. Adjust valve HA-115 water flow rate of 9.8 $m^3$/h. (It is already set to 9.8 $m^3$/h).
65. Set pressure reducing valve (Throttle-01) to 4 barg. (It is already set 4 to barg).
66. Set chiller water temperature to 8 °C.
67. Adjust Pump-01 mass flow rate to 0.15 kg/s via HA-133 (globe valve) and HA-142 (by-pass valve).
68. Adjust frequency inverter to a percentage that gives 14 barg pump discharge pressure. (Should be above the value of case "Start-up C").
69. Check level gages and take actions if levels are both not around mid-level. Refer "Actions to be taken" at the end of the document.
70. Under steady state conditions, it is expected that TT-3 is 57 °C and TT-10 is 13 °C. Process circulation is going on without interruption.
71. When "Start-up D" conditions are fulfilled, skip to the "Start-up E" conditions.
72. Set oil temperature to 70 °C. (It is already set to 70 °C).
73. Set pressure reducing valve (Throttle-01) to 4 barg. (It is already set to 4 barg).
74. Set water temperature to 5 °C.
75. Adjust valve HA-115 water flow rate of 9.8 $m^3$/h. (It is already set to 9.8 $m^3$/h).
76. Adjust Pump-01 mass flow rate to 0.2 kg/s via HA-133 (globe valve) and HA-142 (by-pass valve).
77. Adjust frequency inverter to a percentage that gives 14 barg pump discharge pressure. (Should be above the value of case "Start-up D").
78. Check level gages and take actions if levels are both not around mid-level. Refer "Actions to be taken" at the end of the document.
79. Under steady state conditions, it is expected that TT-3 is 57 °C and TT-10 is 13 °C. Process circulation is going on without interruption.
80. When "Start-up E" conditions are fulfilled, skip to the "Testing A" conditions.
81. Set water temperature to 5 °C (It is already set to 5 °C).
82. Adjust valve HA-115 water flow rate of 9.8 $m^3$/h. (It is already set to 9.8 $m^3$/h).
83. Set pressure reducing valve (Throttle-01) to 4 barg. (It is already set to 4 barg).
84. Set oil temperature to 73 °C .

85. Adjust Pump-01 mass flow rate to 0.25 kg/s via HA-133 (globe valve) and HA-142 (by-pass valve).
86. Adjust frequency inverter to a percentage that gives 14 barg pump discharge pressure. (Should be above the value of case "Start-up E").
87. Check level gages and take actions if levels are both not around mid-level. Refer "Actions to be taken" at the end of the document.
88. Under steady state conditions, it is expected that TT-3 is 57 °C and TT-10 is 13 °C. Process circulation is going on without interruption.
89. When "Testing A" conditions are fulfilled, skip to the "Testing B" conditions.
90. Set water temperature to 11 °C.
91. Set pressure reducing valve (Throttle-01) to 5 barg.
92. Adjust valve HA-115 to set water flow rate which is 9.8 $m^3$/h. (It is already set to 9.8 $m^3$/h).
93. Set oil temperature to 79.5 °C.
94. Adjust Pump-01 mass flow rate to 0.25 kg/s via HA-133 (globe valve) and HA-142 (by-pass valve). (It is already set to 0.25 kg/s).
95. Adjust frequency inverter to a percentage that gives 17 barg pump discharge pressure. (Should be above the value of case "Testing A").
96. Check level gages and take actions if levels are both not around mid-level. Refer "Actions to be taken" at the end of the document.
97. Under steady state conditions, it is expected that TT-3 is 65 °C and TT-10 is 19.5 °C. Process circulation is going on without interruption.
98. When "Testing B" conditions are fulfilled, skip to the "Testing C" conditions.
99. Set oil temperature to 85 °C.
100. Set water temperature to 14 °C.
101. Set pressure reducing valve (Throttle-01) to 6 barg.
102. Adjust valve HA-115 to set water flow rate which is 7.5 $m^3$/h.
103. Adjust Pump-01 mass flow rate to 0.25 kg/s via HA-133 (globe valve) and HA-142 (by-pass valve). (It is already set to 0.25 kg/s).
104. Adjust frequency inverter to a percentage that gives 20 barg pump discharge pressure. (Should be above the value of case "Testing B").

105. Check level gages and take actions if levels are both not around mid-level. Refer "Actions to be taken" at the end of the document.
106. Under steady state conditions, it is expected that TT-3 is 72 °C and TT-10 is 24.5 °C. Process circulation is going on without interruption.
107. When "Testing C" conditions are fulfilled, skip to the "Shut-down A" conditions.
108. Set oil temperature to 73 °C .
109. Set water temperature to 5 °C.
110. Set pressure reducing valve (Throttle-01) to 4 barg.
111. Adjust water flow rate to 9.8 $m^3$/h.
112. Adjust Pump-01 to mass flow rate of 0.25 kg/s via HA-133 (globe valve) and HA-142 (by-pass valve). (It is already set to 0.25 kg/s).
113. Adjust frequency inverter to a percentage that gives 14 barg pump discharge pressure. (Should be below the value of case "Testing C").
114. Check level gages and take actions if levels are both not around mid-level. Refer "Actions to be taken" at the end of the document.
115. Under steady state conditions, it is expected that TT-3 is 57 °C and TT-10 is 13 °C. Process circulation is going on without interruption.
116. When "Shut-down A" conditions are fulfilled, skip to the "Shut-down B" conditions.
117. Set oil temperature to 60 °C .
118. Set water temperature to 5 °C. (It is already set to 5 °C).
119. Set pressure reducing valve (Throttle-01) to 4 barg. (It is already set to 4 barg).
120. Adjust valve HA-115 to set water flow rate which is 9.8 $m^3$/h. (It is already set to 9.8 $m^3$/h).
121. Start Pump-01 and adjust mass flow rate to 0.25 kg/s via HA-133 (globe valve) and HA-142 (by-pass valve). (It is already set to 0.25 kg/s).
122. Adjust frequency inverter to a percentage that gives 6 barg pump discharge pressure. (Should be below the value of case "Shut-down A").
123. Check level gages and take actions if levels are both not around mid-level. Refer "Actions to be taken" at the end of the document.

124. Under steady state conditions, it is expected that TT-3 is 29 °C and TT-10 is 13 °C. Process circulation is going on without interruption.
125. When "Shut-down B" conditions are fulfilled, skip to the "Shut-down C" conditions.
126. Set oil temperature to 40 °C.
127. Set water temperature to 10 °C.
128. Set pressure reducing valve (Throttle-01) to 4 barg. (It is already set to 4 barg).
129. Adjust valve HA-115 water flow rate of 9.8 $m^3$/h. (It is already set to 9.8 $m^3$/h).
130. Adjust Pump-01 mass flow rate to 0.1 kg/s via HA-133 (globe valve) and HA-142 (by-pass valve).
131. Adjust frequency inverter to a percentage that gives 6 barg pump discharge pressure. (Should be below the value of case "Shut-down B").
132. Check level gages and take actions if levels are both not around mid-level. Refer "Actions to be taken" at the end of the document.
133. Under steady state conditions, it is expected that TT-3 is 29 °C and TT-10 is 13 °C.
134. Stop Heater, Pump-02 and Pump-01 in this sequence. Close valve HA-136.
135. Wait for the liquid phase stabilize and accumulate at the bottom of the cycle (pump inlet-pump outlet-evaporator-condenser).
136. Close all the valves to localize possible liquid phase leakages during stand still.

## J.6. Actions to Be Taken

- If liquid level in the evaporator exceeds the mid-level;
  - (i) Decrease the flow rate of process pump (Pump-01).
  - (ii) Increase heater temperature.
- If liquid level in the evaporator drops below the mid-level;
  - (i) Increase the flow rate of process pump (Pump-01).
  - (ii) Decrease heater temperature.
  - (iii) Start-stop the oil pump (Pump-02).

- If liquid level in the condenser exceeds the mid-level;
  (i) Decrease water flow rate via globe valve HA-115.
  (ii) Increase water temperature from chiller.
- If liquid level in the condenser drops below the mid-level;
  (i) Increase water flow rate via globe valve HA-115.
  (ii) Decrease water temperature from chiller.
- Fine adjustment of flow rate and discharge pressure of the process pump (Pump-01) can be done by;
  (i) Adjusting frequency inverter.
  (ii) Adjusting HA-133 (globe valve) and HA-142 (by-pass valve).
- If pump discharge pressure increases above design point which is 25 barg;
  (i) Immediately open valve HA-110. Pressure safety valve PSV-001 is also set to the same pressure, but capacity is not checked.
  (ii) Push emergency shut down (ESD) button.
  (iii) Close the valve HA-110 once pressure drops below 20 barg.
- If there is no liquid phase at the pump suction and level sensor would not shut down the system;
  (i) Push the emergency shut down (ESD) button.
  (ii) In any case when Pump-01 is not running, press the ESD button.